University of Reading

Generation and characterisation of functional astrocytes from embryonic stem cells

PhD Thesis

School of Biological Sciences

Deppo Singh Juneja

November 2018

Supervisors:

Dr. Evangelos Delivopoulos **Prof. Slawomir J Nasuto**

Abstract

Astrocytes are considered a default developmental state in mammalian nervous system differentiation. Even though astrocytes are involved in the maturation of the nervous system, information regarding their own development is sparse. Evidence has shown that astrocyte development (astrocytogenesis) commences after neurogenesis, leading to a heterogeneous population of astrocytes within the CNS. However, generating astrocytes *in vitro* has proven to be more challenging than previously thought, where complex use of morphogens, long time culture incubation (>180 days), and reduced focus on subtype astrocyte generation prevents full understanding of astrocytes. By modifying previous methodologies, here we describe a quick and efficient method to generate functional and heterogeneous astrocytes from mouse embryonic stem cells (mESC) which contributes towards ever growing need towards standardising protocols for in vitro astrocytogenesis. Under the cell suspension protocol, mESCs formed embryoid bodies (EBs), which were then inducted into a neural lineage using retinoic acid (RA) (DIV 3). At DIV 6 EBs were seeded onto laminin coated glass coverslips, in astrocyte differentiation media, containing heparin and N2. Cells morphologically resembling astrocytes were observed migrating from attached EBs, two days post seeding. Migrating cells stained positive for astrocyte markers GFAP, ALDH1L1 and S100β. When astrocytes were stimulated with adenosine triphosphate (ATP), intracellular calcium concentration was elevated, as revealed by Fluo4. Analysis of P2X and P2Y purinoreceptor pathways, revealed significant contributions of each pathways and a functional diversity of the generated astrocytes. Furthermore, these generated astrocytes displayed potential to be used as a tool for future studies via successful removal from substrate, and rescuing damaged neuron rich network. In summary, we describe here the generation of functional astrocytes derived from mESCs, which display heterogeneity in form and function that is commonly observed in astrocytes *in vivo.*

Declaration of original authorship

Declaration: I confirm that this is my own work and the use of all material from other sources has been properly and fully acknowledged

Signed: Deppo Singh Juneja

Acknowledgments

Even though words will not suffice, I take this opportunity to express my deepest gratitude to my PhD supervisors, Dr. Evangelos Delivopoulos and Prof. Slawomir Nasuto, for the knowledge and guidance they provided throughout the past 4 years. As reviewers of the methods I applied, the results I produced and the writing I used to summarised, Evan and Slawek provided me with knowledge and skills that I benefited from substantially. Also, I want to highlight Evans continuous scientific enthusiasm, without which the research provided here would not exist.

Furthermore, I'd like to thank my family and fiancé who have been extremely patient with me through all of this. Without their love and support, this would not have been possible. Finally, I'd like to dedicate this thesis to my father who passed away during my PhD, this is for you Dad.

List of achievements

Publications

Deppo Juneja, Slawomir Nasuto, Evangelos Delivopoulos (2019)
Deriving Functional Astrocytes from Mouse Embryonic Stem Cells with a Fast and Efficient Protocol. IEEE Engineering in Medicine & Biology Society

Juneja, D.S, Nasuto, S and Delivopoulos E. (2017) Differentiation of functional astrocytes from mESC European Meeting on Glial Cells in Health and Disease

Deppo Singh Juneja, Slawomir Nasuto, Evangelos Delivopoulos. (2017) Generating heterogeneous populations of astrocytes from mouse embryonic stem cells. Glio-vascular Coupling. The Physiological Society.

Significant Presentations

Deppo Singh Juneja, Slawomir Nasuto, Evangelos Delivopoulos. (2017) Temporal functional differences in mouse embryonic stem cells derived astrocytes. University of Reading, Doctoral Research Conference

Deppo Singh Juneja (2017) Astrocytes: The Stars of the show. Research Image Competition. University of Reading, Doctoral Research Conference

Juneja, D.S, Nasuto, S and Delivopoulos E (2015) Quick and efficient generation of astrocytes from stem cells. School of Neurotechniques, University of Padua, Italy

List of Abbreviations

ALDH1L1 - aldehyde dehydrogenase 1 family member L1
ATP – Adenosine Triphosphate
BBG – Brilliant Blue G
BMP - Brain morphogenetic protein
bHLH - Basic helix–loop–helix
Ca^{2+} - Calcium
$[Ca^{2+}]_{i.}$ – cytosolic/intracellular calcium
CNS – Central Nervous System
CNTF - Ciliary Neurotrophic Factor
DIV – Day *in vitro*
EB - Embryoid Body
ECM – Extracellular Matrix
ER - Endoplasmic Reticulum
ESC - Embryonic Stem Cell
FBS – Foetal Bovine Serum
GFAP - Glial Fibrillary Acidic Protein
GFP – Green Fluorescent Protein
GJB6 - Gap Junction B6 (Cx40)
GPCR – G Protein Coupled Receptor
hESC - Human Embryonic Stem Cell
hPSC – Human Pluripotent Stem Cell
IP_3 - Inositol Trisphosphate
ICM – Inner Cell Mass
IL6 – Interleukin 6
iPSCs – Induced Pluripotent Stem Cell
LIF – Leukaemia Inhibitory Factor
MEA - Multi-electrode array
mESC – Murine Embryonic Stem Cell
mESCDA – Mouse Embryonic Stem Cell Derived Astrocytes
PBS - Phosphate Buffered Saline
PCC - Pearson's correlation coefficient
P2YR1 – Metabotropic Purinergic Receptor 1
P2X7 – Ionotropic Purinergic Receptor 7
PKC - Protein Kinase C
RA – Retinoic acid
RGC - Retinal Ganglion Cell
SC – Stem Cell
SHH – Sonic Hedgehog
SOCE – Store operated calcium entry

List of Figures and Tables

Table of Contents

1. Introduction

The central nervous system (CNS) consists of interconnected networks composed of variety of neuronal and non-neuronal glial cells such as macroglia and microglia. Microglia originates from different ontogenic sources: hematopoietic system and the main embryonic cells from yolk sac (Alliot et al. 1999; Ginhoux et al. 2013). Whereas macroglia encompasses cells which originate from the neuronal tube such as: oligodendrocytes and astrocytes (Nedergaard et al. 2003). The term glia derives from the Greek word for 'glue' and the study of glial cells dates back to the 19th century, where they were first described and made public by Rudolph Virchow in 1858 (Kettenmann & Verkhratsky 2008). Virchow described the works of Remak, Muller, and Bremann, who revealed the presence of Muller and Bregmann glia within the CNS, and based on their discoveries coined the term neuroglia (nervenkitt) - where glial cells were seen as 'glue' to support neurons and maintain the vasculature of the CNS, with no clear defined function – placing neurons at the centre and sole contributors to cognitive function (Virchow 1858; Fields & Stevens-Graham 2002).

Pioneer work conducted by Dieters and Golgi in the mid-19th century on glial morphology showed differences and similarities between neurons and glia, and brought forward the idea of glial cells as separate cell-type when compared to neurons (Kettenmann & Verkhratsky 2008). This led to the conclusion that glial cells share the same developmental origin as neurons (Oberheim et al. 2012). Over the next few years, work conducted by Santiago Ramon y Cajal, von Lenhossek, William Lloyd Andriezen and Rio-Hortega, provided seminal evidence towards glial biology, by introducing astrocytes and oligodendrocytes to the field of neuroscience (Araque & Navarrete 2010; Verkhratsky et al. 2014).

Astrocytes were first described by von Lenhossek as star shaped cells of the neuroglia, which display elaborate morphology (Matyash & Kettenmann 2010; Fields et al. 2015). Later Andriezen and Cajal built upon these observations and descriptions, and placed astrocytes into different subtypes based on their morphological features and introduced the terms fibrous and protoplasmic astrocytes (Eng et al. 1971; Miller & Raff 1984; Gleichman & Carmichael 2014). Nevertheless, despite these findings, similar to previous conclusions, astrocytes were still relegated to secondary role – providing support to neurons (Miller and Raff 1984, Belanger et al 2009). In the last several decades however,

this view of astrocytes has changed, and ample of evidence now exists which challenges places astrocytes as key players in regulating neural transmission (Hu et al. 2016).
The functional importance of astrocytes both in development, maintenance, and maturity of the CNS has become an area of increasingly intense research (Volterra & Meldolesi 2005; Clarke & Barres 2013). Evidence has now shown that astrocytes are the most abundant type of glial cells within the CNS (Verkhratsky & Butt 2018) and ratio of astrocyte to neuron is mainly 1:1 – although shown to be highly variable depending on the brain region (Herculano-Houzel 2014). This further challenges the idea neuronal dogma, and now ample of studies have now provided evidence towards the active involvement of astrocytes in various important processes, such as: providing metabolic support to neurons (Bouzier-Sore & Pellerin 2013), buffering of extracellular potassium (Bellot-Saez et al. 2017), uptake and recycling of neurotransmitters (Petrelli & Bezzi 2016), ion distribution (Rose & Chatton 2015), sleep (Rusakov et al. 2014), neurogenesis (Kempermann et al. 2015), neurodegeneration (Phatnani & Maniatis 2015), synaptogenesis (Tsai et al. 2012), modulating synaptic activity, and more recently learning and information processing in the brain (Savtchouk & Volterra 2018).

Until recently, astrocytes have been studied as a homogeneous cell population (Matyash & Kettenmann 2010; Farmer & Murai 2017). Since their discovery the classic subdivision of astrocytes into protoplasmic and fibrous cell type has dominated the field (Miller & Raff 1984; Yong et al. 1990; Oberheim et al. 2012). However, this does not account for heterogeneous subpopulations of astrocyte that have been identified in recent experiments (Xin & Bonci 2018). The understanding of the diversity of astrocytes lags far behind that of neurons - in terms of functionality and morphology (Petravicz et al. 2010; Farmer & Murai 2017). The invention of usage of stem cells, embryonic stem cells (ESCs) and/or induced pluripotent stem cells (iPSCs) opens future prospects for understanding astrocytes, given that physiologically functional, cellular model systems can be generated from these cells (Kuegler et al. 2012; Santos et al. 2017; Xin & Bonci 2018). This can allow researchers to begin to unravel the complexity of astrocytes and its heterogeneity and help solidify the definition and function of astrocytes within the CNS.

1.1. Development of Astrocytes – Astrocytegenesis

During development gliogenesis generally follows neurogenesis in the developing brain (Miller & Gauthier 2007; Rowitch & Kriegstein 2010; Peljto et al. 2010). Neural tissue of developing vertebrates is specified from the ectoderm germ layer during embryogenesis (Suda et al. 1987; Reubinoff et al. 2000; Sadler 2005). The ectoderm, most of which will eventually give rise to the epidermis, contains a subset of neuroepithelial cells that will develop into the neural tube, which give rise to the spinal cord and the CNS (Sadler 2005). The neural tube is patterned throughout the dorso-ventral axis by morphogens (SHH, BMPs, and Wnts) (Le Dréau & Martí 2012), which regulate the expression of homeodomain transcription factors forming domains leading to neurons and glial cells (Fig. 1) (Le Dréau & Martí 2012; Rowitch & Kriegstein 2010). Initial evidence displayed astrocyte emerge from the ventral P2 progenitor domain (Molofsky & Deneen 2015). Fate mapping of astrocytes by (Tsai et al. 2012), revealed astrocytes emerge from all of the domains during development, with the ventral domains contributing towards 80% of astrocytes (Fig.4) (Molofsky et al. 2014). Regionally specified neural progenitor cells (NPC) – called radial glia, will initially give rise to neurons and then eventually give rise to regional astrocyte progenitors. This process is called the neural-glial switch (Molofsky & Deneen 2015). Within the developing neural tube, the development of astrocytes and the regulation of neural-glial switch is controlled by several key transcription factors, such as Neurogenin 1/2, a bHLH transcription factor (Sun et al. 2001; Kessaris et al. 2008; Velkey & O'Shea 2015; Bayraktar et al. 2015). These factors control and supress astrocytic genes (GFAP, S100β, and ALDH1L1) by hypermethylation (Sun et al. 2001; Cahoy et al. 2008; Takouda et al. 2017), and prevent the development of astrocytes. Therefore, downregulation of pro-neural genes (such as Neurogenin) and upregulation of pro-astrocyte genes (such as Notch, transcriptional repressor N-CoR, Nuclear Factor I-A, Sox9) is required to induce astrocytogenesis (Velkey & O'Shea 2015; Takouda et al. 2017). For example, Nuclear Factor I-A was identified and found to be both necessary and sufficient for astrocytogenesis in developing mice (Wilczynska et al. 2009; Kang et al. 2012). Changing the expression of NFI family genes altered the neural-glial switch, led to decreased astrocyte numbers within the developing brain (Sloan & Barres 2014).

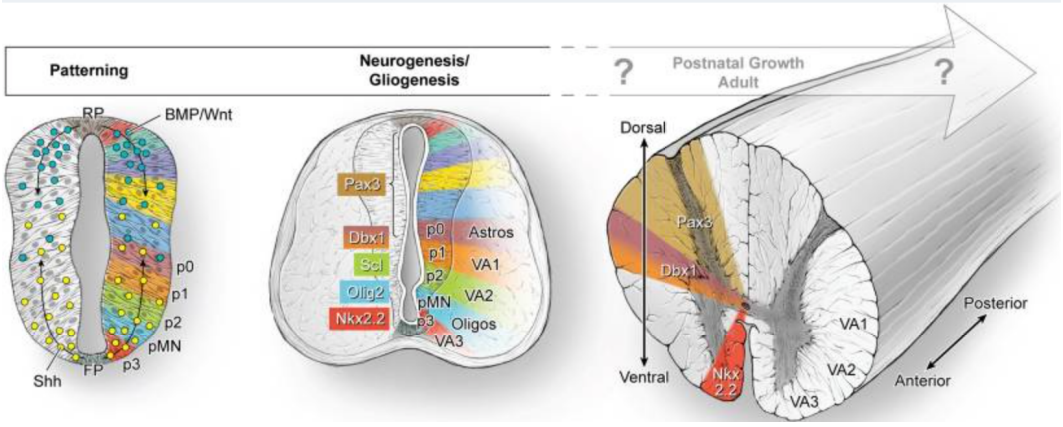

Figure 1: Graphical overview of astrocyte development. Interaction of multiple transcription factors in the neural tube leads to astrocyte development. Image adapted and reproduced from Molofsky et al 2012 under a Creative Commons 4.0 license.

As the transition towards astrocytogenesis occurs by inhibition of pro-neuronal factors, the astrocyte precursors become primed to be induced by cytokines such (Ciliary neurotrophic factor) CNTF (Hughes et al. 2010; Yang et al. 2013), (Leukemia inhibitory factor) LIF (Asano et al. 2009) and growth factors like (bone morphogenetic proteins) BMPs (Kohyama et al. 2010; Le Dréau & Martí 2012) which act to activate signalling pathways such as STAT, SMAD or PI3K-Akt pathway necessary for astrocyte development and maturity (Fig.5) (Hong & Song 2014; Wang et al. 2014). For example, the STAT pathways is one of the key pathways which is required in astrocyteogenesis (Hong & Song 2014). The pathway requires combinatorial work by Neurotrophins (NTF) and LIF to bind to gp-130, a cell surface co-receptor and leads to dimerization with LIF receptors (Nakashima et al. 1999; Hong & Song 2014). Dimerisation of LIFR leads to activation of (Janus kinase) JAK/STAT pathway, which causes the activated STAT locate from cytoplasm to the nucleus and relaxes the chromatin structure GFAP promoter region and triggers transcription of GFAP leading formation, maturity and differentiation of astrocytes (Fig.5) (He et al. 2005; Asano et al. 2009; Hong & Song 2014). Several studies have shown the necessity of gp-130 activation for astrocytogenesis, for example Nakashima et al 1999 shown that gp-130 null mice present reduction in STAT and GFAP when compared to control mice, and these mice showed impairment in astrocyte induction with significant reduction led to significant neuronal defects which is controlled by maturing astrocytes (Nakashima et al 1999).

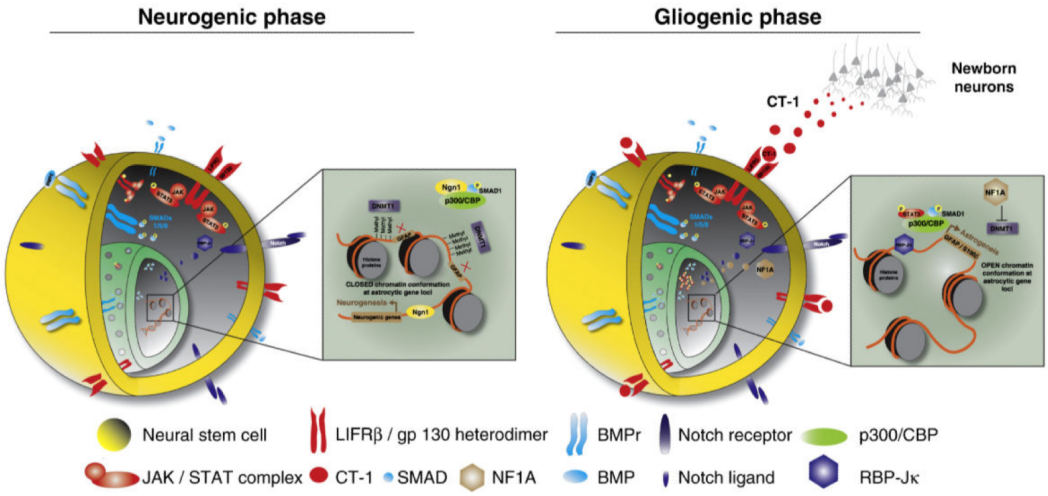

Figure 2: Graphical overview of astrocyte development pathways. Interaction of multiple transcription factors in the neural tube leads to astrocyte development. Image adapted and reproduced from Rowitch and Kriegstein 2010, Sloan and Barres 2014 under a Creative Commons 4.0 license.

A major limitation of all these studies investigating the gliogenic switch is that, they all converge at the expression of GFAP as "the" marker to understand the commitment towards astrocytic lineage (Eng et al. 2000; Bayraktar et al. 2015; Molofsky & Deneen 2015; Hol & Pekny 2015). Therefore, further studies are required to relate the expression of other important astrocytic markers like ALDH1L1 and S100ß (Raponi et al. 2007; Cahoy et al. 2008; Roybon et al. 2013; Kleiderman et al. 2016). Also, it remains to be elucidated whether or not these pathways are working in parallel or one pathway can compensate for the lack of the other or whether they exhibit a temporal pattern. Also, further investigation is also required to study the relation between these different ways of initiating astrocytic differentiation in order to build a better temporal model for understanding astrocytogenesis (Sloan & Barres 2014; Xin & Bonci 2018).

1.2. *In vitro* astrocytogenesis

To gain clearer understanding on astrocytogenesis, *in vitro* assays have been performed ubiquitously using variety of methods and cell types (Mccarthy & Vellis 1980). Majority of initial studies have used primary monolayer cultures as a model of studying astrocytes *in vitro* (Mccarthy & Vellis 1980; Schildge et al. 2013). For example, the first human astrocytes were cultured from foetal and adult post- mortem tissue (Ennas et al. 1992; Schildge et al. 2013) but were often contaminated with microglia and other cell types which were difficult to separate during dissections (Crocker et al. 2008). The

contamination of other cells raises severe disadvantages when studying astrocytes specifically (Crocker et al. 2008; Schildge et al. 2013). Furthermore, as primary astrocytes are more committed in terms of region specific roles and gene expression, they are not a suitable alternative to fully recapture and unravel role of astrocytes and astrocytogenesis (Hewett & Hewett 2012). Moreover, inaccessibility of tissue, mainly human, due to ethical concerns and potential health risks also leads to primary sources as not a viable option for studying astrocytogenesis (Lange et al. 2012).

In vitro astrocytogenesis using other alternatives methods, such as stem cells or partially differentiated cells stem cells (such as glial or neural progenitors) unravel new possibilities to investigate development and the complex roles of astrocytes (Kleiderman & Kirner 2017; TCW et al. 2017; Li et al. 2018). Stem cells, initially studied by Becker et al (1963), are a group of highly specialised cells that have become exceedingly attractive for many applications in tissue engineering, pharmaceutical screening and cellular therapies (Becker, A.J. McCulloch, E.A. Till 1963; Gardner 2007). Stem cells have attracted a large amount of attention in recent years because they are able to provide inexhaustible source and a large pool of cells to be used (Ying et al. 2003; Gardner 2007), by having the ability of self-renewal and differentiate (Ying et al. 2003).

Stem cells have been broadly categorised into two subtypes, adult and embryonic (Biehl & Russell 2009; Chagastelles & Nardi 2011). Adult stem cells are generally tissue and region restricted, and their roles and numbers tightly controlled and only used for maintenance and when in demand throughout the life of an organism (Chagastelles & Nardi 2011; Gao et al. 2017). Stem cells residing in the adult tissues are extremely interesting for several reasons, as they are closer to fully specialised cell types and may therefore be more readily manipulated (Biehl & Russell 2009). However, this is also their downfall as these cells are unipotent and require significant changes and alteration to be differentiated to other cells type (Kleiderman et al. 2016; Gao et al. 2017). For example, Gao et al 2017 were able to show de-differentiation of astrocytes towards neuronal lineage via expression of pro-neuronal transcription factors, however they were not able to create specific neuronal subtypes and lacked expression which matched primary cells. Therefore, embryonic stem cells (ESC) have shown to be more favourable and have the main focus for future studies (Conley et al. 2004; Kuegler et al. 2012). Embryonic stem (ESC) cells are unique in their ability to differentiate into cells from each of the three germ layers, ectoderm, endoderm and mesoderm – they can make all the tissues of the adult organism (a property termed pluripotency) (Martin 1981; Reubinoff et al. 2000). This, together with their ability to multiply in culture without apparent limit,

makes and made them an attractive source for the *in vitro* generation of cell types that may be of use to study disease or to provide a limitless source of cells for cell-replacement therapies (Suda et al. 1987). Using and understanding mechanisms which keep ESC in their pluripotent stages *in vitro*, researchers were able to reverse the process and able to derive stem cells, which can be kept in their pluripotent stage, from adult stem cells – termed induced pluripotent stem cells (iPSCs) (Stadtfeld et al. 2010). Pioneer work by Kazutoshi, Takahashi and Yamanaka, 2006, on mouse lines, they were able to show that by using Oct4, KLF4, Sox and cMy, termed Yamanaka factors, adult stem cells can be kept in undifferentiated stage and can be formed into of a pool of induced pluripotent stem cells (iPSCs) (Stadtfeld et al. 2010). The establishment of an ES like cell line from human cells was achieved also achieved using the four Yamanaka factors (Takahashi et al. 2006; Liu et al. 2008) or new factor LIN28, allowing for the production of human iPSC lines (Takahashi et al. 2006; Liu et al. 2008; Stadtfeld et al. 2010).

To employ *in vitro* systems for studying and trying to capture astrocytogenesis, it is important to mimic *in vivo* conditions (Nagao et al. 2016; Sloan et al. 2017). With the growing use of stem cells, there have been several well defined protocols for their differentiation into different subtypes of neurons, but only few protocols exist for the generation of towards astrocytes (Falsig et al. 2004; Kuegler et al. 2012; Roybon et al. 2013; Shaltouki et al. 2013; Chandrasekaran et al. 2016; Li et al. 2018). Also, very few protocols exist which utilise ESC, which will fully allow to recapitulate *in vivo* astrocytogenesis (Kuegler et al. 2012; Kleiderman & Kirner 2017). ESC were first isolated in 1981 by Martin Evans, Matthew Kaufman, and Gail R. Martin (Kaufman et al. 1983). In 1995, Martin Evans and Austin Smith described the culture of mouse ESC with LIF, which keeps the cells in their pluripotent, self-renewing state. Human ESC were isolated later in 1998 by James Thomson from the inner cell mass (ICM) of residual blastocysts of *in vitro* fertilisations (Ying et al. 2003; Conti et al. 2005). Using and understanding mechanisms which keep ESC in their pluripotent stages *in vitro*, researchers were able to induce these ESC into neuronal and glial subtypes. For example, Ying et al 2003 described that pure population of neural stem cells can be generated from mESC and subsequently provided a platform for generation of glia and neurons which was used by Conti et al 2005 to generate neurons, oligodendrocytes and astrocytes (Ying et al 2003; Conti et al 2005). However, research into mESC was arrested and the focus was shifted towards using human ESC. Although human ESC isolation was defined before by (Zhang et al. 2001), where they were able to obtain neural precursors, the usage of human ESC gained traction more recently (Zhang et al 2001). For example, Krenick et al 2011 displayed differentiation potential of human ESC, and generated functional

astrocytes in 160 days (Krencik & Zhang 2011). This was further optimised by Gupta et al. 2012 and using functional assays such as glutamate uptake and kinetic assays, they showed that the human ESC astrocytes can be used effectively to model neuron–astrocyte interactions and investigate their mechanism (Gupta et al. 2012; Santos et al. 2017). However, the differentiation of human embryonic stem cells to astrocytes is much more complicated when compared with mouse systems (Keugler et al. 2012), since human development proceeds in a different time scale (Santos et al. 2017). Although using human systems would be more desirable, similar to *in vivo* experimental planning and protocols are far more complex that their murine counterparts. Additionally, current protocols for the generation of astrocytes require longer incubation period, and are harder to maintain (Li et al. 2018). Also, the differentiated astrocytes in most protocols are not fully mature and do not fully represent the diversity seen during *in vivo* astrocytogenesis (Roybon et al. 2013). Furthermore, employing human sources of stem cells presents itself with its own challenges, such as ethical and availability issues. Thus, for studies, which require representative populations of astrocytes to fully unravel their complexity, astrocytes generated from murine stem cells are still the best approach.

Since the pioneering studies, there have been assortment of methods which have generated functional astrocytes from mouse embryonic stem cells (mESC). However, the methodologies used either produced other cell types, such as neurons and oligodendrocytes, alongside astrocytes, were large in their timescales or required alteration of protocol which deviated from *in vivo* astrocytogenesis (Kamnasaran et al. 2008). For example, Kamnasaran et al. 2008 transiently transfected cells, which had already been through morphogens which selectively induced gliogenesis in the media. Furthermore, alongside morphogen usage, they used a human (h) GFAP: GFP plasmid to selectively induce transcription for GFAP, and accelerate the generation of astrocytes. This protocol is sufficient for understanding astrocyte function, however it is a protocol which was difficult to replicate and does not follow astrocytogenesis principles. In order to precisely mimic *in vivo* astrocytogenesis, Kuegler et al (2012), refined previous methodologies from Falsig et al 2004, and generated astrocytes which were GFAP negative – displaying heterogeneity in marker expression (Falsig et al. 2004; Kuegler et al. 2012). These astrocytes were immunocompetent and expressed majority of astrocyte specific markers. Nevertheless, the protocol requires adaptations and further specifications to reduce the timeline (Keugler protocol generated astrocytes in 50+ days) and requires stringent validation assays to show production of high quality, pure astrocytes.

Majority of the above studies are limited by the requirement of a long differentiation time to attain astrocyte rich cultures. Also, they use of either serum or expensive growth factors to recapture developmental principles. But above all, majority of protocols rely largely on the expression of GFAP to mark the completion of astrocyte differentiation and maturation, and provide reduced data on step by step temporal analysis of developing astrocytes (Wang & Bordey 2008; Gupta et al. 2012; Yang et al. 2013). This has resulted in overlooking astrocyte heterogeneity and developmental principles while employing *in vitro* methods, thereby highlighting the need for an economical and less time consuming method for the generation of different possible subtypes of astrocytes (Molofsky & Deneen 2015). Furthermore, it is important *in vitro* to develop standardised protocols for the *in vitro* generation of astrocyte subsets with defined maturity status, phenotypic properties and which captures developmental principles in a timely and efficient manner.

1.3. Classification of an astrocyte

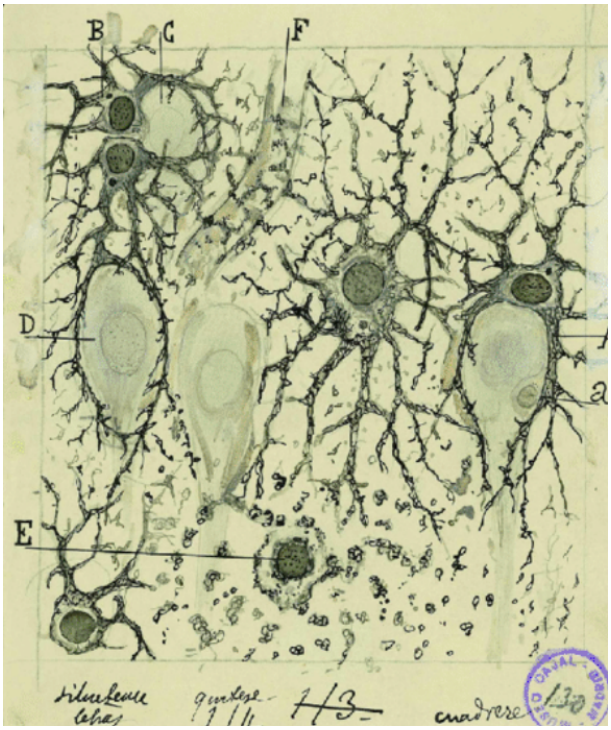

Figure 3: Original Cajal drawing illustrating the human neuroglia in the pyramidal and radiated layers of Ammon's horn with the gold chloride method: A represents thick astrocyte wrapping a pyramidal cell; B, sibling astrocytes forming a nest around a cell (C), one of them extend two processes to another nest (D); E: cell with autolysis sign'. F: Astrocyte close to blood vessels. Image adapted from Cajal Legacy, Instituto Cajal, CSIC under a Creative Commons 4.0 license.

Since the discovery of astrocytes in the early 19th century (Fig. 3), astrocytes have been shown to be a heterogeneous group of cells (Oberheim et al. 2012). Although, due to the neuronal dogma taking centre stage, astrocytes have been treated as a homogenous groups of cells (Verkhratsky & Butt 2018). The full scope of astrocytic heterogeneity, however, has not been realised and it is only now beginning to unravel (Oberheim et al. 2012; Hu et al. 2016; Farmer & Murai 2017; Xin & Bonci 2018). However, in comparison to neuronal diversity, understanding astrocyte heterogeneity still remains rudimentary (Farmer et al 2017; Xin et al 2018). This heterogeneity is not only of morphological nature, but also phenotypic, functional, regional, and local aspects, which are closely linked to each other and the environmental niche they encompass (Okuda 2018).

Classically, astrocytes have been divided into subgroups based on their morphological appearances (Fig. 3). The protoplasmic astrocytes, usually found in the grey matter, and the fibrous astrocytes, which are located in the white matter. This classical subdivision, although rudimentary, was still one of the most defining means of classifying astrocytes. The phenotype of cells can be easily assessed by PCR on mRNA level and by immunocytochemistry on protein level. PCR provides an early response to changes in the environment, but does not allow single cell analysis. Immunocytochemistry is therefore crucial to examine the distribution of marker expression and protein localization in single cells of a possibly heterogeneous population. There are several specific astrocyte markers, which can be detected by one or both methods.

As seen until now, most of the studies for defining astrocytes and their development depend largely on the expression of GFAP (Sofroniew & Vinters 2010; Hol & Pekny 2015). But with more detailed studies of astrocytes, it is becoming clear that not all astrocytes are labelled uniformly with GFAP (Zhang & Barres 2010). Also, the type B stem cells in adult SVZ stains positive for GFAP (López-Hidalgo & Schummers 2014). In addition, GFAP expression is augmented in reactive astrocytes as well as serum derived cultured astrocytes. These findings suggest that the use of GFAP as ‘the prototypical’ astrocytic marker is highly disputable. There are several markers in which one can distinguish astrocytes.

S100β

S100β belongs to the family of Ca^{2+}, Zn^{2+}, Cu^{2+} binding proteins, and is highly expressed in the brain. It has been reported that the initiation of S100β expression (at around E13 in mouse) in astrocytes marks the loss of their NSC potential, thereby stabilizing their commitment towards the astrocytic lineage (Raponi et al. 2007). Expression of S100β in astrocytes is seen in all regions of the brain, occupying both cytoplasmic and nuclear location. Although the exact physiological function of S100β is unknown, it has been attributed to play a crucial role in cytoskeleton organization, calcium binding, and scavenging of toxic substances (Brozzi et al. 2009). Also, intracellular S100β is considered to stimulate cell proliferation, migration along with inhibition of apoptosis and differentiation (Hachem et al. 2007; Donato et al. 2008). In astrocytes, S100β is also known to regulate their response to inflammation in a receptor for advanced glycation end products (RAGE) dependent manner (Selinfreund et al. 1991; Hachem et al. 2007).

EAAT/GLAST

The activation of excitatory amino acid transporter 1 (EAAT1 or sodium dependent glutamate- aspartate transporter GLAST) promoter overlaps its expression with neuronal migration (Shibata et al., 1997. In the murine forebrain, Ullensvang et al 1997 showed that the expression of GLAST occurs at the start at the second embryonic week and reaches a maximum level by P5. Ullensvang et al 1997 also showed that the expression was mainly present in glial cells in both young and adult animals (Ullensvang et al. 1997). Excitatory amino acid transporter 2 (EAAT2 or Glutamate transporter 1) is the second most dominant glutamate transporter expressed by astrocytes performing a similar function in glutamate clearance as described for EAAT1 (Yang et al. 2011). EAAT2 expression begins late in development and increases in a region based manner till development (Desilva et al. 2012). Also, DeSilva et al 2012 showed that by performing western blots, EAAT2 undergoes glycosylation and this increases during development (DeSilva et al. 2012).

ALDH1L1

Aldehyde dehydrogenase 1 light chain 1 (ALDH1L1, as known as 10- formyl tetrahydrofolate dehydrogenase (FDH)) is a folate metabolizing enzyme, first shown to be expressed in rodent astrocytes, making them an important site for folate metabolism (Anthony & Heintz 2007). Later, using P0 mouse, it was reported that ALDH1L1 labels

all astrocytes throughout the brain, whereas GFAP was predominantly expressed in the white matter. Also, it does not co- stain with neuronal or oligodendrocyte markers, thereby promoting the use of ALDH1L1 as a highly specific, 'pan' astrocytic marker which could be employed for preparation of pure astrocytic cultures by performing FACS (C(Vasiliou & Nebert 2005; Foo & Dougherty 2013; Molofsky et al. 2013). By means of GLT1+, ALDH1L1+ reporter mice; another study has reported a decrease in the expression of ALDH1L1 with maturation of spinal cord astrocytes (Yang et al. 2011).

GFAP

Glial fibrillary acidic protein (GFAP) has been widely used as "the" mature astrocytic marker to identify them both *in vivo* and *in vitro* and also to elucidate the signalling cascade for their differentiation (Eng et al. 2000). However as mentioned before, a deeper analysis of the expression of GFAP has revealed that not all the astrocytes express GFAP, its level being higher in white matter, fibrous astrocytes and almost insignificant in grey matter, protoplasmic ones (Kimelberg 2010). Protoplasmic astrocytes can however be identified by the presence of other pan astrocyte markers like ALDH1L1, GS and functional marker like EAAT2. In addition, glia limitans (astrocyte foot processes) and another subtype of astrocytes called interlaminar astrocytes also express GFAP. Its expression has been observed to start at E16 in mouse and at 23 gestational weeks in humans and peaks till E18 and 41 post conception week in mouse and humans respectively (Desilva et al. 2012; Mamber et al. 2012). Protoplasmic astrocytes when turned reactive upon inflammatory insult, retain the ability to exhibit GFAP expression. GFAP ICC does not sufficiently reveal astrocyte morphology. Using dye filling experiments it has been illustrated that *in vivo* astrocytes possess far more processes than those observed with GFAP immunostaining, and GFAP represents only 15% of the total cell volume (Oberheim et al. 2012).

1.4. Roles and functions of Astrocytes

Alongside astrocyte morphology, recent observations of astrocyte functions have also revealed heterogeneity. For example, Martin et al 2015 show Circuit-specific signalling in astrocyte-neuron networks in basal ganglia pathways, where each subpopulations of astrocytes selectively responded to specific neuronal activity (Martin et al. 2015; Okuda 2018).

The brain is one of the most energy demanding organ in the body, and since the discovery of astrocytes, the conclusions have been that sole purpose of these cells is to provide nutrients and support to neurons (Raichle & Gusnard 2002). Based on our recent understanding of astrocytes, we now know that these cells perform many other complex functions such as regulation of neural activity and transmission, neuroprotection (Fields & Stevens-Graham 2002; Agulhon et al. 2008) regulation of memory (Lee et al. 2014), sleep (Rusakov et al 2014), contribute towards formation of the blood-brain barrier (Nedergaard et al. 2003), guidance during migration and many more other functions which are outline below. However, the initial observations were correct, and astrocytes do provide metabolic and physical support to neurons and this is indeed one of their key roles within the CNS (Fields and Graham 2002).

Evidence has shown that astrocytes are involved in providing energy to neurons (Dienel 2015) under basal and energy demanding conditions, via the astrocyte-neuron lactate shuttle (Suzuki et al. 2011; Jakoby et al. 2014). Using fluorescent glucose probes Jakopy et al 2014, showed that astrocytes show preferential transport and metabolism of glucose when compared to neurons from primary hippocampal and cortical cultures. This glucose via glycolysis gets converted into Adenosine Triphosphate (ATP) and pyruvate, however due to high uptake of glucose by astrocytes excess pyruvate is produced. This excess pyruvate gets converted into lactate for neurons to use and directly produce ATP for their function. This lactate shuttle provides evidence of astrocyte supporting neurons in performing their functions (Suzuki et al. 2011; Dienel 2015).

Further evidence of neuronal support is astrocyte involvement in preventing runaway excitation via uptake of glutamate from extracellular space (Petrelli et al 2016). Glutamate is one of the primary neurotransmitter alongside ATP within the CNS. Excess glutamate can lead to glutamate excitotoxicity – where neuronal firing rates increases leading neuronal loss (Schousboe & Waagepetersen 2005; Risher et al. 2014). Because astrocytes are overburdened with excess glutamate, astrocyte metabolise glutamate in

many ways. Mainly, glutamate is converted to glutamine through the action of glutamine synthase and shuttled to neurons for further signalling purposes or recycled (Zou et al. 2011). Zou et al that effecting glutamine synthase activity was inhibited by applying an antagonist or cytokines, it significantly reduced GS expression and inhibited glutamate-induced GS activation resulting in increased excitotoxicity to neurons – shown via glutamate uptake assay (Zou et al. 2011).

1.4.1 Non-conventional roles of Astrocytes

Due to astrocyte ability to interact with neurons in a support manner, researchers began to unravel further roles of astrocytes which challenged the dogma and showed that astrocytes are more than just support cells. One of these functions was the identification of the tripartite synapse – where astrocytes survey, prune and form, influence and for a network that influences the neural activity that is occurring between pre-and post-synapses (Araque et al. 1999; Clarke & Barres 2013; Chung et al. 2015).

Evidence from Halassa et al 2007 led to identification of extent to which a single astrocyte can interact neurons. Using mouse cortex, Halassa et al 2007 quantified the number of synapses which are in contact with a single astrocyte, and found that 100,000 synaptic connections were formed by a single astrocytes (Michael M Halassa et al. 2007; Farhy-Tselnicker & Allen 2018). This showed that astrocytes can influence and modify the working of neural circuitry and signalling in a more direct way.

One of the most direct way that an astrocyte can influence neural activity is through the release of transmitters (Savtchouk & Volterra 2018). The transmitter which are released from astrocytes are termed gliotransmitters and astrocytes have been shown release all of the transmitter which are released by neurons (Zorec et al. 2012; Petrelli & Bezzi 2016; Zorec et al. 2015; Savtchouk & Volterra 2018). This places astrocyte right at the centre of mediating activity in the brain. Astrocytes membrane currents are passive and they display no ability to generate action potentials (Dallérac et al. 2013). Given these findings, the majority stance was that astrocytes were silent support elements in the brain. As astrocytes are incapable of generating action potentials, their excitation cannot be revealed via conventional methods such as, electrophysiology (Dallérac et al. 2013). Several key observations in the early 90's, provided evidence that calcium, rather than electrical signalling is a substrate for astrocyte excitability. When activated by internal or external signals, calcium waves were observed (Henneberger et al. 2010) (Hennebereger

et al 2000) and these waves led to the release transmitters (gliotransmission) (Araque et al 1999).

Calcium signalling and generation of calcium wave is important for astrocytes, as it is an important method of communication (intercellular) and influencing the environment around them (intracellular) (Navarrete et al. 2013; Bazargani & Attwell 2016). The complexity and mechanisms of astrocyte calcium signalling are only recently beginning to unravel, however full comprehension of its nature compared to neuronal signalling is still in its infancy (Volterra et al. 2015; Bazargani & Attwell 2016; Savtchouk & Volterra 2018). Calcium waves have been observed in cultured astrocytes after stimulation by various methods, including application of glutamate (Innocenti et al. 2000), ATP (Guthrie et al. 1999), endothelin-1 (Venance et al. 1997), noradrenaline (Tordjmann et al. 1997), and mechanical stimulation by poking with a pipette tip (Lee et al. 2015). The mechanism of calcium wave propagation from the stimulated cell to adjacent regions has generally been identified to be from two potential pathways: 1) the autocrine/paracrine activation of metabotropic P2 purinergic receptors (Pascual et al. 2005), and/or 2) through the diffusion of inositol 1, 4, 5-trisphosphate (IP3) through open gap junctions and ionotropic P2 purinergic that connect adjacent astrocytes (Kaja et al. 2014) (Yamane et al. 2002). The exact interplay between the two mechanisms seems to depend on culture conditions and the ostimulating event (Scemes & Giaume 2007). For example, Salter and Hicks 1995, provided evidence of extracellular ATP activating metabotropic or ionotropic purinergic receptors, causing an elevation of intracellular calcium in astrocytes. Using whole patch clamp recording on wistar rat cultures, they showed that application of ATP led to an elevation of intracellular calcium, and release of gliotransmitters (Salter & Hicks 1995).

1.5. ATP and Purinergic receptors

A greater appreciation has been developing for the importance of ATP signalling in physiological and pathological brain function. As mentioned above, extracellular ATP activates the P2 purinergic family of receptors (Burnstock et al. 2010). There are two major groups of P2 receptors: P2X, which are ion channels, and P2Y, which are metabotropic G-protein coupled receptors (Bernstein et al. 1998; Burnstock et al. 2010; Pascual et al. 2016). P2X receptors are ionotropic with two transmembrane domains. There are seven cloned P2X subtypes; P2X1-7, which all respond to ATP as their endogenous agonist. P2X receptors act as cation channels and upon activation by ATP, allow the flow of sodium, potassium and calcium. This causes depolarization of the cell

membrane, which in turn can open calcium channels (Vizi et al. 2006; Suadicani et al. 2009). P2X1-6 are all very similar in structure while P2X7 has an elongated intracellular peptide sequence. When exposed to ATP it initially functions as the other P2X receptors, however if the ATP exposure is prolonged its pore enlarges and larger molecules can flow through.

P2Y receptors are G-coupled with seven transmembrane spanning domains. There are eight P2Y receptor subtypes that have been cloned; P2Y1, P2Y2, P2Y4, P2Y6 and P2Y11 through P2Y14 (Fam et al. 2003; Gallagher & Salter 2003; Puchałowicz et al. 2015). P2Y receptors respond to a more varied array of endogenous agonists, including ATP, ADP and even uridine nucleotides UTP and UDP. The strength of response to these agonists varies by receptor subtype, which is sometimes used for subtype identification. For instance, if a cell exhibits a physiological response to ATP and UTP, but not ADP then the responsible receptor is likely either P2Y2 or P2Y4. G-proteins utilized by P2Y receptors are Gi, Go, Gs, Gq/G11, G/G12 and Gi/Go (Centemeri et al. 1997; Gallagher & Salter 2003). Some P2Y receptor subtypes have specific G-proteins they associate with, but many can associate with multiple. For example, the P2Y2 receptor can activate Go, Gq/G11 and G12. Stimulation of these G-proteins by recombinant P2Y receptors can either activate phospholipase C (PLC) or adenylate cyclase, causing intracellular calcium release or changes in cAMP levels, respectively (Venance et al. 1997).

Extracellular ATP can activate calcium responses from astrocytes and is the primary signalling molecule in astrocyte communication (Guthrie et al. 1999; Anderson et al. 2004). In addition, ATP is involved in mediating the release of neurotransmitters through several different signalling mechanisms (Centemeri et al. 1997; Tang et al. 2015). ATP activation of P2X7 receptors, which are found in large numbers on astrocytes, can lead to the release of glutamate (Fellin 2009; Kang & Othmer 2009). In addition, the activation of several P2Y receptors, and, specifically, the P2Y1 receptor, can cause the release of glutamate from astrocytic vesicles in a PLC-mediated calcium-dependent manner (Burnstock et al. 2010). ATP activation on astrocytes can also cause the release of addition ATP, as mentioned above (Anderson et al. 2004). In this way, astrocyte activation can have a direct effect on the environment they encompass (Hashioka et al. 2014).

2. Aims of the study

The *in vitro* generation of astrocytes stem cells has reached a state where the cells can be considered for clinical applications. However, remaining research needs to work toward protocols that provide standardised sets of cells which capture the process of astrocytogenesis *in vitro*. To do this, the cell population will need to be characterised for: (a) Excess of positive and negative markers (b) for maturity - by using markers, and gene expression profiling which measure astrocyte at different stages of development (c) function - by functional assays like looking at calcium dynamics or receptor specific dynamics. To our knowledge, the field still lacks sufficient standardisation of the available protocols. The available protocols have drawbacks such as: (a) some of the protocols do not provide sufficient detail for reproduction, or deviate away from capturing astrocytogenesis (b) astrocyte purity and maturity is not comparable to that obtained with primary or in vivo astrocytes (c) there are technical issues that prohibit widespread use, even though the protocol may be suitable (e.g., long-term induction, or long term generation >100 days of astrocytes) and (d) the emerging astrocytes are often poorly characterised (e.g., are only stained GFAP), but hardly for maturity markers, regional identity, negative markers and additional astrocyte functional characterisation. For this reason, there was no protocol when this study was being conducted that was the gold standard for astrocytogenesis. As depicted in Table. 1 plethora of studies (16 at the time of the literature review) utilised ESC's, and verified the need for further protocol optimisation and for better characterisation and standardisation of the resultant cell types. The present work aims to contribute and reduce the time taken towards generation of astrocytes from stem cells. By using mouse embryonic stem cells (mESC), the developmental transition of astrocytes, similar to what is seen during gliogenensis *in vivo*, can be fully captured and assessed. Therefore, initially the work will focus on the question of how to generate astrocytes from embryonic stem cells. These generated cells will be characterised with respect to their phenotypic and genetic features. Subsequently, once characterised these generated astrocytes will be subjected to functional analysis via assessing their ability to generate calcium dynamics – observed via calcium imaging. Furthermore, the main pathway/s in which the generated astrocytes influence and govern calcium activity will also be tested across the developmental day *in vitro* (DIVs). Lastly, once characterised the generated astrocytes will be subjected to multiple isolation protocols, and characterised again post isolation. This is essential for future storage (creating a cell bank) and testing integration ability of the generated astrocytes in multiple cell assays.

3. Generation of astrocytes from embryonic stem cells

3.1. Introduction

Neurons have been for long the major neural cell type differentiated from stem cells. Plethora of developmental pathway based protocols have been put utilised to generate several functional neuronal subtypes ranging from cortical dopaminergic, cholinergic, GABAergic, glutamergic neurons, cerebellar purkinje neurons to spinal motor neurons (Peljto et al. 2010). The generation of subtypes of astrocytes from stem cells has been greatly limited due to lack of our understanding about their specification and consistent markers (Bayraktar et al. 2015). Also, there are no well described markers or assays to differentiate the subtypes of astrocytes (Imura et al. 2006; Bayraktar et al. 2015). Additionally, most of the studies reporting the generation of astrocytes rely on the expression of GFAP which is not ubiquitously expressed in all astrocytes (Eng et al. 2000). Studies done for establishing differentiation of stem cells towards astrocytes show a long culture time required for their acquisition of gliogenic potential (Krencik et al., 2011, Roybon et al., 2013, TCW et al. 2017). Although, these protocols have successfully generated astrocytes which closely resemble the *in vitro* counterparts, till date there is no well-defined and commodious protocol for the generation of well characterised astrocytes and their subtypes in a quick and efficient manner.

Reference	Cell Source	Supplements Used	Time Taken
Rajan and McKay 1998	ESCs	CNTF	-
Reubinoff et al 2001	ESCs	FGF2, EGF, BDNF	40 Days
Zhang et al 2001	ESCs	FGF2, EGF, BDNF, LIF	45 Days
Barberi et al 2003	ESCs	bEGF, EGF, N2, CNTF, PDGF	30 Days
Tabar et al 2005	ESCs	FGF, EGF, Nogging	56 Days
Uzzman et al 2005	Transgenic ESCs	EDGF, PDGF2, Laminin	20 Days
Beneviste et al 2005	Transgenic ESCs	EDGF, PDGF2, Laminin	20 Days
Johnson et al 2007	ESCs	Heparin, FGF2, BDNF, GDNF, cAMP	67 Days
Kamnasaran et al 2008	Transgenic ESCs	N2, B27, Heprin Suphate, EGF	35 Days
Asano et al 2009	NPC	bFGF, RA, LIF	-
Hui et al 2010	ESCs/iPSCs	RA, SHH, cAMP	90 Days
Emdad et al 2012	ESCs/iPSCs	SB43152, Noggin	37 Days
Gupta et al 2012	ESCs	B27, BMP2, BDNF	55 Days
Krencik et al 2012	ESCs/iPSCs	RA, FGF8, SHH, EGF, CNTF, LIF	90+ Days
Keugler et al 2012	ESCs	bFGF, EGF, N2, Heparin	49 Days
Juopperi et al 2012	iPSCs	bFGF	90 Days
Shi et al 2012	ESCs/iPSCs	-	45 Days
Shaltouki et al 2012	ESCs/iPSCs	bFGF, CNTF, BMP, Heregulin	37 Days
Espuny-Comacho et al 2013	ESCs/iPSCs	-	87 Days
Roybon et al 2013	ESCs/iPSCs	RA, BDNF, GDNF, SB431542, LDN193189, CNTF, FBS, bFGF	80 Days
Mormone et al 2014	iPSC	FGF2, EGF, CNTF, Noggin	35 Days
Muratore et al 2014	iPSCs	-	100+ Days
Palm et al 2015	iPSCs	SB-431542, N2, B-27, EGF, LIF, TGFB3, CHIR 99021, ascorbic acid, PMA	21 Days
Kleiderman et al 2016	ESCs	EGF, FGF, BMP4	45 Days
Zhou et al 2016	iPSCs	LDN193189, SB43152	30 Days
Santos et al 2017	iPSCs	Commerical cocktail supplmeneted with Noggin, PDGF, FGF2, N2, B27, LIF	42 Days
Sloan et al 2017	ESCs	-	172 Days
TCW et al 2017	NPC/iPSCs	Commercial cocktail	30 Days
Li et al 2018	Transgenic PSCs	DMH1, SB43, FGF2, EGF2, BMP4, CNTF	52 Days

Table 1: Studies which use stem cells to derive and differentiate astrocytes. The arrow indicates starting of the study to contribute towards standardisation of protocols.

3.1.1. EB's and spontaneous emergence of astrocytes

To mimic the *in vivo* mechanisms governing early neurogenesis, two major classes of protocols are utilised: an EB-based technique and a single cell monolayer-based method. The 3D aggregation system is thought to better maintain the "stemness" of stem cells and to allow better cell-to-cell and cell-to-matrix interactions (Sloan et al. 2017). Other vital considerations for improved neural cultures are media composition, exogenous growth factors or small molecules, and most importantly the timing of the procedure itself (Molofsky & Deneen 2015). Zhang et al 2001 was the first to develop a novel technique to isolate and culture human astrocytes in serum-free conditions, thus recapitulating the resting, non-reactive state normally observed in healthy astrocytes *in vivo*. The group differentiated 3D spheres, now known as Embryoid Bodies (EBs), in chemically defined medium containing FGF-2, which later form neural rosettes. By day 7, almost all EBs expressed neural progenitor cells and neural stem cells markers, confirmed by the expression of neural markers nestin. Subsequently the prolonged culture of the protocol

led to the development of GFAP positive astrocytes. Later other EB based differentiation studies were published (Reubinoff et al. 2000; Carpenter et al. 2001). In one of the protocols by Carpenter et al 2001, EBs were differentiated into neuronal progenitors in the presence of retinoic acid (RA) along with selective morphogens (Carpenter et al., 2001). All of the studies obtained populations with a wide panel of morphological characteristics, positive for neuronal and astrocyte progenitors and led to the usage of EB culture system *in vitro* to model developmentally relevant culture system to generate neuronal and astrocyte subtypes (Tabata 2015).

Astrocytes can also emerge spontaneously in cultures by the "spontaneous emergence approach". For example, human iPSC-derived NPCs have been differentiated toward various neuronal lineages such as cortical neurons (Shi et al. 2012; Chandrasekaran et al. 2016), and spinal MNs, where astrocytes and oligodendrocytes frequently appear as secondary by-products in these preparations, however, the efficiency is low and not reliable. A recent study showed the emergence of endogenous astrocytes from neuronal cultures via increased expression of the glial fibrillary acidic protein (GFAP), at day 100, with confirmation through the NanoString platform (Muratore et al. 2014). Other groups have also confirmed the emergence of astrocytes with long-term differentiation of hiPSCs-derived neural progenitors and primary stem cells (Shi et al. 2012; Espuny-Camacho et al. 2013). However, all of these protocols are complex in methodology replication and astrocytes that are produce have fewer functional properties such as: being immunoreactive (Roybon et al. 2013), reduced ability to form synapses (Boehler et al. 2008; Tyzack et al. 2016) than their *in vivo* counterparts.

3.1.2. Generation of astrocytes from stem cells

Recent advances in understanding the complex molecules involved in astrocytogenesis has enabled *in vitro* protocols to produce astrocytes efficiently from stem cells. Several studies have utilised embryonic and neural stem cells from a variety of species, ranging from human to mice, to mimic and confirm *in vivo* astrocytogenesis (Table 4) (Roybon et al 2017, TCW et al 2017). Nevertheless, replication of astrocytogenesis *in vitro* has shown to be more challenging than previously thought (Rajan & McKay 1998; Reubinoff et al. 2000; Zhang et al. 2001; Barberi et al. 2003; Tabar et al. 2005). The current challenge is to further clarify the developmental mechanisms of astrocyte generation and establish simple and efficient protocols to unravel complexity in astrocytes (Uzzaman et al. 2005; Johnson et al. 2007; Emdad et al. 2012; Juopperi et al. 2012). As differentiation of human embryonic stem cells to astrocytes is much more complicated compared with

mouse systems and current protocols for the generation of astrocytes require long-term cultures (Palm et al. 2015; Li et al. 2018). Thus, for studies and considering the limited time available to dully unravel the complex process of astrocytogenesis, astrocytes generated from murine stem cells are still the best approach. Here, we describe the derivation of astrocytes from mouse embryonic stem cells mESC to produce a protocol which contributes towards standardisation of protocols to generate astrocytes.

The derived protocol combines and alters two existing protocols from Peljto et al 2010 and Keugler et al 2012 to accelerate astrocytogenesis. The rationale behind using and coalescing these two protocols are the following: both protocols utilise mESCs and do not use and transgenic manipulation, Peljto et al 2010 does not use excessive morphogens – to induce semi-spontaneous emergence of desired cells, and neuralises (directs cells into neurons) mESCs in short timeframe compared to other published protocols using mESCs (Ban et al 2001), and Keugler et al 2012 protocol uses 3D aggregation method which closely mimics *in vivo* astrocyte development. Further to this, both protocols use key factors (morphogens) such as retinoic acid (RA), heparin and N2, at crucial time points to develop desired cells. In addition to all of the above, Keugler et al 2012 develops astrocytes which are also GFAP negative in expression. Therefore, for the acceleration of neurogenesis and development of heterogeneous population of astrocytes, these two protocols were altered and used.

3.2 Method and Materials

3.2.1. Materials

Culture Materials	Catalog Number	Provider
DMEM (Dulbecco's Modified Eagle Medium)	11965092	Thermo Fisher
Advance DMEM/F-12	12634028	Thermo Fisher
Neurobasal	21103049	Thermo Fisher
DPBS	A1285801	Thermo Fisher
Knock out serum (KSR)	17502048	Thermo Fisher
N2 Supplement (100X)	17502048	Thermo Fisher
Fetal Bovine Serum (FBS)	F2442	Gibco
Pen/Strep	15140	Invitrogen
L-Glutamic Acid	G1624	Sigma
ß-Mercaptoethanol	1350	Gibco
Leukemia inhibitory factor (LIF)	L5158	Sigma
Retanoic Acid (RA)	302794	Sigma
Heparin	H3149	Sigma
Bovine serum albumin (BSA)	A2058	Sigma
Laminin	L2020	Sigma
Gelatin	G1393	Sigma
Triton-X100	9002931	Sigma
Formaldehyde (PFA)	130525894	Sigma
Hoechst 33342	H3570	Molecular Probes
Trypsin Solution	59427C	Thermo Fisher
Taq DNA Polymerase Kit	201203	Qiagen
Taq PCR Core Kit	201203	Qiagen
Taq PCR Master Mix	201203	Qiagen
Rnease Mini Kit (RNA Isolation)	74104	Qiagen
Primers (see primer table for primer list)	3222431	Thermo Fisher
Agarose	A6877	Sigma
DNA Ladder	15628	Invitrogen
Loading Dye	18116	Invitrogen
SYBR Green Master Mix	14928100	Thermo Fisher

Table 2: Materials used for generation of mESCDA

3.2.1. Maintenance of murine embryonic stem cell line

The murine embryonic stem cell (mESC) (line derived from Mus musculus, strain 129) were used for all of the experiments.

Media Recipe

mESC media

- DMEM
- 10% Foetal bovine serum (FBS)
- 1% Penicillin/Streptomycin
- 1% L-glutamine
- 100uM 2- Mercaptoethanol
- 1000units/mL - Leukaemia Inhibitory Factor

Step by Step method for maintenance and passaging

1. T-25 flasks were coated with 0.1 geltain (diluted in PBS) 2 hours before experimentation
2. Gelatin coated flasks were rinsed with 5mL of PBS twice
3. When the mESC reached confluence, 2mL of Trypsin/EDTA was added and cells were gently agitated the cells until they formed a suspension
4. After 2 minutes, 3 mL of mESC media was added to neutralise the trypsin
5. Cells were transferred to a 15mL falcon and centrifuged for 5 minutes at 180 Rcf and acceleration of 4.
6. Supernatant was aspirated and mESC were resuspend in the pellet in an appropriate volume for the split ratio of 1:8
7. An even suspension was ensured by gently pippeting up and down, five or six times
8. Media was changed every other day and flask assessed every day for confluency

3.2.2. Incubation and generation of embryoid bodies – a push towards neural lineage

Cultures of mESC were used when they reached 80% confluency, with a serum based media containing DMEM and FBS with 1uM of LIF to prevent spontaneous differentiation.

Media Recipe

Aggregation Medium (ADFNK)

- Advanced DMEM/F12 – Neurobasal (1:1)
- 10% Knockout Serum Replacement
- 1% Penicillin/Streptomycin
- 1% L-Glutamine
- 100uM 2-Mercaptoethanol
-

Step by step method

1. Confluent flask of mESC cells (around 80%) was taken and medium aspirated from the flask.
2. The flask was then washed in 5 ml PBS.
3. PBS was aspirated and cells in flask were exposed to 2 mL Trypsin/EDTA for 2 minutes
4. Flask was gently agitatated until top layer of mESC cells were detached
5. Trypsin/EDTA was inactivated with 3 mL mESC media (See above) and the lifted cells were transferred to a 20mL universal tube.
6. Cells were centrifuged for 5 minutes at 180g
7. Supernatant aspirated and cells were resuspend cells in 2mL ADFNK medium
8. Cells counted haemocytometer
9. Cells were seeded in mESC cells in ADFNK medium, at a density from 2 x 10^4 to 2.5 x 10^5, (recommended 50,000 cells/mL) in either non-tissue culture treated 6-well plates or petri dishes. For a petri dish, 500,000 cells per 10 mL is sufficient.
10. Cells were incubated at 37°C for 2 days, by which time aggregates were formed and found to be floating in the medium.

11. After 2 days EBs were exposed to fresh ADFNK media containing either containing retinoic acid (RA) at 1uM or no retinoic acid (depending on the methodology required and tested, see results). Media was also changed to remove non-EB formed cells and any debris
12. At day five, if RA was added it was removed and fresh ADFNK media was added by transferring medium containing EBs to a 15 mL centrifuge tube. The EBs were allowed settle under gravity.
13. The supernatant was aspirated and EBs were gently re-suspend in fresh ADFNK media and transferred to petri dish for further incubation
14. At DIV 6 EBs were ready for further experimentation

3.2.3. Differentiation of mESC into Astrocytes (mESCDA) – single cell and EB based methods

The process of differentiation tried to recapture astrocytogenesis. For differentiation of astrocytes, both a single cell monolayer and EB based technique was used (Chandrasekan et al 2016). Both methodologies, employed an altered astrocyte differentiation media (Keugler et al. 2012).

Media Recipe

<u>mESCDA media</u>

- ADMEM/F12
- 2% FBS
- 1% N2 (x100)
- 1% L-glutamine
- 1% Pen/Strep
- 100uM β-mercaptoethanol
- 50ug/mL heparin

Step by step single cell method

1. Laminin coated glass coverslips for 12/24 well plates were prepared by adding 2μg/cm^2 laminin in PBS for 2 h at 37°C
2. After 2 hours, coverslips were washed 2x with PBS and coverslips incubated overnight

3. Generated DIV 6 EBs were removed from plates and suspended onto 15mL falcon.
4. Media was aspirated and EBs were suspended in Trypsin/EDTA and incubated for 60 seconds to allow EBs to dissociate
5. To neutralise the trypsin, cells were suspended in mESCDA media
6. Cells were the passed through 70 µm cell strainer to ensure efficient removal of EBs which were not properly dissociated
7. Cells were centrifuged at 180 Rcf for 5 minutes
8. Supernatant was removed and cells were re-suspended in mESCDA media
9. The incubated coverslips were washed 2x with PBS
10. Cells were plated at a density of 50,000 cells/cm2 in 12/24 plates coated with 2µg/cm^2 laminin

Step by step EB based method

1. Similar to above, laminin coated glass coverslips for 12/24 well plates were prepared by adding 2µg/cm^2 laminin in PBS for 2 h at 37°C
2. After 2 hours, coverslips were washed 2x with PBS and coverslips incubated overnight
3. Generated DIV 6 EBs were removed from plates and suspended onto 15mL falcon.
4. Media was aspirated and EBs were re-suspended in mESCDA media
5. 10-20 intact EB's were directly plated in 12/24 plates coated with 2µg/cm^2 laminin

3.2.4. Immunocytochemistry and image acquisition

Images were taken using an Axio Imager microscope (Zeiss, Germany).
Separate digital images (red 568nm, green 468nm, blue 350nm - RGB) of astrocyte stains (green and red light) and DNA (Hoechst 33342) were captured with a ×20 objective (1040x1388 pixels) from the same nine non-overlapping microscopic fields per well AxioCam CCD digital camera (Carl Zeiss) mounted to an inverted AxioVert 135 Carl Zeiss epifluorescence microscope. Focus was adjusted for each new field, but fluorescent illumination and exposure were kept constant to improve consistency during analysis. Scale bars were calibrated using AxioVision software (release 4.6.3; Carl Zeiss). Files were saved in tagged image file format (.tif) and JPEG (.jpeg).

Antibody	Type	Concentration	Source
GFAP	Chicken Polyclonal	1:500	Aves
ALDH1L1	Rabbit Polyclonal	1:100	Abcam
S100β	Rabbit Polyclonal	1:250	Abcam
Nestin	Rat Monoclonal	1:500	Santa Cruz
P2X7	Rabbit Polyclonal	1:250	Alomone
P2YR1	Rabbit Polyclonal	1:250	Alomone
488	Anti-Rabbit	1:500	Alexa Fluor
594	Anti-Chicken	1:500	Alexa Fluor
594	Anti-Rat	1:250	Alexa Fluor
594	Anti-Mouse	1:500	Alexa Fluor

Table 3: Antibodies and their concentrations used for immunohistochemistry

Primary antibody process

1. Remove the media in which cells were incubated in and wash coverslips with PBS x 3
2. Coverslips were incubated with 1 ml of paraformaldehyde (PFA) and left to incubate at room temperature for 30 mins
3. Coverslips were washed again three times with PBS
4. Once washed 400ul of Triton was added. (Note that Triton is x100 concentrated (we need around 0.02% of triton - therefore add 200ul of triton in 10ml of PBS)
5. Samples were placed on the rocker for 10 mins and washed again with PBS three times.
6. 10% Goat serum was prepared. (2.5ml of goat serum in 25ml of PBS) and coverslips were incubated for 2 hours.
7. Desired antibodies (Table 2) in 10% goat serum
8. Petri dishes were prepared. Briefly: cut out a circle of tissue and place it inside the petri dish. Slightly wet the circle of tissue; to keep it stabilised in the Petri dish, and cover the circle of tissue with parafilm to create a hydrophobic later. Label the petri dish.
9. The antibodies were made at the desired concentrations (Table 2)

10. Using fine tip forceps, coverslips were removed from the well plate and placed it on the earlier prepared petri dish
11. Antibodies was directly applied on the coverslip - add around 150ul.
12. Samples were incubated overnight in the fridge.

Secondary antibody process

1. Fresh 10% goat serum was prepared
2. Petri dishes with primary incubated coverslips were washed with PBS
3. Once washed 150ul of secondary antibodies (Table 2) was added onto the coverslips
4. The coverslips were incubated secondary antibody for 2 hours at room temperature - the samples are wrapped in foil to prevent any light coming in
5. Hoechst was prepared at the concentration of 1:1000
6. After secondary incubation, coverslips were washed 3 times with PBS.
7. After washings, Hoechst was added and coverslips incubated for 1 mins and washing process was repeated
8. Microscope slides were washed with 70% ethanol to clean and remove debris
9. Once microscope slides were cleaned, a small drop (10ul) of mounting media was added in the middle of microscope slide
10. Coverslips were removed with fine tip forceps and placed onto the microscope slide
11. Coverslips were left to dry - nail polish around the coverslip was added to prevent the coverslips from moving around
12. Samples were stored in slide box in the fridge in the dark for analysis

3.2.5 Image analysis for quantification and co-localisation of cell body and nuclei

All of the image analysis was initially performed manually, utilising ImageJ (NIH - National Institutes of Health), and later were performed on bespoke algorithms using MATLAB. For analysis of cell body and nuclei, images were split into individual channels from RGB (red 568 nm and green – cell body 488 nm, Blue – Nuclei (Hoescht). To analyse these images, we developed a workflow (See appendix). Initially, the images were thresholded utilising the Otsu method of thresholding (Vala & Baxi 2013) to remove any potential uneven illumination. Additionally, debris and unwanted cellular artefacts were also removed. Finally, original image was overlaid on top of the altered image and Pearson's correlation analysis was performed to assess its distance to the

original image. The altered image was then analysed for astrocyte stain positive cells and percentage area covered by astrocyte positive cells (see Appendix). Co-localisation analysis was performed on co-localised astrocyte positive stains manual counting. Percentage co-localised cells was assessed by measuring the number of co-localised cells/number of total cells multiplied by 100.

3.2.6. Reverse Transcription Polymerase Chain Reaction

Total RNA was isolated using the QIAGEN RNeasy Kit according to the manufacturer's instructions (see step by step below). Eluted RNA was measured in a spectrophotometer and purity ensured by 260/280 nm ratio of greater than 1.95 for all samples. Each RNA sample was treated with DNase I from the RNeasy Kit, to eliminate any genomic contamination. The QIAGEN QuantiTect Reverse Transcription Kit was used to transcribe 1µg of RNA to cDNA. PCR was conducted with the DreamTaq Green PCR Master Mix (ThermoFisher). The protocol consisted of an initial denaturation step at 95°C for 2 min and 35 cycles of: i) denaturation step 30 s at 95°C, ii) annealing step 30 s at 55°C and iii) extension step 1 min at 72°C. A final extension step of 5 min at 72°C was conducted at the end. Separation of PCR products was performed in a 1% agarose gel via electrophoresis and visualization was done with SYBR safe DNA gel stain (ThermoFisher). Digital photographs of the gels were taken with the Syngene U Genius 3 System (SLS) and cDNA levels relative to the housekeeping gene Gapdh were calculated using PCR band densitometry (See Appendix).

Gene	Ref Sequence	Forward Sequence	Reverse Sequence
ALDH1L1	NM_027406	5'-CTCGGTTTGCTGATGGGGACG-3'	5'-GCTTGAATCCTCCAAAAGGTGCGG-3'
AQP4	NM_009700	5'-GCTCAGAAAACCCCTTACCTGTGG-3'	5'-TTCCATGAACCGTGGTGACTCC-3'
GAPDH	NM_008084	5'-GCCTCGTCCCGTAGACAAAATGGTG-3'	5'-GTAGTTGAGGTCAATGAAGGGGTCGTTG-3'
GFAP	NM_001131020.1	5'- CCTGAGAGAGATTCGCACTCAATACG -3'	5'- CTCTAGGGACTCGTTCGTGCC -3'
GJB6	NM_001010937	5'-CGTACACCAGCAGCATTTTCTTCC-3'	5'-AGTGAACACCGTTTTCTCAGTTGGC-3'
Iba1 (Aif1)	NM_019923.4	5'-AGCCTGAGGAGATTTCAACAGAA-3'	5'-TTTGGACGGCAGATCCTCAT-3'
IL-6	NM_031168	5'-CCTCTGGTCTTCTGGAGTACCATAGC-3'	5'-GGAGAGCATTGGAAATTGGGGTAGG-3'
iNOS	NM_010927	5'-TTGCCACGGACGAGACGGATAGG-3'	5'-GGGGTTGTTGCTGAACTTCCAGTC-3'
IR3R2	NM_019923.4	5'-ACCTGGTCTAAAGAGTCCCCC-3'	5'-TGCCCAGCATTTACAGGCAT-3'
S100ß	NM_009115	5'-GGTTGCCCTCATTGATGTCTTCCAC-3'	5'-CTTCCTGCTCCTTGATTTCCTCCAG-3'
Nanog	NM_028016.2	5'-CAGAAGGGCTCAGCACCAGTG-3'	5'-CAAGTTGGGTTGGTCCAGGTCTG-3'
Nestin	NM_016701	5'-CTGGAAGGTGGGCAGCAACT-3'	5'-ATTAGGCAAGGGGGAAGAGAAGGATG-3'
Olig 2	NM_016967	5´-CCCTGAGGCTTTTCGGAGCG-3´	5´-GCGGCTGTTGATCTTAGACGC-3´
P2YR1	NM_008772.5	5´- TGAATTTGCGAGCACGGTTG-3´	5´- CTCACTCAGGTGGCACACAC-3
P2XR7	NM_011027.3	5´-CGGTGTGTTTCCTTTGGCTG -3´	5´-GACGGTGCCATAATTCGTGC -3´

Table 4: RT-PCR: Primers used for each tested gene

Primer design and optimisation

Genes were chosen for validation from categories that were enriched in both the symptomatic and the late-stage time-points. Primers were designed for genes of interest using the Primer Blast tool from NCBI (http://www.ncbi.nlm.nih.gov/tools/primer-blast/) (Table 3). Primers were designed to produce amplicons of 50- 150bp in length and to overlap an exon boundary. If an exon boundary could not be overlapped controls were used which had received no reverse transcriptase enzyme during cDNA synthesis, thus checking for the presence of genomic DNA. Primers were ordered from Sigma Aldrich at a synthesis scale of 0.025µmol and desalt purification and were kept at a stock concentration of 100µM at -20°C according to manufacturer's instructions.

Purification of Total RNA from Animal Cells using Spin Technology

1. Buffer RPE is supplied as a concentrate. Before using for the first time, 4 volumes of 100% ethanol was added as indicated to obtain a working solution
2. Cells were harvested via cell scraping (see chapter 4)
3. Cells were disrupted by adding 600 µl of supplied Buffer RLT to lyse the cells

4. Lysate was pippeted directly into a QIAshredder spin column (supplied) and centrifuge for 2 min at full speed at a table top centrifuge
5. 600mL of ethanol was added to the lysate and mixed well by pippeting
6. 700µl of the sample, including any precipitate that may have formed, was collected to an RNeasy spin column placed in a 2 ml collection tube (supplied).
7. Lid was closed gently, and the spin column was centrifuged for 15 s at ≥8000 x g (≥10,000 rpm). Flow-through was discarded post centrifuge.
8. Post centrifuge, the column was collected and 700µl Buffer RWI was added and centrifuged at 15 s at ≥8000 x g (≥10,000 rpm)
9. After centrifugation, spin column was removed from the collection tube and new collection tube was used
10. 500µl of Buffer RPE was added to RNeasy spin column and centrifuged for 15 s at ≥8000 x g (≥10,000 rpm) – this was repeated again
11. The RNeasy spin column was placed in a new 1.5 ml collection tube (supplied).
12. 30–50 µl RNase-free water directly added to the spin column membrane and centrifuge for 1 min at ≥8000 x *g* (≥10,000 rpm) to elute the RNA
13. Eluted RNA was measured by NanoDrop™ 2000/2000c Spectrophotometer (Thermo)

Reverse Transcription with Elimination of Genomic DNA for PCR

1. Genomic DNA elimination reaction was prepared by mixing 2µl of supplied gDNA Wipeout Buffer, with 1µg of RNA and RNAse free water with total volume of 14µl
2. The reaction was incubated for 2 min at 42°C. Then place immediately on ice
3. Reverse-transcription reaction components were prepared by combining supplied 1µl Quantiscript Reverse Transcriptase, 4µl Quantiscript RT Buffer, 1µl RT Primer Mix
4. Template RNA from step 1 (14 µl) was added to component transcription master mix
5. Using a thermal cycler, the cDNA was made by incubating the prepared sample for 15 min at 42°C
6. Then the thermal cycler was switched to 95°C for 3 min at to inactivate Quantiscript Reverse Transcriptase reaction
7. Samples were stored at –20°C for further experiments

Preparation of PCR mixture

1. Thermo Scientific™ DreamTaq™ Green PCR Master Mix (2X) was used to prepare PCR mixture
2. 25µl of Green PCR Master Mix was added with 1µl of forward primer, 1µl of reverse primer, 10µl of template DNA and nucleus free water to make up final solution of 50µl
3. Sample was gently vortexed and PCR was performed on a thermal cycler for denaturing, primer annealing, extension and final extension steps

- Initial denaturation step for 3 minutes at 95°C with 1 cycle
- Denaturing step for 30 seconds at 95°C
- Annealing step for 30 seconds for primer melting temperature of 65°C
- Extension step for 30 seconds at 72°C
- These steps were performed at 35 cycles
- Final extension step for 15 minutes at 72°C

Agarose gel electrophoresis

Agarose gel electrophoresis was used for the separation of DNA fragments according to their size in an agarose gel matrix. This method was employed to confirm the specificity of amplified PCR products as well as for restriction analysis of expression and reporter DNA constructs.

1. Agarose gel density of 1-2% agarose was prepared by melting agarose in 100 ml of TBE buffer
2. 5 µl (0.5 µg/ml) of ethidium bromide was added to the agarose to stain the DNA fragments.
3. The resultant solution was poured in an electrophoresis chamber.
4. Samples (PCR products and DNA ladder) were loaded into the gel pocket
5. Electrophoresis was carried out at 100 V for approximately 1 hour.
6. The Invitrogen DNA ladder (Invitrogen) was used to verify the size of the separated DNA fragments.
7. DNA samples were visualised using Syngene U Genius 3 System (SLS) and cDNA levels relative to the housekeeping gene Gapdh were calculated using PCR band densitometry

2.2.7 Statistical Analysis

Experiments with immunofluorescent labelling and PCR were performed in triplicates. In each experiment 3 glass coverslips for each timepoint (7, 14, 21 and 28 DIV) were cultured and fixed and 9 images were collected from each glass coverslip (27 images were analysed per timepoint per experiment). Immunofluorescence and gel analysis was performed using bespoke MATLAB algorithms (see appendix) and published algorithms via Image J. Furthermore, to confirm algorithm specificity gel densomitary for gel electrophoresis, and cell profiler for immunocytochemistry was used (Livak et al., 2001). Data are presented as means +/- SEM and the statistical differences were tested by Unpaired T-Tests, ANOVA with Bonferroni's Multiple Comparison post-hoc or Mann-Whitney tests where appropriate, using GraphPad Prism 6.0 (Graphpad Software, La Jolla, CA). Statistical significance was assumed when $P<0.05$, and was indicated by an asterisk on the respective data point in figure. Two asterisks indicated $P<0.01$ and three $P<0.001$.

3.3. Results

3.3.1 Critical conditions for the development of astrocytes from mouse embryonic stem cells

The conditions for generating and culturing stem cells to develop astrocytes in vitro show a high degree of variability. Limitations such as growth factor concentration and combination, incubation period, and type of surface substrate used are all factors influencing the development of cells (Falsig et al. 2004; Krencik & Zhang 2011). These limitations could be overcome by identifying optimal methods which best mimic astrocyte development occurring *in vivo* (Molofsky & Deneen 2015; Tabata 2015). Derived mouse embryonic stem cells (mESC) were initially subjected to different culture conditions: spontaneous emergence, semi-directed, 3D aggregation, or mono-layer methodologies, to identify the best approach for generating astrocytes (mESCDA) (Carpenter et al. 2001; Chandrasekaran et al. 2016).

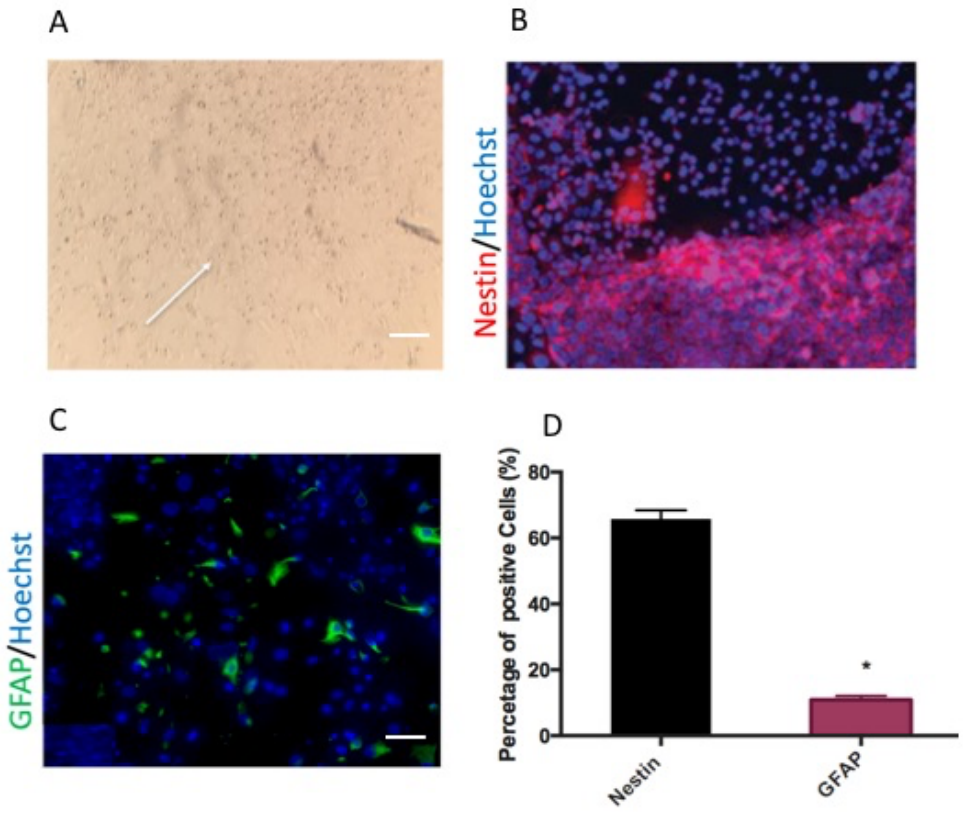

Figure 4: Monolayer methodology for astrocyte development. (A) Single cell seeding of mESC for astrocyte development failed to form clusters required. (B) Nestin stain was used for cell immaturity and immunoflouresence show attached cells are nestin postive (C) GFAP was used to confirm astrocyte presence and GFAP positive cells are seen - however they sparsely labelled. C: Analysis reveals attached cells unclustered cells are

significantly postive for nestin instead of GFAP. Cultures have been counterstained for cell nuclei marker H- 33342 (blue stain). Scale bar = 20μm. All data are expressed as mean ± SEM from three separate experiments, *P < 0.05, **P < 0.01, ***P < 0.001) from Unpaired T statistical test.

Each method tested used a reformed version of established protocols from Peljto et al 2010, and Keugler et al 2012 (Peljto et al. 2010; Keugler et al. 2012). The expression level of astrocyte marker GFAP, via immunofluorescence, was used to observe the emergence of astrocytes and also used to confirm the endpoint for each method (Carpenter et al. 2001). Firstly, the mono- layer method was implemented (Fig.4). The mono-layer method followed 2:3:1 neuralisation protocol, which generated spherical embryoid bodies (EB) (Asano et al. 2012; Peljto et al. 2010). 650,000 cells/ml were dissociated (via trypsin) from generated EB's and plated onto laminin- coated coverslips - which contained heparin rich astrocyte media altered from Keugler et al 2012. Assessment of cultures at DIV 28 revealed poor attachment of neuralised mESC to the coverslips (Fig.4A - white arrow). The single cell suspension failed to form clusters required for astrocyte emergence and development (Rujano et al. 2004). Almost all cells expressed high levels of the neural stem cell marker nestin (Fig.4B-4D <65.77% ± 4.31%, $p<0.05$) and held neurogenic potential, this was further confirmed lower than the expected expression of GFAP (Fig.4B-4D <10% ± 1.03%) (Conti et al. 2005). This subsequently led to using 3D aggregation methodology (direct seeding of EBs) for subsequent experiments (Santos et al. 2017).

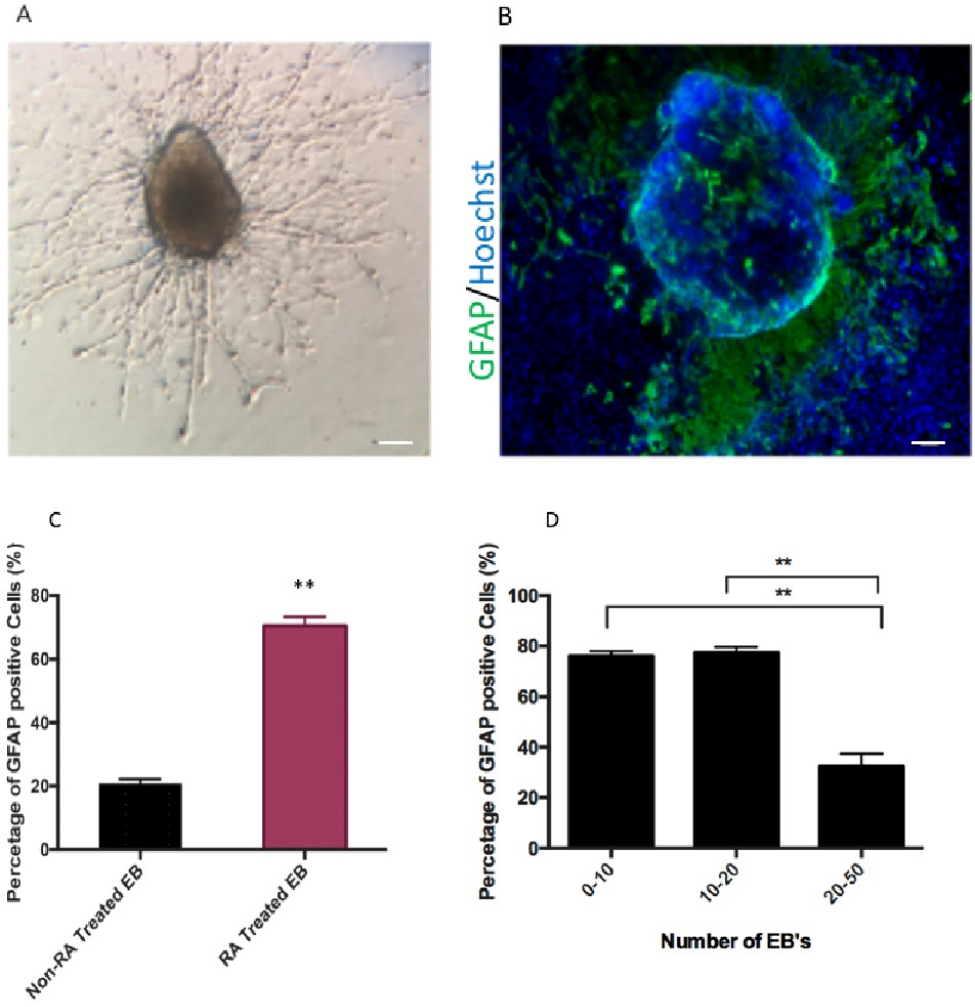

Figure 5: Semi Directed approach leads to mESCDA. Brightfield (A) and GFAP stained image (B) of plated Embryoid Body (EB's). The protrusion and extension of its processes and abdication of cells astrocytes from EBs can be seen. (C) Comparison between RA treated and non-RA treated reveals a significant increase in GFAP positive cells in RA treated cells. Cultures have been counterstained for cell nuclei marker H- 33342 (blue stain). Scale bar = 50µm. All data are expressed as mean ± SEM from three separate experiments, *P < 0.05, **P < 0.01, ***P < 0.001) from ANOVA with Bonferroni's Multiple Comparison post-hoc or Mann-Whitney tests.

The 3D aggregation method contained 2 conditions: 1) following 2:3:1 neuralisation protocol, which contained retinoic acid (RA) – semi-directed approach (Fig.5) (Shi et al. 2012; Peljto et al. 2010) and 2) removal of retinoic acid (RA) from neuralisation protocol – spontaneous emergence approach (Fig.5) (Carpenter et al. 2001; Reubinoff et al. 2001; Peljto et al 2010). Both conditions generated spherical embryoid bodies (EB), which were directly seeded onto laminin-coated coverslips (Fig.5A). The generated EBs attached to the surface and extended protrusions in each condition (Fig.5A). These protrusions formed a scaffold which allowed EBs to anchor (Goh et al 2013). Immunostaining at DIV28 showed GFAP positive astrocytes to emerge from EBs (Fig.5B). The semi-directed approach, which contained RA, produced significantly more GFAP positive cells (Fig.5C. 71.22% ± 8.11% $p<0.05$) compared to the spontaneous approach (Fig.5C 21.42% ± 6.21%). Based on these results, all of the experiments performed later for this study were carried out using direct EBs seeding method in heparin rich astrocyte media. Next, it was essential to determine the suitable number of EBs which would allow the successful and accelerated generation of mESCDA (Keugler et al 2012). Low (0-10), medium (10-20) and high (20-50) density of EBs were plated onto laminin-coated coverslips. Assessment of GFAP positive stain at DIV 28 revealed high-density EBs lead to a significantly reduced number of GFAP positive cells (Fig.5D 30.12% ± 4.41% $p<0.001$) when compared to low (0-10) and medium density (10-20). No significant difference was observed between low (Fig.5D 77.11% ± 1.13%) and medium (Fig.5D 79.01% ± 1.85%) EB numbers. Therefore, to maximize astrocyte development and provide uniformity in methodology, subsequent experiments were performed on medium density EBs, as it provided a slightly higher number of GFAP positive cells.

3.3.2. Rapid generation of mESCDA and genetic analysis of differentiated cells

After having established the protocol necessary for mESCDA (Fig.5A), temporal mRNA marker expression patterns in cell populations were analysed by reverse transcriptase-PCR. Migrating cells on the laminin-coated coverslips were harvested via cell scraping methodology (see chapter 4) and total RNA was extracted and screened for the genetic expression of markers was assessed temporally (DIVs 7-28) post seeding (Cahoy et al. 2012) (Table 1). Firstly, stem cell pluripotency gene, Nanog was assessed. Nanog expression was at its highest at DIV 7 (Fig.5C 13.92% ± 1.86%, N=3), with a significant downregulation at DIV 28 (Fig.5C 2.77% ± 2.6%, N=3), indicating the limited presence of stem cells amongst the generated astrocyte population as the cultures progress temporally. Additionally, there was absence of neural progenitor gene Nestin (Cho et al. 2013), microglial marker IBA1 (Hopperton et al. 2018) and oligodendrocyte gene Olig-2 (Zhou & Anderson 2002) at DIV 7 or later, suggesting absence or non-detectable presence of neural progenitors, and macroglial cells during the EB seeding/astrocyte induction phase of protocol.

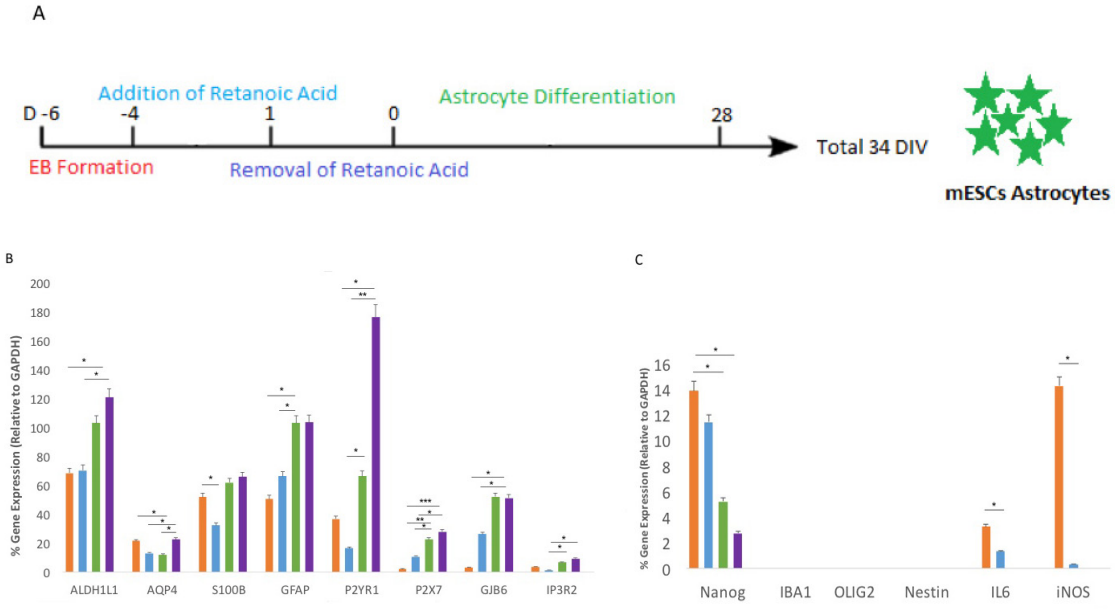

Figure 6: Rapid generation of non-proliferating, mature astrocytes from mESC. (A) Heterogeneous populations of mESCDA were generated from murine embryonic stem cells (mESC) in the presence of RA. EBs were generated and plated in the presence of RA, N2 and Heprain on laminin coated coverslips produced heteregenous populations of astrocytes. (B,C) Expression of genes of mESCDA across DIVs (from DIV 7-28) measured by PCR. Data are given in percent expression relative to the housekeeping gene

Gapdh. (C) Nestin, Olig2 (oligodendrocyte lineage transcription factor; neuroectodermal marker), IBA1 and Nanog were used as other cell markers (B) GFAP (glial fibrillary acidic protein), S100β (S100beta), AQP4 (aquaporin), EAAT2 (Slc1A2, glutamate transporter), and ALDH1L1 (aldehyde dehydrogenase) were used as astrocyte markers. All data are expressed as mean ± SEM from three separate experiments, *P < 0.05, **P < 0.01, ***P < 0.001) ANOVA with Bonferroni's Multiple Comparison post-hoc tests.

Astrocytic markers, GFAP (Eng et al 2000), S100β (Pinto et al 2000), ALDH1L1 (Cahoy et al. 2008), and AQP-4 (Szu & Binder 2016), were also investigated. ALDH1L1 is a pan-astrocytic marker and an early marker of astrocyte maturation (Eng et al 2001). Analysis revealed a significant ($p<0.05$) upregulation of ALDH1L1 from DIV 7 (Fig. 6B 67.5% ± 3.6%, N=3) to DIV28 (Fig.6B 120.7% ± 27.5%, N=3,). GFAP, an established astrocytic marker, was also upregulated between DIV 7 (Fig.6B 53% ± 11.9%, N=3) and DIV 28 (Fig.6B 102.9% ± 28.2%, N=3). In contrast, S100β (Fig. 6B) and AQP-4 (Fig. 6B) exhibited aberrant expression patterns, with the highest expression at DIV 28. Analysis of S100β revealed the characteristic downregulation of the gene at DIV 14, as its main role switches from a GFAP conformation regulator to a calcium-binding protein (Fig.6B from 32.3% ± 2.04% to 65.9% ± 3.78%, N=3). AQP-4, a water channel protein, analysis revealed early expression at DIV 7 (Fig.6B 21.62% ± 2.9%, N=3), with a significant downregulation at DIV 21 (Fig.6B 12.04% ± 2.1%, N=3),, and a significant upregulation at DIV 28 (Fig.6B 22.73% ± 3.1%, N=3), similar to what is reported *in vivo* (Fallier-Becker et al 2014).

Purinergic receptor specific markers P2YR1, P2X7, endogenous calcium mediating receptor marker IP_3R_2 (Hamilton et al. 2008) and connexing - Cx30 (GJB6) (Pannasch & Rouach 2013) were also examined. Expression of these genes was upregulated throughout temproally. Differences between DIV 7/DIV14 and DIV 28 were statistically significant between of: P2YR1: (At DIV 7 Fig.6B 36.81% ± 3.01%, N=3 - DIV 28 Fig.6B 176.27% ± 13.11%, N=3, $p<0.05$) P2X7: (Fig.6B At DIV 7 Fig. 2.27% ± 0.88%, N=3 - DIV 28 Fig.6B 27.93% ± 4.12%, N=3, $p<0.001$) IP3R2: (At DIV 14 Fig.6B 1.38% ± 0.38%, N=3 - DIV 28 Fig.6B 9.39% ± 1.91%, N=3, $p<0.05$) and GJB6: (At DIV 7 Fig. 6B 3.40% ± 1.21%, N=3 - DIV 28 Fig.6B 51.16% ± 10.29%, N=3, $p<0.05$).

3.3.3. Immunocytochemical phenotyping of mESCDA

A time course study of the expression of established astrocytic proteins, using immunocytochemistry was also performed. Since a single positive marker, such as GFAP, is not sufficient to characterise the extent of astrocyte differentiation, select astrocytic markers were used: GFAP (Fig.7), S100β (Fig.11) and ALDH1L1 (Fig.13) and astrocyte negative marker Pan-neuronal was used (Fig. 8).

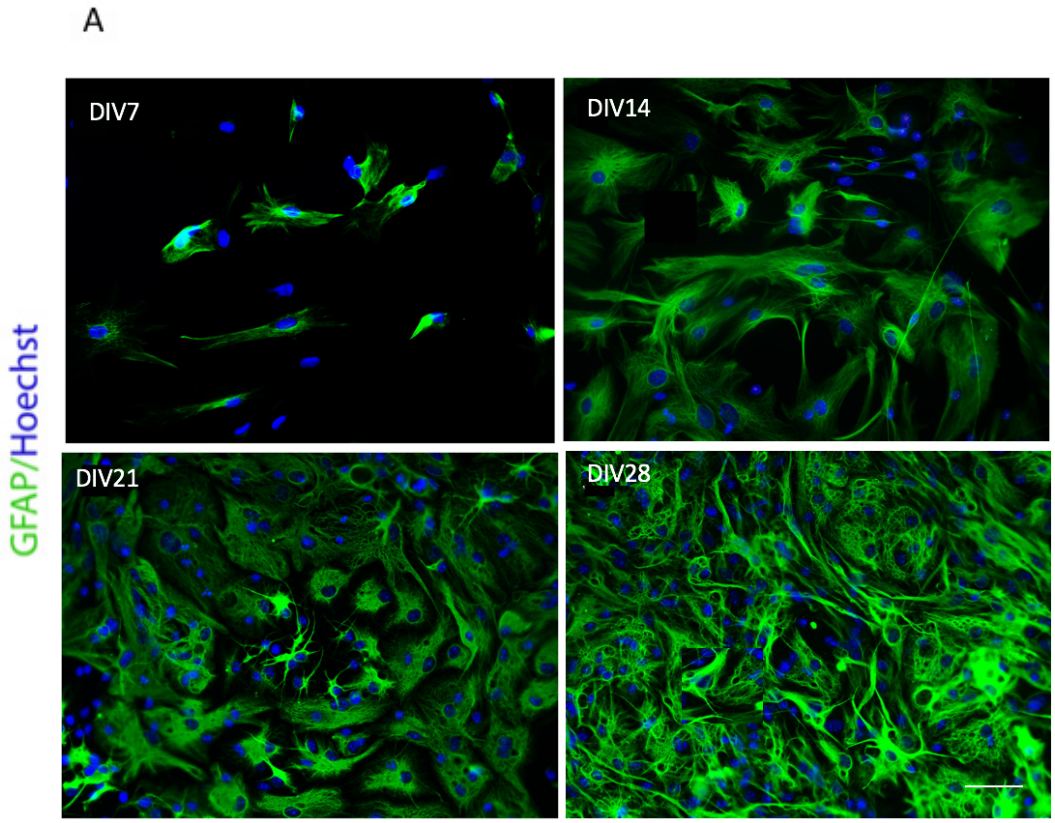

Figure 7: Immunocytochemical phenotyping of mESCDA. (A) DIV 7-28 fluorescent images of astrocytes RA inducted from mESC, labelled for established astrocytic marker GFAP. Cultures have been counterstained for cell nuclei marker H- 33342 (blue stain). Scale bar = 20μm.

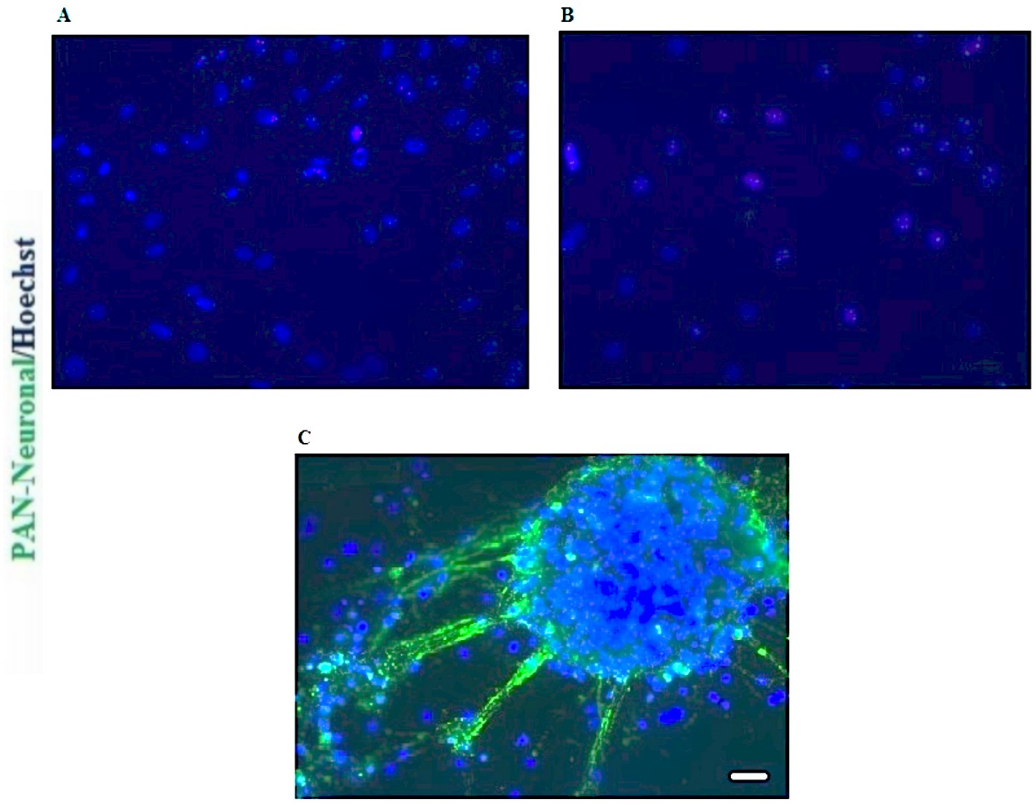

Figure 8: Cells negative for neurons: Cells were immunostained at DIV 28 for neuronal markers. No neurons were visible when cells were stained for pan-neuronal (A) (left panel) and nestin (B) (right panel). (C) Experiment performed on a neuronal protocol from Peljto et al. 2010 positively stained for pan-neuronal (mature neurons). Nuclei were counterstained with Hoechst (Blue) with H-33342. Scale bar = 50µm.

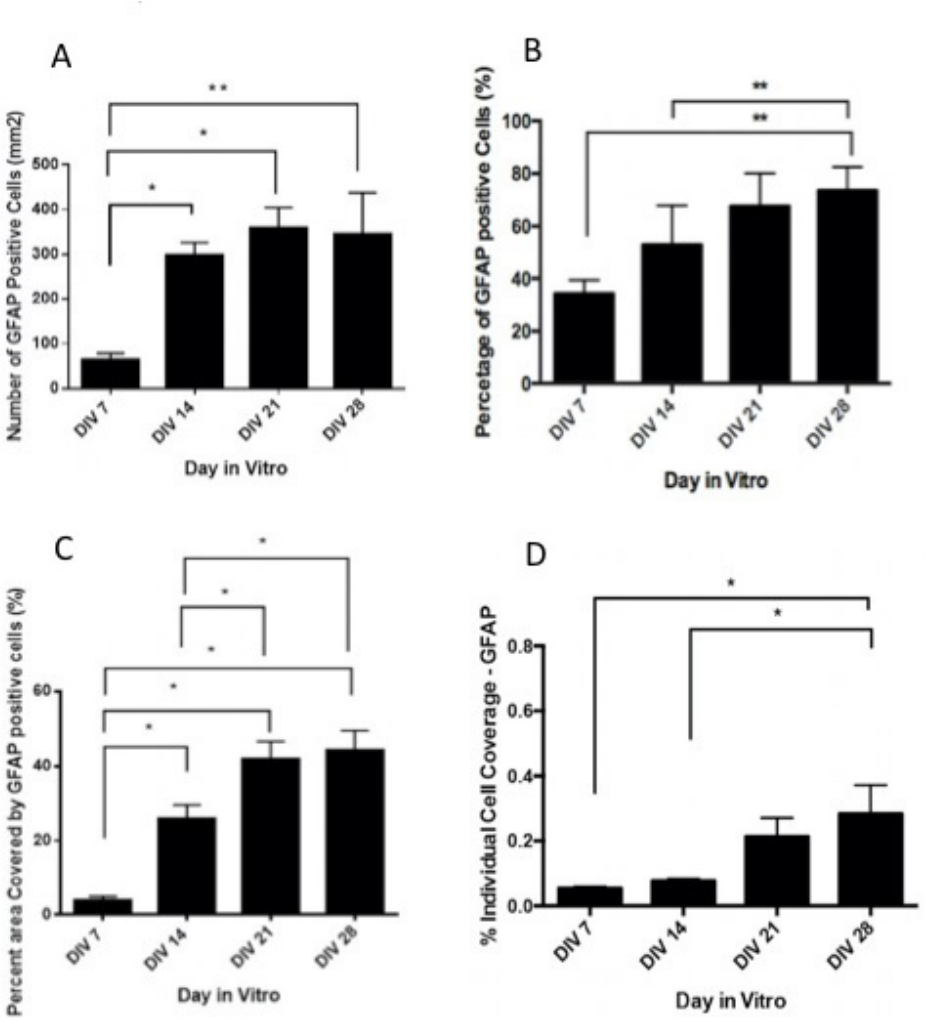

Figure 9: Quantification of GFAP marker expression. (A) Absolute number of marker positive cells per mm2. (B) Percent (%) area covered by marker positive cells. (C) Percent (%) of marker positive cells. (D) Percent of area covered by an average marker positive cell. All data are expressed as mean ± SEM from three separate experiments, *P < 0.05, **P < 0.01, ***P < 0.001) ANOVA with Bonferroni's Multiple Comparison post-hoc tests.

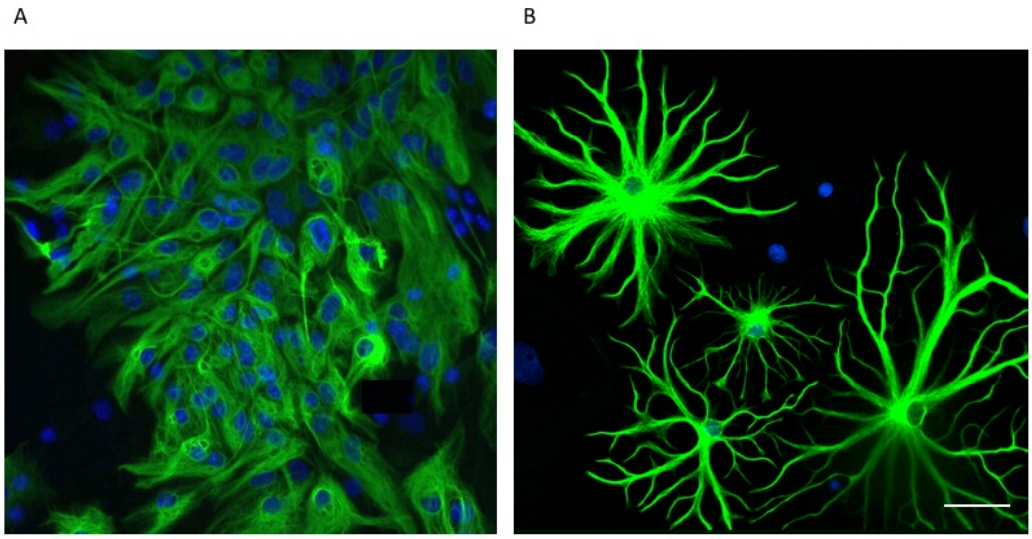

Figure 10: Heterogeneity in morphology of mESCDA. Cultures immunostained for the astrocytic marker GFAP, alongside counterstained for cell nuclei marker (blue) with H-33342. Scale bar = 20µm. (A) Reveals typical dinnerplate morphology. (B) Displays more elaborate morphology with extended protrusions of processes – revealing heterogeneity in morphology expression in mESCDA

At DIV 14 approximately half of the cell population was GFAP positive (Fig.9B 52.93% ± 14.94%, n=9) and exhibited typical astrocytic morphology (Fig.10). This percentage significantly increased during the following weeks and plateaued at DIV 28 (Fig.9B 73.68% ± 9.03%, n=9). Assessment of the relative surface area covered by GFAP positive cells revealed a statistically significant increase ($p < 0.05$) from less than 5% surface coverage at DIV7 (Fig.9C 3.88% ± 1.060%, n=9) to more than 40% at DIV28 (Fig.9C 44.23% ± 5.268%, n=9). The area covered by the average individual GFAP positive cell was also analysed at different DIVs (Fig.9D). There was a significant ($p<0.05$) doubling in GFAP positive cell size from DIV 7 (Fig.9D 0.054% ± 0.0057%, n=9) to DIV28 (Fig.9D 0.284% ± 0.088%, n=9). Furthermore, heterogeneous morphology was also observed within the cultures, morphology ranged from a “dinner plate” morphology to an enlarged complex morphology with elongated processes (typically seen in primary astrocytes) across all DIVs (Fig.10).

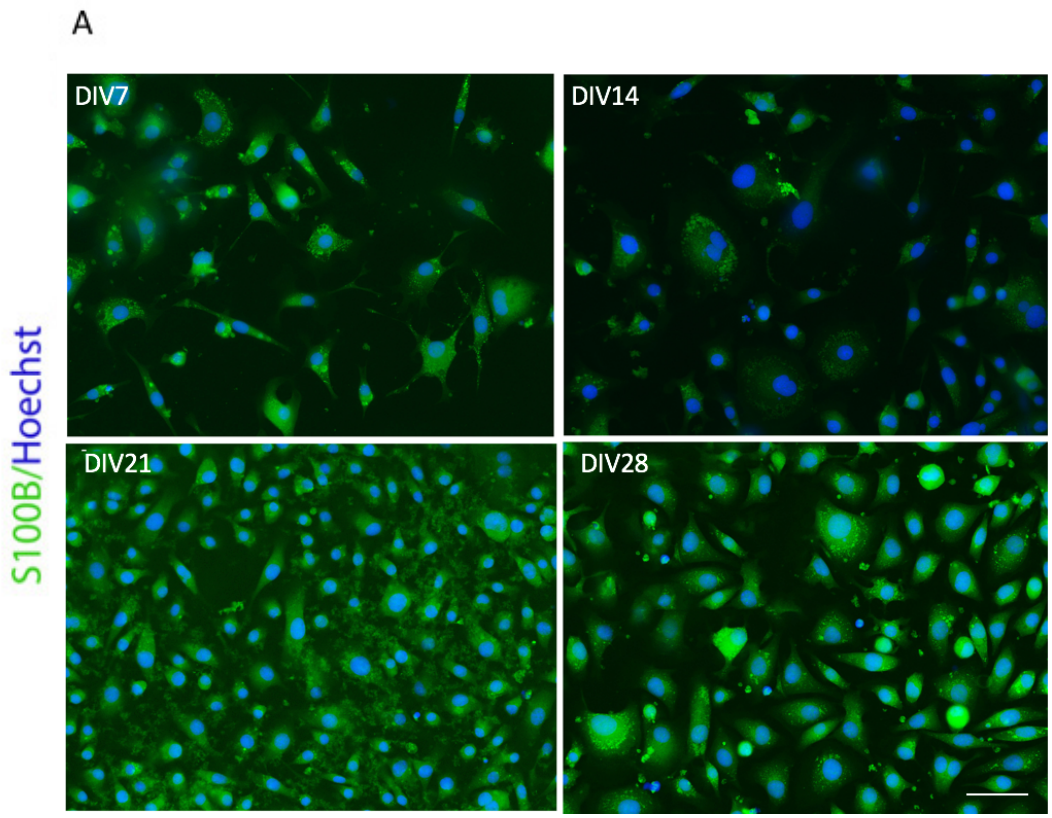

Figure 11: Immunocytochemical phenotyping of mESCDA. (A) DIV 7-28 fluorescent images of astrocytes RA inducted from mESC, labelled for established astrocytic marker S100β. Cultures have been counterstained for cell nuclei marker H- 33342 (blue stain). Scale bar = 20μm.

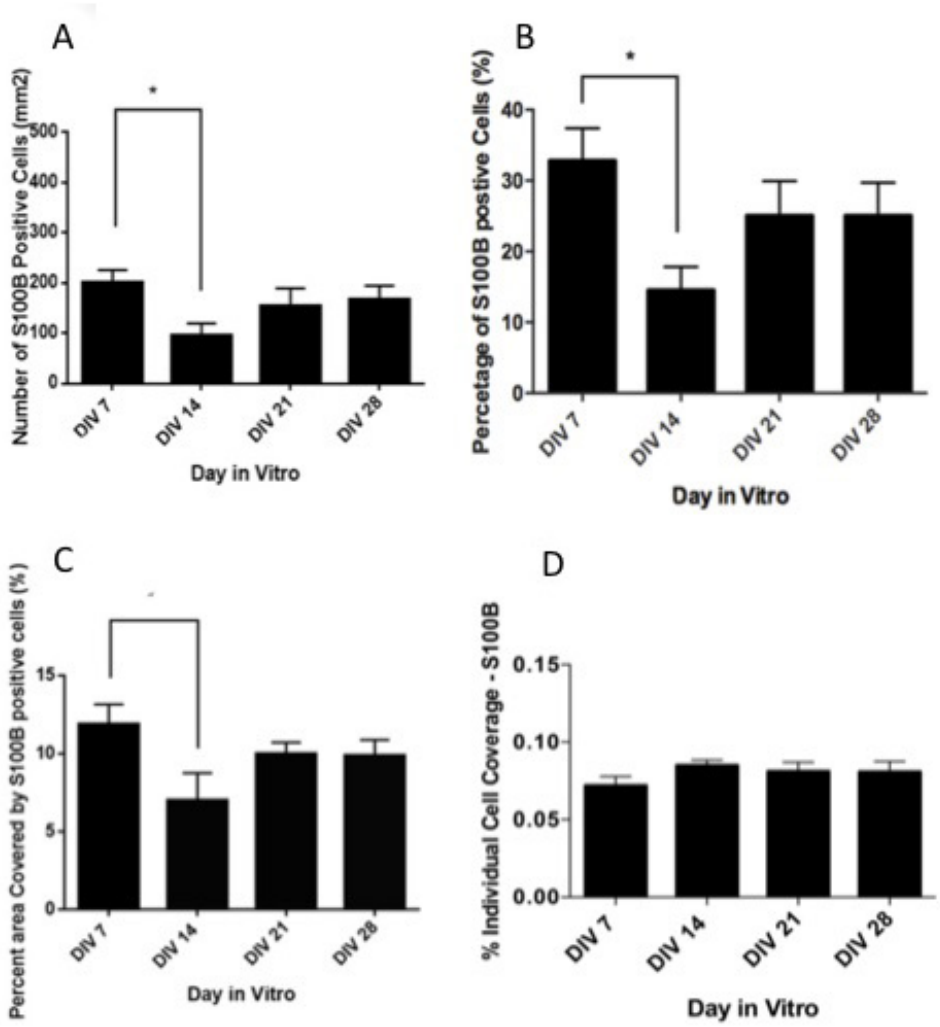

Figure 12: Quantification of S100β marker expression. (A) Absolute number of marker positive cells per mm2. (B) Percent (%) area covered by marker positive cells. (C) Percent (%) of marker positive cells. (D) Percent of area covered by an average marker positive cell. All data are expressed as mean ± SEM from three separate experiments, *P < 0.05, **P < 0.01, ***P < 0.001) ANOVA with Bonferroni's Multiple Comparison post-hoc tests

Further to above examination, there was significant decrease in S100β positive cells ($P<0.05$) between DIV 7 (Fig.12B 32.82% ± 4.61%, n=9) and DIV 14 (Fig.12B14.52% ± 3.29%, n=9). At DIV 28, S100β positive cells recovered and plateaued and maximal expression was achieved (Fig.12B 25.04% ± 4.67%, n=9). The relative surface area covered by S100β positive cells was highest at DIV 7 (Fig. 12C 13.56% ± 1.55%, n=9), with a statistically significant reduction ($p<0.05$) at DIV 14 (Fig. 12C 7.01% ± 1.78%, n=9), which coincided with the decrease in the percentage of S100β positive cells. At later DIVs (DIV 21 and 28), cell coverage plateaued. Analysis of area coverage of an average individual S100β positive cell showed no significant differences across DIVs and was stable at approximately 0.08% (Fig.12D).

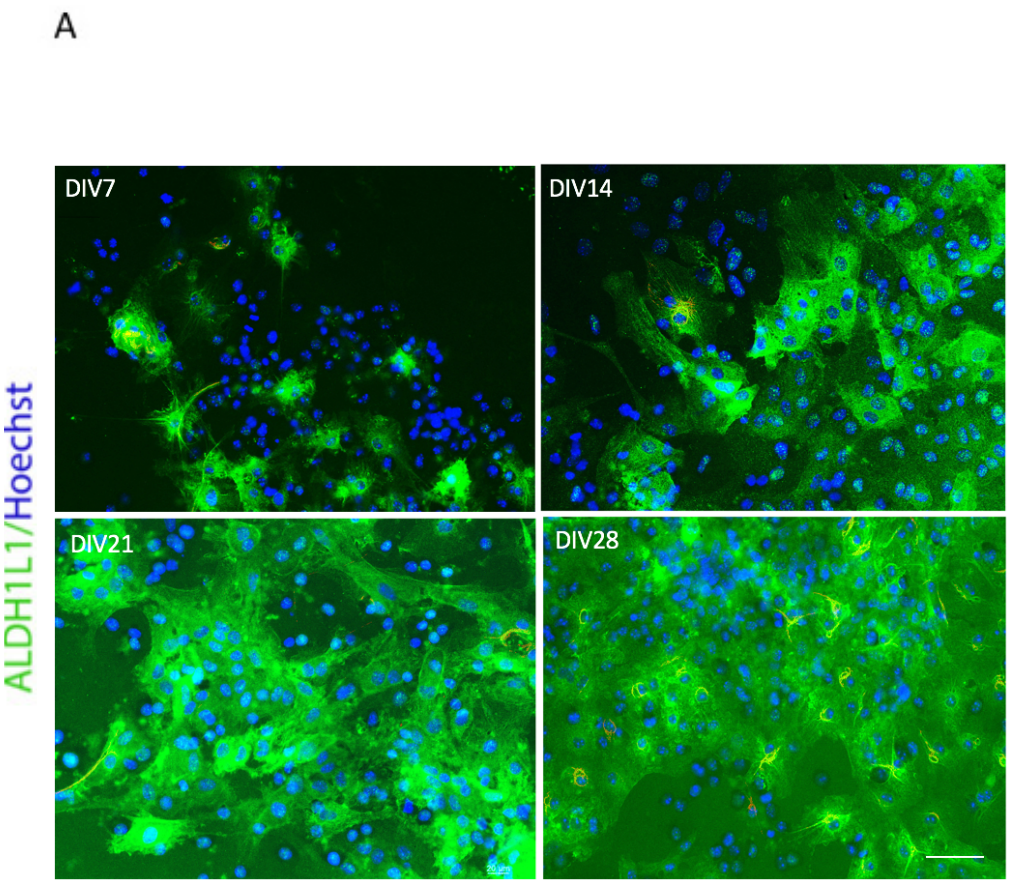

Figure 13: Immunocytochemical phenotyping of mESCDA. (A) DIV 7-28 fluorescent images of astrocytes RA inducted from mESC, labelled for established astrocytic marker ALDH1L1. Cultures have been counterstained for cell nuclei marker H-33342. Scale bar = 20µm

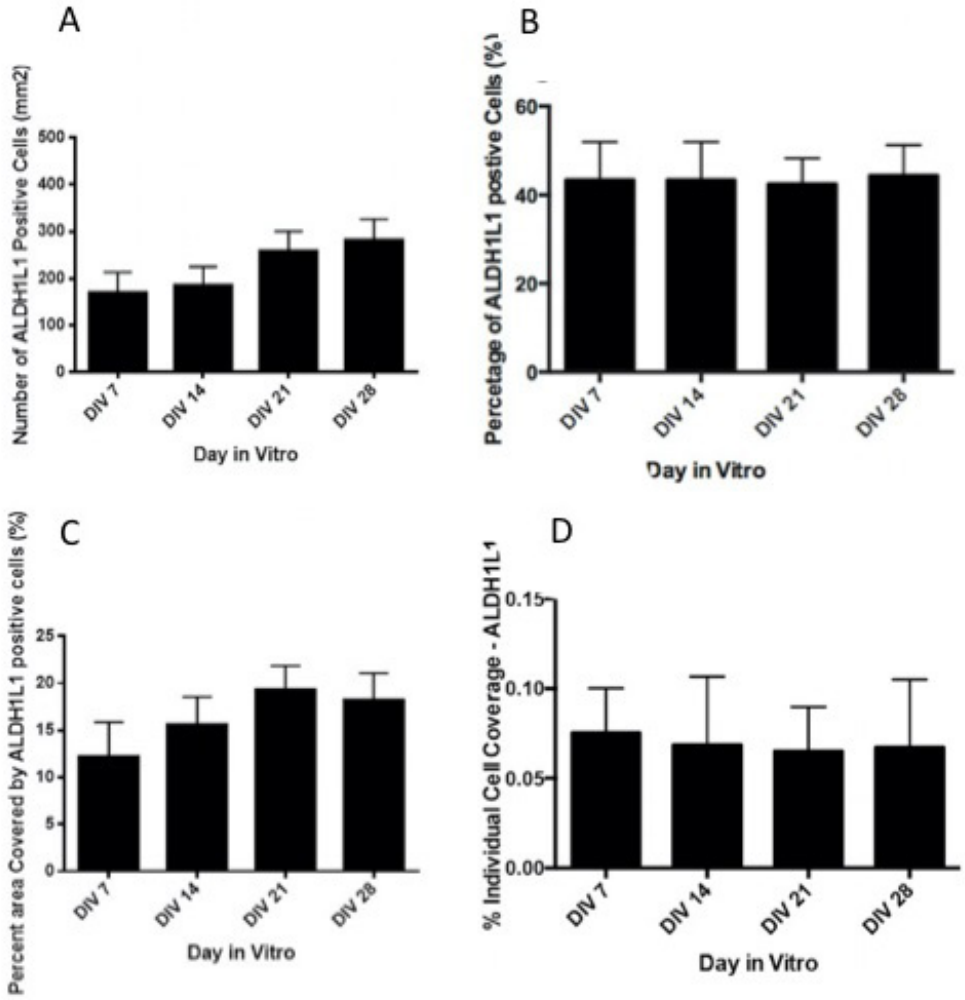

Figure 14: Quantification of ALDH1L1 marker expression. (A) Absolute number of marker positive cells per mm2. (B) Percent (%) area covered by marker positive cells. (C) Percent (%) of marker positive cells. (D) Percent of area covered by an average marker positive cell. All data are expressed as mean ± SEM from three separate experiments, *P < 0.05, **P < 0.01, ***P < 0.001). ANOVA with Bonferroni's Multiple Comparison post-hoc tests

Analysis of ALDH1L1 immunolabelled cultures revealed no significant difference in the percentage of ALDH1L1 positive cells from DIV 7 to DIV 28 (Fig.14A-B stable at approximately 40%). A non- significant upwards trend was observable on the relative surface area coverage (Fig.14C) from DIV 7 to DIV 28, whereas relative area coverage of an average ALDH1L1 positive cell remained stable at approximately 0.07% (Fig.14D).

3.3.4. Co-localisation of astrocytic markers within mESCDA

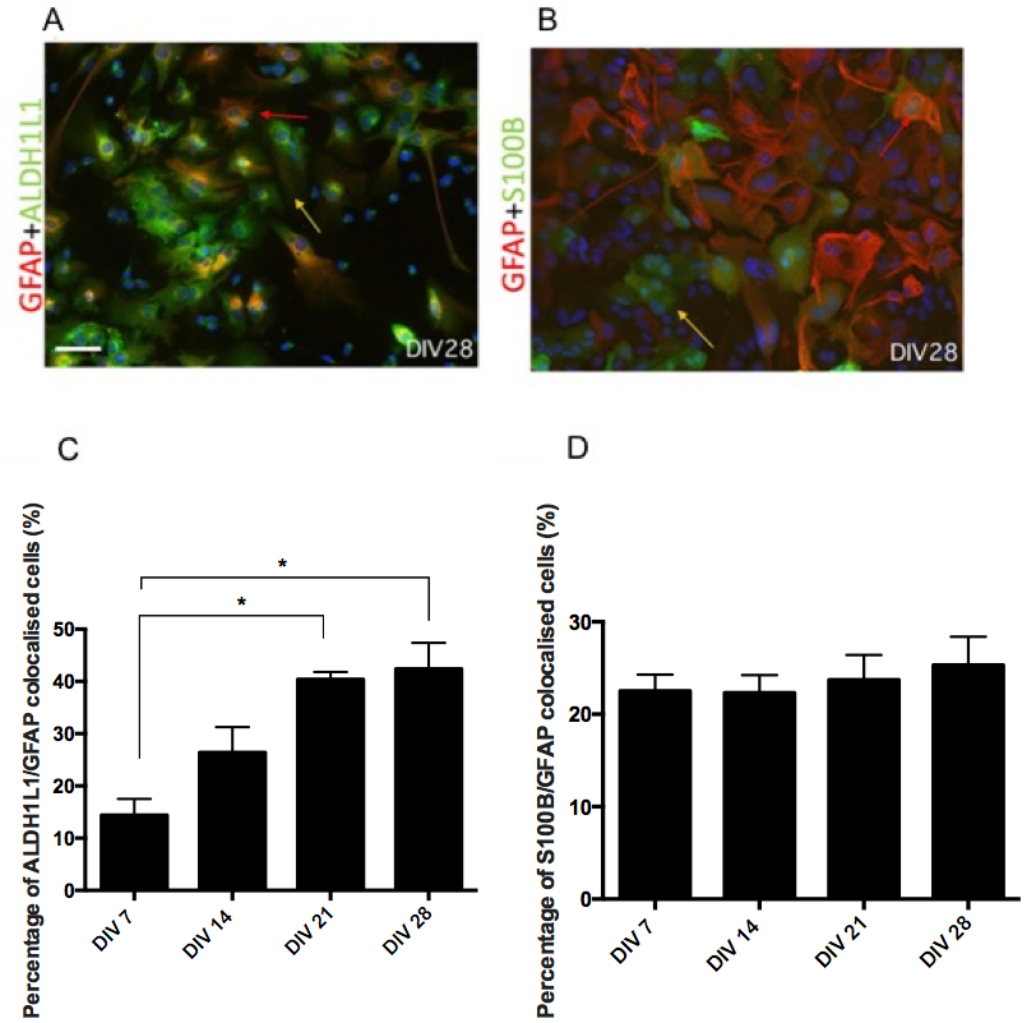

Figure 15: Co-localisation of astrocytic markers (GFAP, ALDH1L1 and S100β). (A and B) Cultures co- immunostained for the astrocytic marker proteins GFAP (red), S100β (green), and ALDH1L1 (green) counterstained for cell nuclei marker with H- 33342 (blue). (A) Culture example at DIV 28 of astrocytes co-expressing GFAP (red) and ALDH1L1 (green) (red arrow) or expressing only ALDH1L1 (yellow arrow). (B) Culture example at DIV 28 of astrocytes co-expressing GFAP (red) and S100β (green) (red arrow) or expressing only S100β (yellow arrow). Scale bar = 20µm. (C-D) Analysis of co-localisation across different days *in vitro* reveals heterogeneity of differentiated astrocytes in protein expression. Percent differences in staining where (C) GFAP/ALDH1L1 and (D) GFAP/S100β stains from DIV 7 to DIV 28. ANOVA with Bonferroni's Multiple Comparison post-hoc tests

Astrocytes generated *in vitro* are not as homogenous in marker expression as previously assumed (Matyash and Kettenman 2010). To highlight the existence of subpopulations of astrocytes, we performed double-immunolabelling of GFAP with either ALDH1L1 (Fig.15A) or S100β (Fig.15B) temporally across DIVs (DIV 7-DIV 28). In figures, 15A and 15B yellow arrows point to cells expressing only one protein ALDH1L1 or S100β, while red arrows point to cells expressing both proteins, in DIV 28 cultures. Quantification revealed that not all cells express all astrocytic markers simultaneously, illustrating the existence of astrocytic sub-populations (heterogeneity in marker expression). Analysis of ALDH1L1 and GFAP co-staining revealed a significant positive increase in number of colocalised cells, which was significantly increasing towards the late time-points (Fig 15C. DIV 7 14.3% n=9 and DIV 28 42.4% 0.04 n=9, $P<0.01$). S100β and GFAP stains were not significantly different throughout the culture (Fig. 15D DIV7 22.51% n=9 and DIV 28 25.31% n=9).

3.4. Discussion

The study of astrocytes, in their resting state or in different defined activation scenarios, faces a number of challenges: 1) measurements *in vivo* require a distinction of astrocytes from sur- rounding cells for the analytical endpoints chosen; 2) ex vivo studies, for example using purified adult astrocytes, suffer from a compromised viability of the obtained cells, and from undefined activation states, when put in culture; 3) *in vitro* studies mainly rely on studies of mixed populations, prepared from relatively immature cells. They may also contain precursor cells, reactive astrocytes and other cell types, such as microglia and oligodendrocytes. Additional approaches would thus be desirable to further explore astrocyte biology. Here, the result provides an alternative strategy via using stem cells, which allows generation of a pure population of non-proliferative, non-activated astrocytes.

Although stem cell derived astrocyte generation is not a relatively unexplored field, as recently new methods of astrocyte generation have been described (Table 4) (Shaltouki et al. 2013; Roybon et al. 2013; Zhang et al. 2016, Chandrasekaran et al. 2016; Kleiderman et al. 2016, TCW et al. 2017, Xi et al 2018 – see Table), there lacks uniformity in all of the protocols. The majority of current protocols are time-consuming, rely on variety of morphogens, lack granularity in astrocytic subtype generation and often are not as efficient as for example neural induction methods (Ban et al. 2007; Kamnasaran et al. 2008; Peljto et al. 2010). Therefore, for efficient development of heterogeneous astrocytes, there was an effort to improve the established protocols by 1) reducing the time frame for astrocytogenesis; 2) preventing excessive use of morphogens and direction towards a lineage to produce physiologically relevant astrocytes, and 3) characterise and provide evidence of subtype (heterogeneous) generation.

2.4.1 Reduction of timeframe via a semi-directed approach

Two major classes of protocols are usually utilised to mimic the *in vivo* mechanisms governing astrocytogenesis: an EB-based 3D aggregation technique and a single cell monolayer-based method (Shi et al. 2012; Chandrasekaran et al. 2016). Here a semi-directed spontaneous emergence based approach for differentiation of mESC towards astrocytes was optimised and developed. Most studies follow a distinct lineage direction pattern where from stem cells, exogenous lineage specific morphogens are used to develop neural stem cells, and then glial progenitor cells and finally astrocytes (Table 4). Here, two established protocols from Pjelto et al 2010 and Keugler et al 2012, were

combined and altered, to minimise morphogen application, accelerate astrocyte development and contribute towards a standardisation of protocols that exists within the literature. The altered protocol led to the generation of heterogeneous populations of astrocytes from different time points.

During development, the regional identity (anterior-posterior, dorsal-ventral) of astrocytes is determined when neural stem cells are patterned to regional progenitors by morphogens such as retinoic acid. The regionalised progenitors first give rise to subclasses of neurons and then, during gliogenesis, generate regional-specific astrocytes with functionally distinct characteristics (Nakashima et al. 1999; Muroyama et al. 2005). Therefore, a combination of extrinsic cues and epigenetic factors contribute to fate specification during development. The idea that extrinsic signals are required for astrocytogenesis *in vitro* first arose from the observation that embryonic cortical precursors produce neurons when cultured on embryonic cortical slices, but astrocytes when cultured on postnatal cortical slices (Morrow et al. 2001). Therefore, by mimicking endogenous signalling pathways *in vitro* is necessary towards an accelerated production of astrocytes.

Peljto et al 2010 protocol was essential in the generation of astrocytes, as it provided endogenous signalling induced by retinoic acid (RA) that direct the generation of specialised cell subtypes with properties that match those of counterpart cells generated *in vivo*. The protocol was initially used for directed generation of motor neuronal subtype via the aid of only RA, and no transgenic manipulation (Fig. 8). Therefore, to induce and accelerate astrocyte development Keugler et al 2012 protocol was used. By using RA alongside heparin and N2 within the cultures, the results showed the accelerated emergence of GFAP positive astrocytes from EBs (71% at DIV 28), when compared to non-RA treated EBs (from 21% at DIV28) (Fig.5). The findings indicate neuralisation of the protocol is essential and RA is a key regulator in inducing astrocyte differentiation within the EB (Fig.5).

Retinoic acid performs its actions by activating endogenous signalling pathways and creating a feed- back loop to allow endogenous production of RA in an autocrine manner (He et al 2005). Pathways such as Bone morphogenetic proteins (BMP) and ciliary neurotrophic factor CNTF that suppresses the potential for neural differentiation are activated during RA application (Rajan & McKay 1998; Miller & Gauthier 2007; Okada et al. 2004) (see literature review chapter 1). BMPs form a complex between the BMP-downstream transcription factor Smad1 and STATs, bridged by the transcription

coactivator p300/CREB-binding protein (CBP), and ciliary neurotrophic factor CNTF suppress the potential for neural differentiation by activating (JAK) signal transducer and activator of transcription (STAT) (gp130-JAK-STAT) pathway (Hong & Song 2014) all of which lead to astrocytogenesis (Asano et al. 2012). This evidence of RA leading to these intracellular pathway changes is shown by expression of IL-6 within the cultures. IL-6 pathway is a family of cytokines which share membrane glycoprotein gp130 as a critical receptor component for activation JAK-STAT pathway required for astrocytogenesis (Yanagisawa et al. 2001; Brown et al. 2014). Evidence by Yanagiswa et al 2001 show IL-6 expression is elevated to induce astrocyte differentiation. Using neuroepithelial cells from mice, the study displayed that IL-6 expression coincided with astrocytogenesis, and this increase in expression is necessary to allow formation of BMP-IL6 complex to induce activation of GFAP promotor leading astrocytogenesis. This is shown within the generated mESCDA, where at DIV 7/14 there is increase in IL-6 expression, and at later DIVs (DIV 21/28) this expression non-existent (Yanagisawa et al. 2001). The reduced expression of nestin and high expression of IL-6, provides evidence towards lineage specification and accelerated astrocyte development by RA application at the neurilisation steps (Fig.6).

Alongside, RA Hepran sulphate and its highly sulphated analogue heparin promote neural and glial phenotypes (Pickford et al. 2011). Several studies have demonstrated the proof of concept of using heparin to enhance the maintenance of ESCs as well as to stimulate their differentiation into therapeutically relevant cell types (Furue et al. 2008; Pickford et al. 2011). Given that physiological heparins modulates important cell signalling pathways and cell fate, exogenously supplemented heparins have shown to manipulate cell signalling and direct cell fate choices of cells during development towards astrocytes (Nagayasu et al. 2005). Therefore, to accelerate astrocytogenesis within the cultures, heparin rich media obtained from Keugler et al. 2012 was used to develop astrocytes from neuralised mESC. This strategy is now widely employed (TCW et al. 2017), however during the establishment of protocol Heparin usage for astrocytogenesis was a novel route, subsequently preventing the use of further morphogens to direct astrocyte differentiation. This semi-directed approach via combination and alteration of two established protocols led to generation of astrocyte within 13 days within the cultures, confirmed via immunocytochemistry and RT-PCR (Fig.6-14), contributing towards a growing need to 1) reduce the time frame for astrocytogenesis and 2) prevent excessive use of morphogens and direction towards a lineage to produce physiologically relevant astrocytes.

2.4.2 Characterisation and evidence of subtype (heterogeneous) generation of mESCDA

Heterogeneity of astrocytes derived from rodent brains or from stem cells has been underestimated. Astrocyte are a heterogeneous group of cells within the CNS. There exists genetic, protein, functional, morphological, and regional heterogeneity (Farmer et al. 2017; Xin et al. 2018). In *in vitro* astrocytogenesis, it has been common in the field to strongly rely on a few single markers, such as GFAP (Namihira et al. 2009; Kamphuis et al. 2012). Also, morphologically cells are homogeneous cells are mainly developed and show a single 'dinner plate' morphology (Fig.10) (Olude et al. 2015). Nevertheless, most of the published protocols for differentiation of astrocytes from stem cells (independent of the use of serum or culture duration) judge differentiation maturity, efficiency and subtype generation exclusively via by the expression of GFAP (Krencik & Zhang 2011; Palm et al. 2015; Kleiderman 2016). Therefore, for comparison, it was essential to perform GFAP analysis on the generated protocol.

GFAP is a type III intermediate filament protein and an important component of the astrocyte cytoskeleton (Eng et al. 2000). Here immunocytochemical and PCR analysis revealed a significant increase in GFAP positive cells across time (from DIV7 to DIV 28), which plateaued at DIV 21 (Fig 6). This temporal expression reflects *in vivo* changes seen in GFAP expression. Temporal analysis performed on mouse GFAP mRNA by Riol et al 1992 revealed significant increase and a plateau in expression of GFAP during development and this GFAP increase coincides with appearance of astrocytes. This expression of GFAP mRNA is significantly high at birth and continues to increase, donating a period of astrocytic proliferation. Subsequently, during maturation the expression of GFAP was shown to be decreased, coinciding with arrest in astrocyte population - donating a period of astrocytic morphological differentiation (Riol et al. 1992). This has also been observed in human by Rezaie et al 2003, where there is extensive distribution and presence of GFAP-Positive astrocytes in the human foetal brain at 19–20 gestational weeks onwards, which arrests as the brain matures (Rezaie et al. 2003). These temporal changes in expression observed here subsequently suggest temporal maturity of generated mESCDA, and provide direct evidence of astrocyte which are comparable to their *in vivo* counterparts (Freeman 2010). This temporal analysis of GFAP expression has not been performed in recent stem cell derived astrocyte studies, therefore the evidence presented here provides an excellent opportunity to revisit GFAP expression and assess it with an alternative angle.

Additionally, within the cultures heterogeneous morphological populations of GFAP positive cells were also observed across DIVs, i.e. at DIV 21 and 28 – where there was presence of elaborate star shape morphology alongside reduced protrusions and 'dinner plate' morphology observed *in vitro* (Freeman 2010; Olude et al. 2015). However, as a general rule, post DIV 14, as GFAP expression started to plateau, GFAP cells began to lose their radial and 'dinner plate' morphology and adopted a more spongiform/stellate phenotype with extended fine protrusions (Fig.6-10), while doubling in size. These changes in morphology donates to cell maturity, and dictates presence of subpopulations of mature and immature cells present together within the culture (Freeman 2010). Additionally, this double in morphology could dictate the presence of reactive astrocytes (Kamphuis et al. 2012). Using primary astrocyte cell culture, Kamphuis et al. 2012, suggest that an increase in astrocyte cell size and cell morphology and suggests an increased in astrocytes activation. Nevertheless, within the generated mESCDA it is safe to rule out astrocyte activation due to limited/reduced presence of iNOS and IL-6, markers for neuroinflammation and activation, at later DIVs when GFAP expression is at its highest. The assessment here verifies generated mESCDA capability to display complex morphologies which are comparable with *in vivo* and primary astrocytes.

However, expression or absence of single markers cannot sufficiently describe cell populations and therefore other approaches had to be developed. GFAP has been proved not to be "the marker' for all types of astrocytes, as it shows weak expression in grey matter protoplasmic astrocytes (Tabata 2015), which are the major type of astrocytes in the brain, and occupies only which represent ~15% of the total volume of the astrocyte (Farmer 2010). Although GFAP is an important endpoint marker to identify mature astrocytes, astrocytes can also be identified by the expression of calcium-binding protein S100β, ALDH1L1, AQP- 4, ALDH1L1 and additional markers proposed based on microarray gene expression profiles Furthermore, expressions of these markers, as well as astrocyte morphologies, vary considerably amongst cortical regions and at different time points during development (Emsley & Macklis 2006; Bradley & A 2018), suggesting that during *in vitro* astrocytogenesis, temporal analysis of other astrocyte markers is also essential in the identification of astrocyte subtypes.

Developmental studies have shown that the sequence of marker appearance during the initial, embryonic phase of gliogenesis is ALDH1L1 > S100β > GFAP with AQP4 and EAAT1/2 labelling perivascular membranes and mature astrocytes respectively. Therefore, to reliably test the efficiency of protocol in the generation of astrocytes, other well defined markers were used for a better characterisation of astrocytes and its

developmental journey *in vitro*. Within the protocol, mESCDA reliably expressed GFAP negative astrocytic genes (S100β, ADH1L1, AQP4, and receptor-specific genes), revealing heterogeneity of marker expression as observed *in vivo*.

Concerning the problem related to astrocyte identity, several studies have been done to discover pan-astrocyte markers and also to understand the molecular differences in a region specific manner (Yang et al. 2011; Tsai et al. 2012). A couple of studies have described ALDH1L1, a folate metabolizing enzyme, to be expressed specifically in astrocytes in murine brain, making it one of the most widely accepted pan-astrocyte marker and an early astrocyte marker, reliably labelling all subtypes of astrocytes: protoplasmic and fibrous (Cahoy et al. 2008; Tsai et al. 2012). Analysis of ALDH1L1 markers showed that in contrast to GFAP, expression of ALDH1L1 in generated mESCDA produced by the protocol remains stable across different DIVs - when looking at both genetic and immunocytochemical assessments (Fig.14). Evidence by Yang et al 2011 and Roybon et al 2013 show ALDH1L1 expression occurring before GFAP in the sequence of astrocytic markers. Inspection of the data supports this observation, where immunocytochemical expression of ALDH1L1 at DIV 7 (Fig.14) is higher than GFAP (Fig.7). Furthermore, Roybon et al 2013 show that in iPSC derived astrocytes the increase in ALDH1L1 expression correlates with decreased astrocyte proliferation (Roybon et al. 2013). The presence of stability of ALDH1L1 expression across all time points therefore dictates presence of proliferative cells alongside mature cells, across the DIVs within the mESCDA. Furthermore, analysis of cell size and coverage also displays presence of stability in expression. At the time of the study, these analyses of ALDH1L1 positive staining have not been displayed previously and provide novel evidence towards ALDH1L1 expression. This stability in expression of ALDH1L1 in stem cell derived astrocytes has not been reported before, and grants access to highly proliferative population of cells– further confirming subpopulation (heterogeneous) generation of astrocytes.

Additionally, studies claim the expression of ALDH1L1 does not particularly map to the mature astrocyte phenotype (Roybon et al. 2013). The results partly corroborate this claim, as there is sparse co-labelling of GFAP positive and ALDH1L1 positive cells in the cultures, at later developmental stages (DIV 21 and DIV 28) (Fig.15). Nevertheless, this claim warrants further investigation, as within our cultures there are ALDH1L1 positive cells that do not express GFAP (Fig.15A). This indicates the presence of either immature astrocytes or mature astrocytes that lack GFAP expression (Keugler et al 2012, Molofsky et al 2013).

Likewise, S100β is a useful astrocyte marker. S100β is involved in a plethora of intracellular processes within astrocytes, such as cell proliferation, calcium binding, and activity, microtubule stability, cell cycle, and development. The role of S100β in developmental stages has shown to be extremely important. When analysing S100β, there was an existence of GFAP negative cells (Fig.15) (Keugler et al. 2012). Evidence has shown that its expression coincides with GFAP *in vitro* (Brozzi et al. 2009). In generated cultures, there was a presence of S100β at DIV7, with a significant reduction in expression occurring at DIV14 (Fig.12). This reduction has been previously linked to astrocyte maturation and is also involved in the shift of S100β role during development and corroborates with literature, suggesting S100β contribute towards the migratory capacity of undifferentiated astrocytes and that S100β expression needs to be repressed for mature astrocytes to appear (Hachem et al. 2007; Patro et al. 2015). Nevertheless, Patro et al. 2015 using Sprague dawley rats display that once astrocytes lose their potential for proliferation, the S100β expression is repressed (Patro et al. 2015). However once astrocytes reach maturity, S100β expression reappears – making S100β a dual marker for astrocytes. Here, the effects of S100β expression suggest that S100β might contribute to astrocyte development as well as to the maintenance of an undifferentiated phenotype in astrocytic cells by interacting with GFAP as shown by co-localisation analysis. Double- immunolabelling of GFAP positive cells with S100β positive cells at different DIVs performed (Fig.15D), revealed a stability in the expression of both labelled cells, indicating GFAP and S100β are mostly co-expressed together and they are tightly regulated together in determining astrocyte fate.

2.4.3. Study improvements and future directions

Comparatively to other protocols (Table 4) the differentiation of mESCDA is fast and robust, and all steps are easily accessible at every stage. Hence it offers the possibility to investigate assess astrocyte development at every stage. The quick reproducibility and generation of heterogeneous (subtypes) of astrocytes would allow these cells to be used in studies which allow probing of the astrocytes. Although the study does provide a platform for future studies, assessment of further developmental markers along the way would sufficiently benefit the obtained results, and would further allow characterisation of the generated mESCDA. For example, Sun et al 2017 recently used SOX-9 to determine the number of astrocytes in the adult brain outside the neurogenic regions. SOX-9 is an early developmental transcription factor involved in fate switching of astrocytes (Kang et al. 2012; Sun et al. 2017), and using SOX-9 immunolabeling and

isotropic fractionator techniques, Sun et al 2017 were able to quantify astrocytes. Similar staining and technique could be applied in generated mESCDA, and would sufficiently show presence of mature/immature astrocytes.

Furthermore, alongside immunostaining and morphological analysis, western blot analysis would further solidify the results. Although the technique is not short of its pitfalls, and would provide similar semi-quantitative analysis performed above, it would provide confirmation of results seen above. Additionally, the response of mESCDA towards cytokines might help to get new insights into astrocyte behaviour during inflammatory conditions, which occur in most neurodegenerative diseases. Furthermore, a comparison of mESCDA could be performed with iPSC cells, to analyse which is the best methodology which can offer offers new possibilities to investigate the involvement of astrocytes in processes within the CNS.

4. Calcium dynamics of generated mouse embryonic stem cell derived astrocytes (mESCDA)

4.1. Introduction

Astrocytes have emerged as key players in the regulation of synaptic physiology. They display complex and heterogeneous morphological structures and are able to sense and respond to environmental signals, modulate neuronal activity, synaptic transmission, and vascular function (Perea et al. 2014; Petrelli & Bezzi 2016). Synaptic activity is integrated into astrocytes (Perea & Araque 2010) and might result in intracellular calcium (Ca^{2+}) elevations with specific spatial and temporal properties. These might appear as global and local responses within the astrocytic complex morphology. It is yet unclear if global Ca^{2+} elevations are more representative of an integrative response or if they are the result of a summation of Ca^{2+} fluctuations or inositol 1,4,5-trisphosphate (IP_3) levels; nevertheless, these have been used as a hallmark of astrocytic function (Khakh & McCarthy 2015). These calcium elevations may appear spontaneously or may be triggered by endogenous or exogenous stimuli - such as the release of transmitters from adjacent cells such as neurons, or mechanical stimulation and exogenous pharmacological applications (Zorec et al. 2012).

Astrocytes are theorised to modulate synaptic activity through the release of gliotransmitters including glutamate, ATP (which is broken down to adenosine) and D-serine. These transmitters are released from astrocytes in a Ca^{2+} dependent manner in response to either electrical or pharmacological stimulation (Agulhon et al. 2008). In the hippocampus, ATP-evoked astrocyte Ca^{2+} was shown to promote glutamate release, which consequently facilitating synaptic transmission via activation of mGluRs (Perea et al. 2014; Panatier & Robitaille 2015). Nevertheless, attempts from multiple studies have shown that astrocyte calcium signalling has failed to affect the neurogenic niche it surrounds. These studies have used readouts of synaptic transmission and plasticity in the hippocampus using a variety of mouse models such as MrgA1 and IP_3R2 KO (Petravicz et al. 2010; Li et al. 2013) to show astrocytes play a minimal role in mediating neuronal response. However, these studies are limited in terms of their arguments. Multiple pieces of evidence for plethora of studies have shown that there are astrocytes are majorly involved in regulating neural networks. For example, Henneberger et al 2010 show a tight modulation of astrocytic intracellular Ca^{2+} is crucial for D-serine-dependent long-term potentiation (LTP) of hippocampal CA1 pyramidal cells (Henneberger et al. 2010). Accordingly, a recent study has shown that acute blockade of Ca^{2+} dependent IP_3 mechanisms impairs LTP, but that this can be rescued by exogenous D-serine.

The primary mechanism for the elevation of intracellular Ca^{2+} levels in astrocytes is through the Gq-GPCR-PLC-IP_3 pathway (Fiacco & Mccarthy 2004; Michael M. Halassa et al. 2007; Lalo et al. 2011). As astrocytes in the central nervous system possess a full complement of membrane receptors and ion channels (Bernstein et al. 1998; Lalo et al. 2011), this allows them to respond to intercellular signals from both other astrocytes and from neurons on a millisecond timescale (Scemes & Giaume 2007). First shown in culture, the principal mechanism of long-distance signalling in astrocyte networks are intercellular calcium waves mediated by the extracellular diffusion of adenosine 5'-triphosphate (ATP) and related purines interacting with the P2Y family of membrane receptors (James & Butt 2001). This causes a rise in intracellular calcium levels, which is part of a cascade that can result in the vesicular release of gliotransmitters, in particular, ATP, which can signal other downstream astrocytes; thereby causing a propagation of calcium waves (Guthrie et al. 1999; Miller 2010; Kuga et al. 2011; Rusakov et al. 2014). Recently, calcium waves have been shown to occur in situ in brain slices and in vivo in the rat neocortex shown via two-photon microscopy (Wang et al. 2012). Although the physiological and pathophysiological roles of calcium wave *in vivo* are not clearly understood and are very much an area of active research. A particularly intriguing and clinically important function may be the augmentation of calcium wave following disease or injury, for instance, during ischemic insults or seizures, essentially acting as a pathological signalling mechanism that may augment reactive gliosis and secondary injury processes (Delekate et al. 2014).

The functional extent of any physiological or pathophysiological contributions of calcium waves will depend on the dynamics of signal propagation through the network, which will, in turn, depend on the molecular mechanisms that underlie the dynamics. For example, the ability of extracellular ATP in binding to purinoreceptors and causing a cascade of intracellular signalling - inositol 1,4,5-trisphosphate - IP_3 mediated signalling leading to astrocyte environmental niche control. Therefore, analysis of specific receptor pathways mediating and contributing to calcium dynamics is essential.

4.1.1. Purinergic receptor and its components

One of the most important discoveries in the field of purinergic transmission in recent years was the role of ATP as the transmitter mediating intercellular communication in the brain. In astrocytes derived from rat cortex, the generation of a calcium wave was shown to depend most crucially by the activation of either ligand-gated P2X or G-protein-coupled P2Y purinergic receptors (Ceruti & Abbracchio 2006).

The metabotropic P2YR1 and pore-forming $P2X_7$ receptors are regarded as one of the main receptors for astrocyte transmission (gliotransmission) within the CNS. P2YR1 receptors are coupled primarily through the Gαq/11-signalling pathway (Burnstock et al. 2010). The conventional Gαq/11-signalling pathway involves activation of the heterotrimeric G protein and the subsequent dissociation of αq and ßγ subunits. The αq subunit activates PLC, which catalyses the hydrolysis of phosphatidylinositol 4,5-bisphosphate (PIP_2) into IP_3 and diacylglycerol (DAG). IP_3 then binds to IP_3 receptors on the endoplasmic reticulum, triggering a release of intracellular calcium. Therefore, the primary mechanism for the elevation of intracellular calcium levels in astrocytes is through the Gq-GPCR-PLC-IP_3 pathway (Haydon 2001; Fiacco & Mccarthy 2004; Fellin 2009; Sherwood et al. 2017). Although current models of receptor-activated calcium entry focus on this cascade mechanism, there is increasing evidence that this pathway is not the only one whereby calcium elevation occurs (Sherwood et al. 2017).

Recently, ionotropic P2 purinoceptors ($P2X_7$) permeable to calcium have been functionally characterised in astrocytes (Burnstock et al. 2010). Hence, because of the complexity of the P2 purinoceptor mediated calcium signalling, dissecting the relative contribution of the different calcium elevating pathways in each cellular context is of crucial importance in the attempt to determine the biological significance of the mechanisms regulating the intracellular calcium homeostasis (James & Butt 2001). P2X receptors are ligand-gated ion channels conveying the ionotropic actions of extracellular ATP. Until now, seven different subunits of this receptor family have been identified which form functional receptor ion channel complexes in homo/ hetero oligomeric assemblies. Within the P2X receptor family, the $P2X_7$ receptor has a distinguished role in astrocyte calcium activity (Nobile et al. 2003; Vizi et al. 2006). The long intracellular C-terminal domain has been shown to be instrumental for the pore-forming property of $P2X_7$ receptors, which has been involved in calcium influx and has shown to contribute towards store-operated calcium entry and elevation in intracellular calcium and contributing to calcium increase and signalling (Verkhratsky & Parpura 2014).

The identification of mechanisms mediating transmitter release from astrocytes is relevant not only for normal physiological processes but also for pathological states of the central nervous system (CNS). For instance, during ischemic insults and seizures, reduction of calcium concentrations in the extracellular environment may trigger the release of transmitters from astrocytes (Hamilton & Attwell 2010; Ding 2014). The function of the different subtypes of purinoreceptors on astrocytes is not well understood.

Important unresolved questions from previous studies such as, whether calcium signalling occurs in all populations of astrocytes, and which subtypes of purinoreceptors predominantly mediated the response to ATP. Here, the studies aim to show that in developed mESCDA, ATP evokes increased cytosolic calcium via metabotropic P2Y purinoceptors and ionotropic P2X purinoreceptors, which are activated at micromolar concentrations of ATP. Additionally, the study will aim to identify the predominant pathway which leads to changes in calcium dynamics via the application of several receptor specific compounds impeding calcium signalling. Additionally, astrocytic Ca^{2+} signals exhibit critical spatiotemporal features that need to be fully understood to allow for the careful assessment of their functional implications. Among them: fast vs. slow elevations; single vs. multiple astrocytes; receptor-dependent mechanisms. The complementary application of existing tools, as well as the development of accurate models to tackle its unique features, will allow the study to provide novel insights into receptor specific actions and consequences. Therefore, the study here will aim to further the field and contribute to understanding the complexity of astrocyte signalling - particularly in stem cell derived astrocytes.

4.2. Materials and Method

4.2.1 Materials

Culture Materials	Catalog Number	Provider
Calcium Chloride (CaCl2)	12074	Sigma
HEPES	H3375	Thermo Fisher
Bovine serum albumin (BSA)	A2058	Sigma
DPBS	A1285801	Thermo Fisher
ADMEM/F-12	12634028	Thermo Fisher
N2 Supplement (100X)	17502048	Thermo Fisher
Fetal Bovine Serum (FBS)	F2442	Gibco
Pen/Strep	15140	Invitrogen
L-Glutamic Acid	G1624	Sigma
ß-Mercaptoethanol	1350	Gibco
Laminin	L2020	Sigma
Gelatin	G1393	Sigma
Triton-X100	9002931	Sigma
Formaldehyde (PFA)	130525894	Sigma
Hoechst 33342	H3570	Molecular Probes
Trypsin Solution	59427C	Thermo Fisher
Taq DNA Polymerase Kit	201203	Qiagen
Taq PCR Core Kit	201203	Qiagen
Taq PCR Master Mix	201203	Qiagen
Rnease Mini Kit (RNA Isolation)	74104	Qiagen
Primers (see primer table for primer list)	3222431	Thermo Fisher
Agarose	A6877	Sigma
DNA Ladder	15628	Invitrogen
Loading Dye	18116	Invitrogen
SYBR Green Master Mix	14928100	Thermo Fisher
Fluo 4	12312	Molecular Probes
ATP	2135791	Sigma
Suramin	129464	Tocris
Brilliant Blue G	115399	Tocris
EGTA	E3889	Sigma
Ionomycin	I3909	Sigma
MRS2179	0900	Tocris

Table 5: Materials used for assessment of mESCDA calcium dynamics

4.2.2. Generation of mESCDA for calcium imaging

The EB based technique was utilised for calcium experiments as it resulted in successful generated of mESCDA (see chapter 2). 20 intact EB's were seeded directly onto laminin coated 13mm coverslips containing astrocyte differentiation media (ADMEM/F12, 2% FBS, N2, 1% L-glutamine, 1% Pen/Strep, 100μM β-mercaptoethanol and 50μg/mL heparin (Robertson and Goldstein 1988; Nagayasu et al. 2005) (Sigma Aldrich, Poole, UK), were grown from DIV 7- DIV 28 for calcium imaging assessment.

4.2.3. Immunofluorescence and genetic analysis of purinoreceptors

Antibody	Type	Concentration	Source
P2YR1	Rabbit Polyclonal	1:250	Alomone Labs
P2X7	Rabbit Polyclonal	1:250	Alomone Labs
GFAP	Chicken Polyclonal	1:500	Aves
488	Anti-Rabbit	1:500	Alexa Fluor
594	Anti-Chicken	1:500	Alexa Fluor

Table 6: Antibodies used for immunofluorescence

Immunofluorescence was performed with same methodology as in previous chapter (see chapter 2). Cells were washed with PBS, at 7, 14, 21 and 28 DIV, fixed with 3.7% formaldehyde in PBS for 30 minutes, and permeabilised with 0.02% Triton X-100 diluted in 10% goat serum for 10 minutes. Subsequently, cells were washed with PBS and 10% goat serum was added to block against non-specific binding for 2 hours. Cells were then stained with anti- rabbit polyclonal P2YR1 (APR-009) and anti- rabbit polyclonal PX27R (APR-004) $P2X_7$ at 1:250 concentrations, and counterstained with anti-rabbit 488 polyclonal secondary antibodies (Table 6). Nuclei were counterstained with H-33342 (Hoechst dye). Images were taken using an Axio Imager microscope (Zeiss, Germany).

Polymerase chain reaction was performed as per previous conditioned described in chapter 2. The forward and reverse primer (see primer list) and template DNA was added, alongside nuclease-free water to make 50ul reaction for gel electrophoresis. Electrophorese was run on ethidium bromide agarose based gel at 100V for 40 min. 20μl of diluted markers/ladders was ran alongside, 20μl of sample per well. Data gel analysis

was performed using bespoke MATLAB algorithms (see appendix) and published algorithms via Image J. Furthermore, to confirm algorithm specificity gel densomitary for gel electrophoresis was performed.

4.2.4. Calcium Imaging of mESCDA

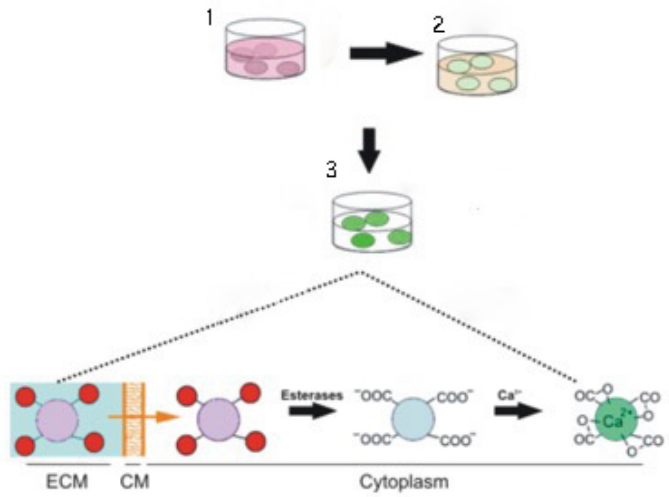

Figure 16: Fluo-4 AM is taken up by the cells and hydrolysed by endogenous esterases thereby rendering the dye fluorescent and sensitive to calcium. ECM= Extracellular medium, CM= Cell membrane. 1 - Astrocyte Medium, 2 - Fluo4 Calcium medium, 3 - HBBS buffer minus Fluo-4. Image adapted from https://www.embl.de/eamnet/html/calcium/dyes/fluorescentdyes3.htm

Calcium imaging was performed using Fluo-4 acetoxymethyl ester dye as it is easily taken up by the cells in the presence of Ca^{2+} and Mg^{2+} and exhibits high fluorescence with a Kd of 335 nM. Once inside the cell, the ester is hydrolysed by endogenous esterases, thereby making it fluorescent and sensitive to calcium (Fig. 16).

Prior to recording, coverslips from different DIVs were loaded with Fluo-4/AM (2.5 µM) within 1M HEPES Buffer, 1M $CaCl_2$, 2mM Bovine Serum Albumin (BSA) and double distilled water (ddH2O) for 30 minutes 37°C, 5% CO_2 (Molecular Probes) (Neary et al. 1999; Lock et al. 2015). Subsequently, post 30 minutes, cells were thoroughly rinsed with Hank's Balanced Salt Solution (HBSS) to remove extracellular traces of the dye and to complete de-esterification and incubated again for 30 minutes 37°C, 5% CO_2. Coverslips were then moved to the recording chamber and all fluorescence measurements were made at 37°C (Warner Instruments) with no CO_2 control for 5 minutes – 300 Seconds.

Excitation and emission wavelengths were 494 nm and 516 nm respectively. Changes in calcium were detected with an inverted Nikon Eclipse TE2000-S microscope (Nikon) equipped with a xenon arc lamp (Sutter Instruments). Imaging Workbench 6.0 (INDEC Bio- Systems) was used to control a Lambda 10-2 shutter system (Sutter Instruments).

4.2.5. Applications of compounds

Suramin hexasodium salt (suramin 100 μM) – General P2 anatgonist, N6-methyl-20-dexyadenosine-30,50- bisphosphate, tetraammonium salt (MRS 2179002050 μM) – P2YR1 antagonist, Brilliant Blue-G (BBG 50 μM) – $P2X_7$ antagonist and U73122 PLC blocker were obtained from Tocris Biosciences. ATP (50 μM), and Ionomycin (100 μM) were obtained from Sigma. Compounds were prepared as stock solutions as per manufactures guidelines and frozen in aliquots. When required, compounds were made up in HBBS. Post Fluo-4/AM, coverslips were incubated with the compounds for 30 minutes pre-recording and then washed three times with HBBS. The concertation of compounds ATP, and Suramin concentration were chosen from Hamilton et al 2008, whereas concentration of other compound concentrations were chosen based on previous experiments performed in the laboratory.

4.2.6. Data Analysis

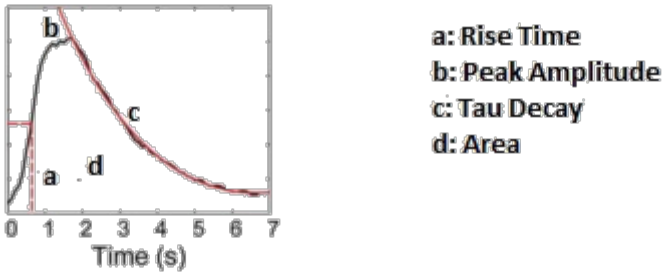

Figure 17: Breakdown of wave components for analysis of ATP evoked calcium dynamics.

Unless otherwise stated, ATP was applied after 30 seconds of background recording (to acquire baseline average fluorescence) at 50μM and was applied post incubation with compounds. Cells with unstable resting calcium in the baseline condition (i.e. fluctuations unlike normally observed calcium transients or a constantly rising baseline) were discarded. Astrocytes were identified at 488 nm excitation, and cell bodies within a single plane of focus were selected as regions of interest (ROI); several ROI were simultaneously recorded from in each experiment. The relative changes in calcium response to all stimulation were quantified as fold increase over baseline and was calculated for each trace and reported as ΔF/F0 (Macleod 2012). The signal was filtered using low pass filtering (Otsu et al. 2014). Area under curve (the area under the curve from the application of agonist till the end of experiment), rise time (10%-90% rise of curve), decay tau (peak maximum till decay curve was fit with the following equation $f(t) = a * \exp(-t/tau)$ and latency were analysed from each ROI and compared across astrocytes which had been treated with ATP (Kang & Othmer 2009; Okada et al. 2012; Hashioka et al. 2014) (Fig. 17). For compound treatment analysis, the fluorescent dynamics were compared against ATP application and peak differences between ATP agonist and purinoreceptors antagonists were measured. The peak response of an antagonist was expressed as a percentage of the response to ATP (denoted % peak change). Number of responding vs non-responding cells were also characterised.

All data analysis was performed offline and data assessed with Clampfit 10, WinFlour software packages (Strathclyde University) and modified MATLAB algorithms (see appendix). Experiments were performed in triplicates and for each of 7, 14, 21 and 28 DIVs. Multiple ROI (cell somata) were analysed n = 30 astrocytes per DIVs with the experimental n=4. Data are presented as means +/- SEM and the statistical differences were tested by ANOVA with Bonferroni's Multiple Comparison Test post-hoc test, or Mann-Whitney tests, where appropriate, using GraphPad Prism 6.0 (Graphpad Software, La Jolla, CA). Statistical significance was assumed when $P<0.05$)

4.3. Results

4.3.1 Expression of purinergic receptors in mESCDA

Calcium oscillations and waves in astrocytes are one of the most well-studied mechanisms for the cells to respond to various stimuli and a mode of intra as well as intercellular signalling (Fiacco & Mccarthy 2004; Rusakov et al. 2014). After having established a methodology to generate mESCDA, it was essential to assess whether mESCDA are functionally mature and are able to respond to the environmental cues as expected. This was done via assessing their calcium dynamics through Adenosine triphosphate (ATP - 50 μM) stimulation of Fluo-4 loaded mESCDA. Prior to calcium dynamics assessment, it was essential to evaluate purinergic receptor expression within the mESCDA. During protocol establishment, purinergic receptors P2YR1 and $P2X_7$ were temporally examined (from DIV7-28) via reverse transcriptase-PCR (see chapter 2). Expression of these genes was up-regulated throughout temporally. Differences between DIV 7/DIV14 and DIV 28 were statistically significant between of: P2YR1: (At DIV 7 Fig 18. 36.81%±3.01%, N=3 - DIV 28, Fig 18. 176.27% ± 13.11%, N=3, $p<0.05$) $P2X_7$: (Fig18. At DIV 7 Fig 14. 2.27%±0.88%, N=3 - DIV 28 Fig 18. 27.93%±4.12%, N=3, $p<0.001$).

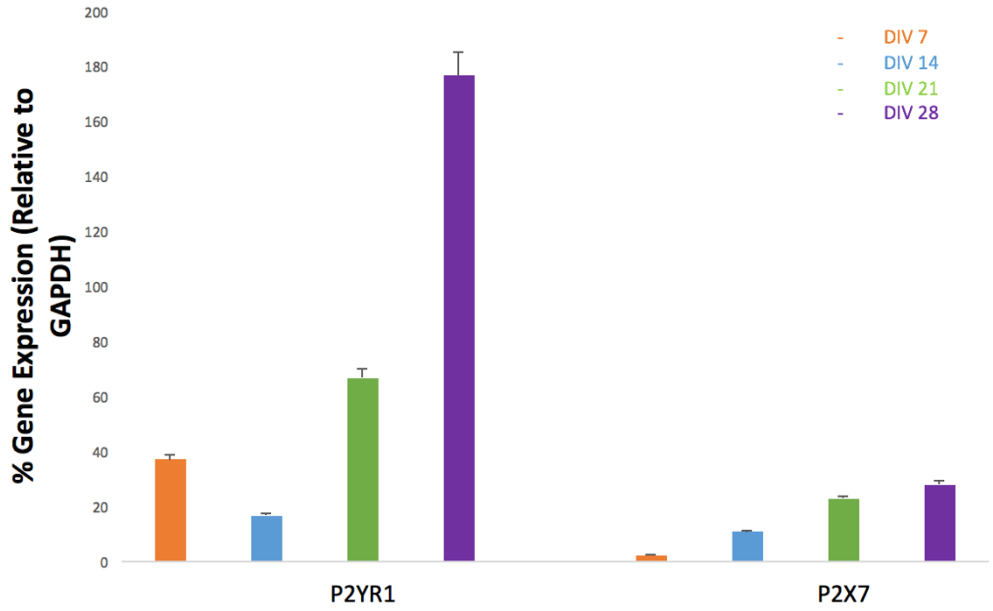

Figure 18: Generation of and development of purinergic receptors in mESCDA. Data are given in percent expression relative to the housekeeping gene Gapdh. (A) P2YR1 expression (B) $P2X_7$ expression across DIVs. All data are expressed as mean ± SEM from three separate experiments, *P < 0.05, **P < 0.01, ***P < 0.001) ANOVA with Bonferroni's Multiple Comparison post-hoc tests

In addition to genetic assessment, it was essential to elucidate protein expression and localisation of the receptors within mESCDA. Temporal immunostaining (DIV 7-28) for both P2YR1 and P2X7 receptors revealed mESCDA reliably expressing both purinergic receptors, confirming genetic analysis (Fig 18-21). The upregulation of receptor was visible in fluorescence images acquired, moreover, looking at co-localisation staining revealed both receptors are expressed in regions occupied by GFAP positive staining (Fig. 19-21). Although, some receptors staining is also visible outside of GFAP positive stains, signifying purinergic receptor expression occurring in GFAP negative mESCDA (Fig 18 -21).

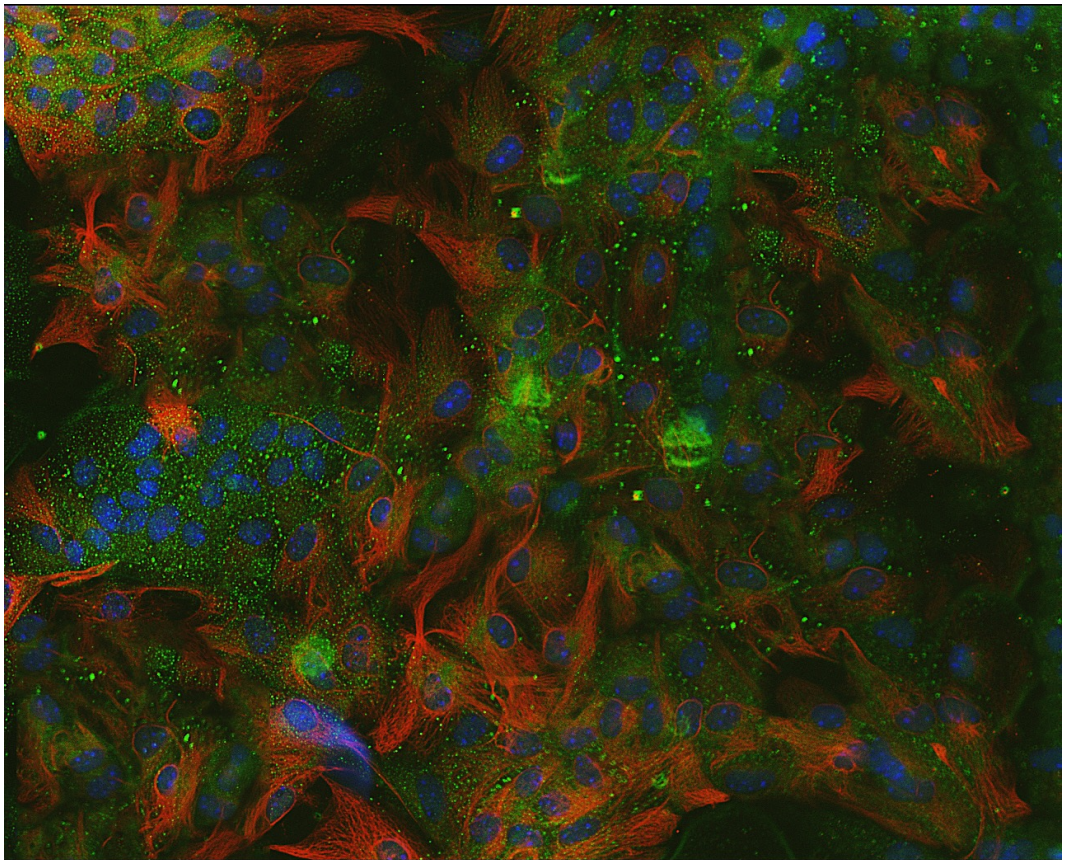

Figure 19: Immunocytochemical phenotyping of purinergic receptors. P2YR1 receptors at DIV 28, immunofluorescent labelled for established astrocytic marker P2YR - green and GFAP – red. Cultures have been counterstained for cell nuclei marker H- 33342 (blue stain). Scale bar = 20μm, image acquired at x20 magnification.

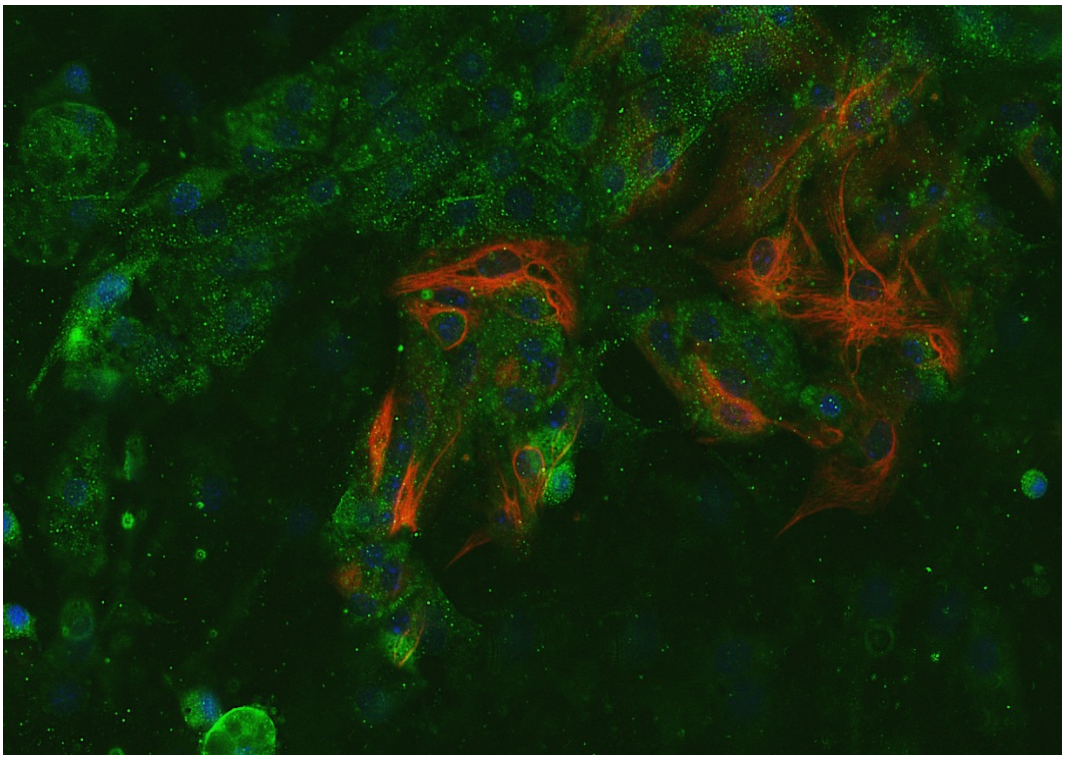

Figure 20: Immunocytochemical phenotyping of for purinergic receptors. P2X7 receptors at DIV 28, immunofluorescent labelled for established astrocytic marker P2X7 - green and GFAP – red. Cultures have been counterstained for cell nuclei marker H- 33342 (blue stain). Scale bar = 20µm, image acquired at x20 magnification.

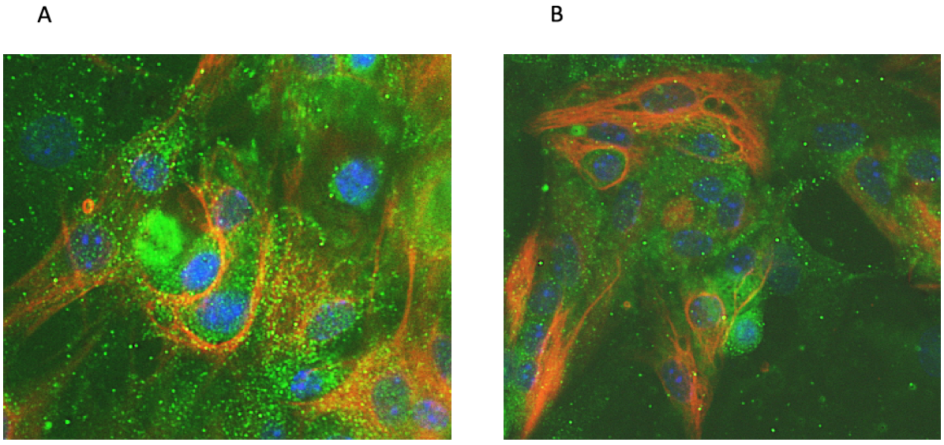

Figure 21: Immunocytochemical images of DIV 28 astrocytes at x40 magnification for (A) P2YR1 receptors –(B) P2X7 receptors - green and GFAP - red. Cultures have been counterstained for cell nuclei marker H- 33342 (blue stain).

4.3.2. Application of ATP leads to calcium transients in mESCDA

A time-lapse sequence of a 5-minute recording is illustrated in figure 22, where calcium concentration in multiple regions of interest (e.g. middle right and middle left) increases (from 30 to 60 seconds) and returns to initial levels (from 90 to 300 seconds). Furthermore, heatmap also revealed that evoked activity travels in a wave-like manner across the regions of interests (ROI) (Fig. 22). Evoked calcium transients displayed a temporal rise, a peak and decay phase post peak, which was expected due to responses seen *in vivo,* a hallmark of astrocyte function (Bazargani & Attwell 2016; Shigetomi et al. 2016). This kinetics varied across DIVs (Fig 24), Indicating this variety and heterogeneity in response can be linked to heterogeneity in expression of purinergic receptors (Fig. 18), and may also linked to increase in response of these cells – indicated by the significant decrease in number of cells responding across the DIVs (Fig. 19-21) (DIV 7 – 20% to DIV 28 – 5%).

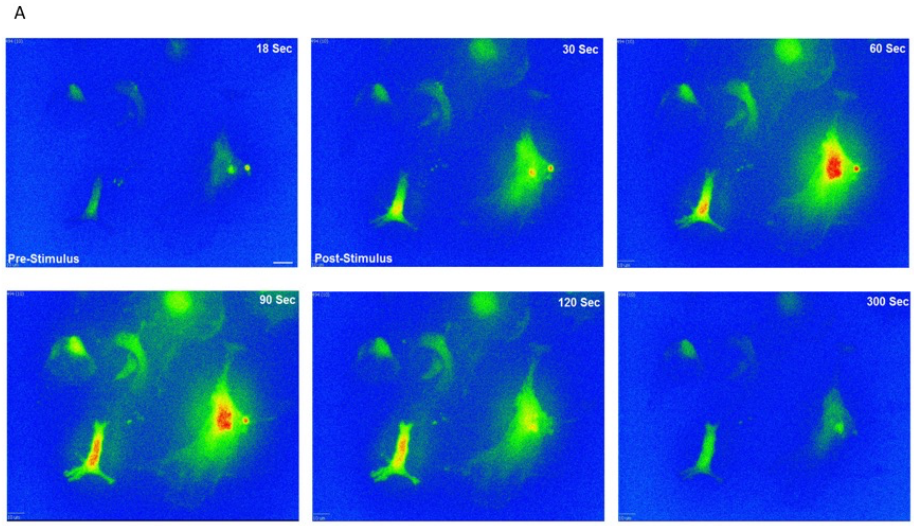

Figure 22: Calcium waves of ATP evoked mESCDA. (A) Heatmap of Fluo4 treated, activated astrocytes when evoked via ATP, starting with pre-stimulus, ending with 300 seconds- end of experiment.

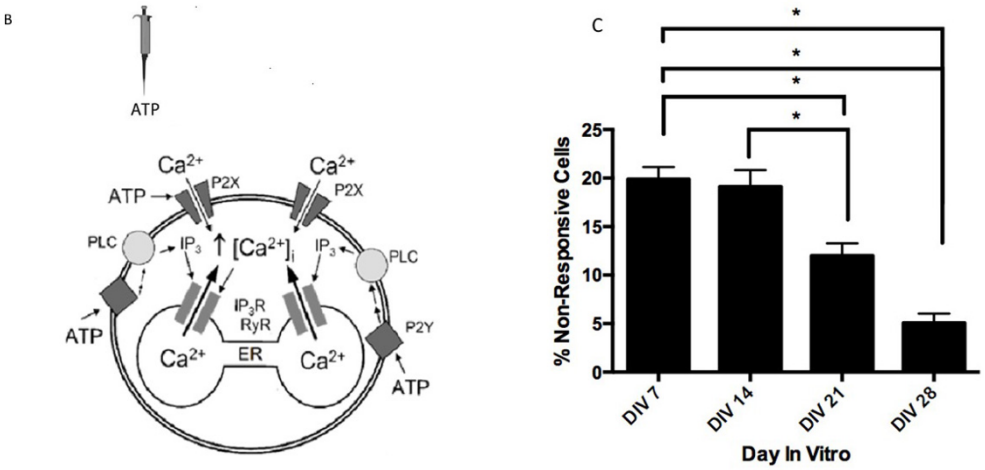

Figure 23: Activation of purinergic pathways within mESCDA. Schematic representation of intracellular processes within astrocytes (B) when purinergic receptors are activated. (B) Number of responsive v/s nonresponsive cells increasing across DIVs. Analysis performed by ANOVA with Bonferroni's Multiple Comparison post-hoc statistical tests.

Heatmap observation revealed cells which do not respond to the exogenous application of ATP, therefore it was essential to assess the number of responsive and non- responsive cells temporally across the cultures. Quantification of the percentage of astrocytes displaying Ca^{2+} transients showed a significant decrease in percent (%) of non-responding cells as we progressed through the DIVs, from approximately 20% at DIV 7 to approximately 5% at DIV 28 (Fig. 19C), revealing temporal changes lead to changes maximal affinity of purinergic receptors (Kuntz et al 1999).

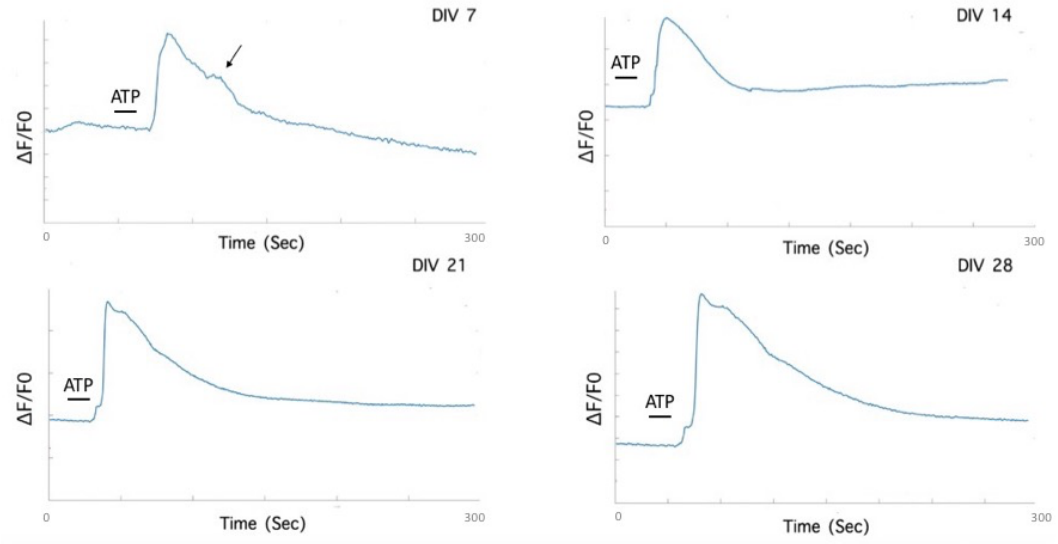

Figure 24: Representative ATP evoked responses of mESCDA. Purinergic response calcium waves from evoked ATP across different DIVs (DIV 7-28) reveal differences in calcium dynamics, the transients are mono and bi-phasic in nature (black arrow at DIV 7 showing bi-phasic response).

Evoked calcium transients displayed a temporal rise, a peak and decay phase post peak, which was expected due to responses seen *in vivo,* a hallmark of astrocyte function (Bazargani and Attwell 2016; Shigetomi et al. 2016). This kinetics varied across DIVs (Fig 24), Indicating this variety and heterogeneity in response can be linked to heterogeneity in expression of purinergic receptors (Fig. 18), and may also linked to increase in response of these cells – indicated by the significant decrease in number of cells responding across the DIVs (Fig. 23) (DIV 7 – 20% to DIV 28 – 5%).

4.3.3 Characterisation of intracellular calcium pool

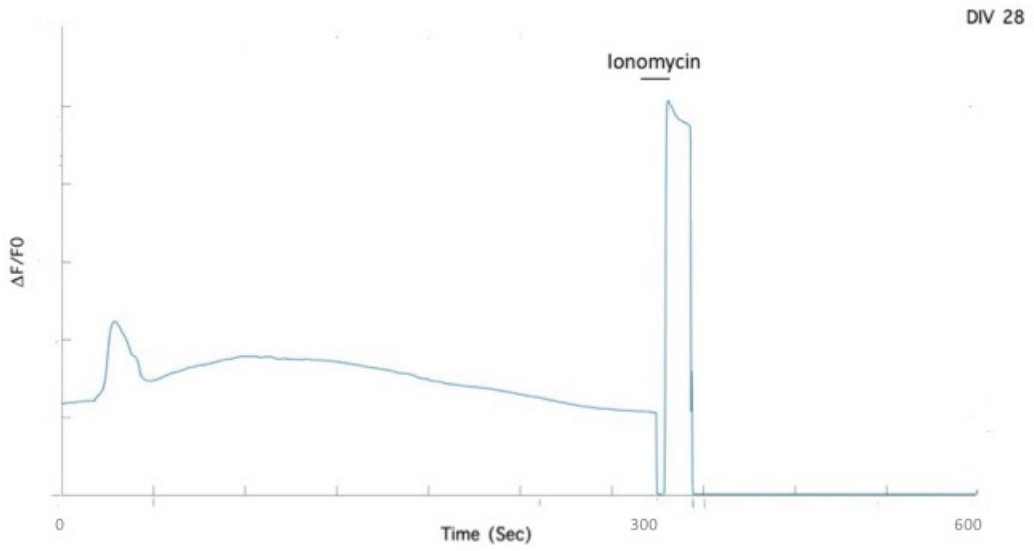

Figure 25: All or nothing response from mESCDA. Application of Ionomycin at the end of the experiment 300 seconds (DIV 28) reveals intracellular stores responsible for evoked calcium transients.

The role of intracellular calcium dynamics being responsible for the observed calcium wave was further confirmed by the application of Ionomycin – a calcium ionophore (Muller et al 2013). Application of 100 μM triggered a phasic increase in cytosolic calcium post ATP evoked calcium transient (Fig. 25). Post application there was a peak which was significantly different from ATP evoked calcium transients. This indicated an all or nothing response and this has occurred due to release of calcium within the intracellular (cytosolic) stores – via IP_3 mediated release (Sherwood et al 2017). The results here confirming involvement of intracellular calcium in the observed ATP induced calcium dynamics (Fig 22).

4.3.4 Temporal analysis of calcium transients

After solidifying that the evoked calcium dynamics occurred mainly due to changes in cytosolic calcium, and were not noise, the Ca^{2+} waveform was decomposed into different components: decay tau, area under the curve (AUC), and rise time (RT). The latency between the application of ATP and the rise in intracellular Ca^{2+} concentration was also assessed (Bernstein et al. 1998).

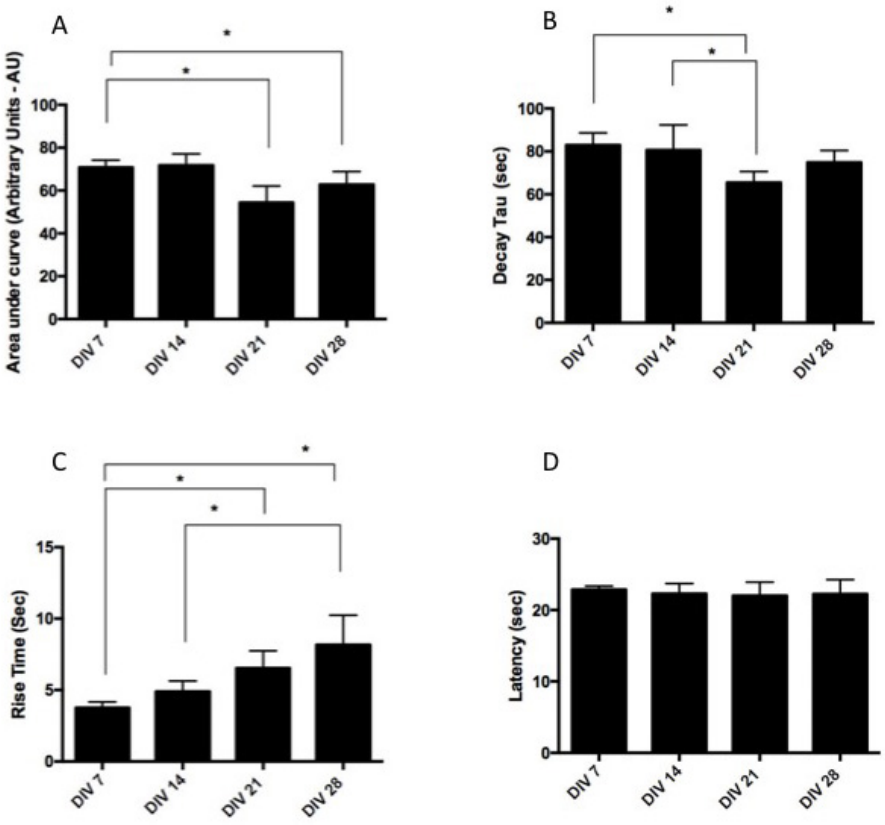

Figure 26: Components of ATP evoked calcium dynamics. Analysis of individual components in ATP evoked calcium transients. From left to right - (A) Area under curve (AUC), (B) decay tau (Tau), (C) rise time (RT), and (D) latency of n = 30 astrocytes reveals heterogeneity in response. All data are means ± SEM from three experiments. n.s., no significant difference (P > 0.05); *P < 0.05, **P < 0.001 ANOVA with Bonferroni's Multiple Comparison post-hoc tests

There was a significant ($p<0.05$) increase in rise time of DIV 7 (Fig. 26C: 3.75s ± 0.202s, n=3) astrocytes when compared to DIV 21 (Fig. 26C: 5.81 ± 0.73s, n=3) and DIV28 (Fig. 26C: 6.04s ± 0.56s, n=3), alongside significant increase when comparing DIV 14 (Fig. 26C: 4.01 ± 0.61s, n=3) to DIV 28 (Fig. 26C: 6.04s ± 0.56s, n=3). Area under the curve

revealed a significant reduction in response of DIV 21 (Fig. 26A: 54.38 ± 2.56s, n=3) and DIV 28 (Fig. 26A: 62.08 ± 4.51s, n=3) when compared to DIV 7 (Fig. 26A: 70.76 ± 5.11s, n=3), revealing a change in number of calcium trafficked in and out of the cell as the cultures matures. The ability to clear the amount of calcium measured via decay tau significantly decreases at DIV21 (Fig. 26B: 65.42 ± 13.56s, n=3) when comparing DIV 7 (Fig. 26B: 82.95 ± 11.16s, n=3) and DIV 14 (Fig. 26B: 80.66 ± 22.21s, n=3) with a decreasing trend at DIV 28. The latency of response of ATP remains the same across DIVs (around 22 Seconds) (Fig. 26D). These temporal changes in astrocyte components show that there is heterogeneity in the response similar to heterogeneity in receptor expression and marker expression seen previously.

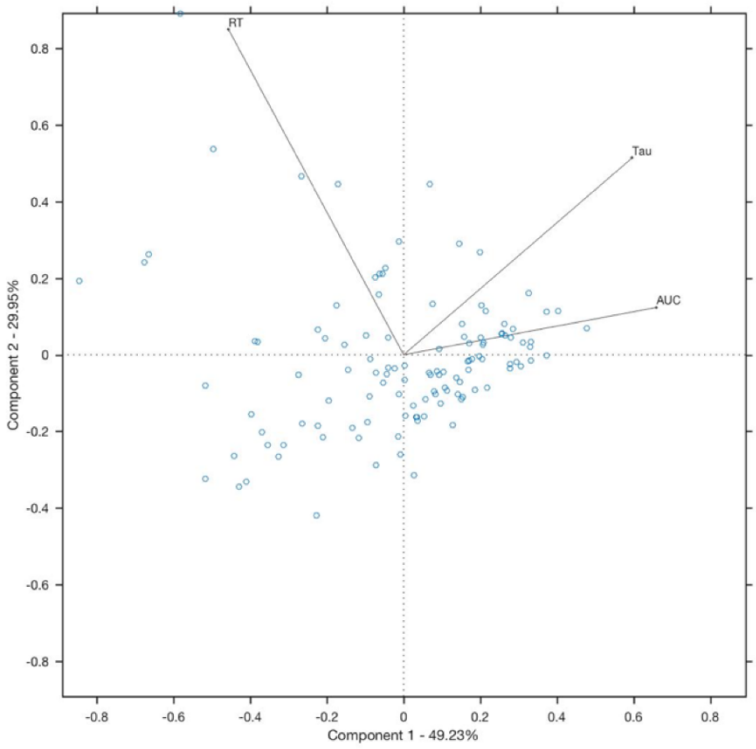

Figure 27: Individual components responsible for calcium dynamics in mESCDA. Principle component analysis (PCA) reveals the major contributors in calcium waves. AUC and Tau are linked with similar directionality, whereas RT is an individual component with its own directionality.

In addition to the above, to further understand which of these different components contribute majorly towards calcium dynamics, principal component analysis (PCA) was performed (Fig. 27). PCA displayed 2 major components: where AUC and decay tau contributing towards one component (around 49.23% contribution together), and RT

contributing towards the second component (around 29.95% contribution alone) demonstrating the involvement of each component towards the calcium wave. Previous evidence has displayed P2YR1, and $P2X_7$ contribute towards RT and Decay tau respectively (Hamilton et al. 2008), therefore to further clarify which receptor is the major contributor towards evoked calcium response, receptor-specific antagonists are required.

4.3.5 Phasic responses in calcium transients dictate the involvement of different purinergic receptors

The evoked calcium transients due to activation of purinergic receptors display either monophasic (Fig. 28A, average traces) or biphasic (Fig. 28B, average traces) response in the decay phase depending on whether there was a sustained response after the half-amplitude of peak response. The percentage of monophasic and biphasic responses varied across different days *in vitro*. Temporal analysis revealed that majority of responding mESCDA display responses, with a slight decrease at DIV 21 from >90% at DIV 7, to >65% at DIV 21 (Fig. 29).

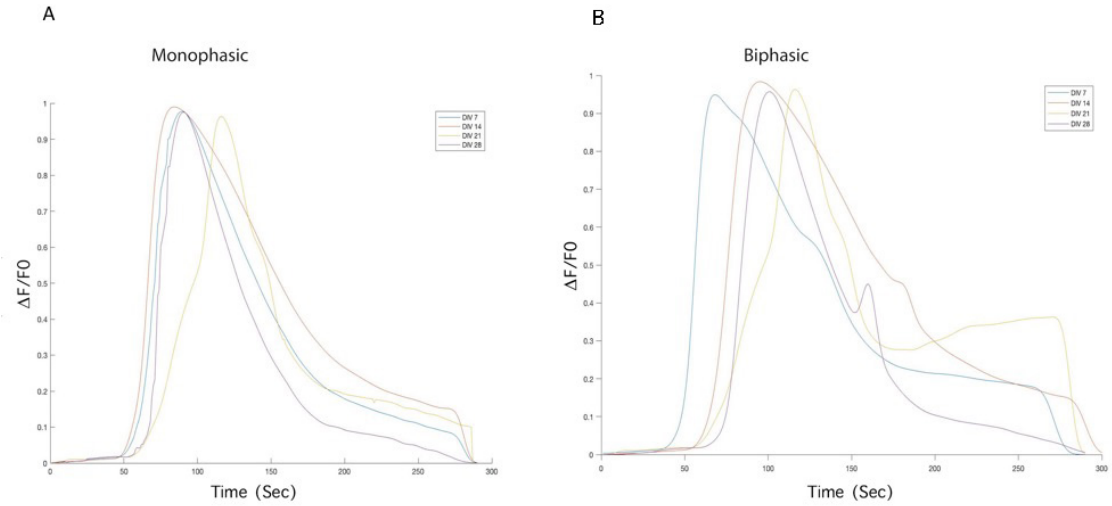

Figure 28: Mono and bi-phasic responses of mESCDA. Average calcium dynamics of ATP evoked calcium transients across DIVs (DIV 7-28) where (A) displays monophasic and (B) displays bi- phasic calcium response.

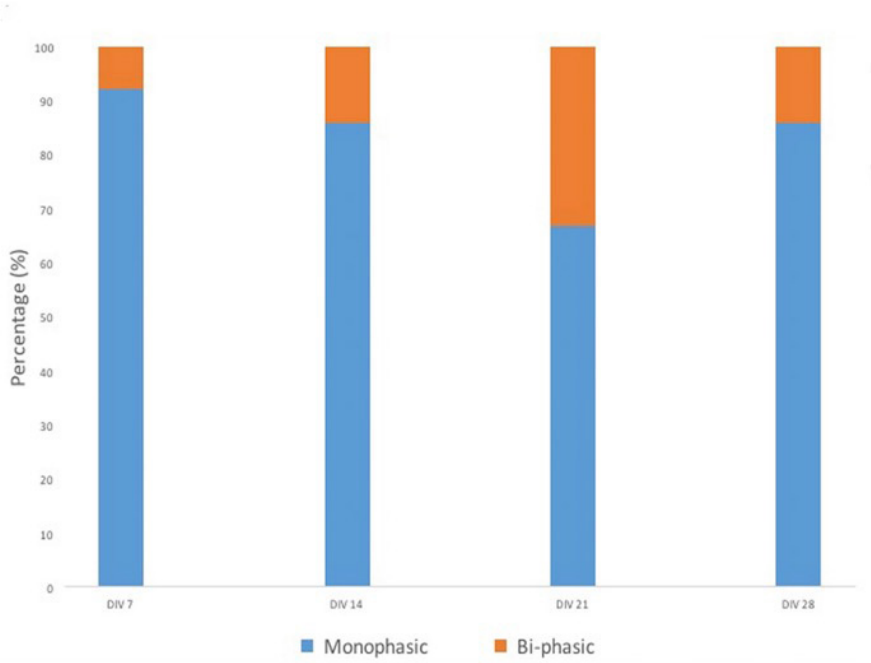

Figure 29: Percentage of monophasic v/s biphasic cells across DIVs

4.3.6 Identification of principle purinergic pathway involved in calcium transient

To identify the principle pathway/s involved in the generation of evoking calcium transient, it was essential to utilise compounds which were selective for specific receptors and pathways (Petravicz et al. 2008). Since ATP is a non-selective P2 purinoceptor agonist, initially non-selective antagonists were utilised. Prolonged bath application of the broad-spectrum P2 antagonist suramin (at 100 μM) reduced evoked calcium transients.

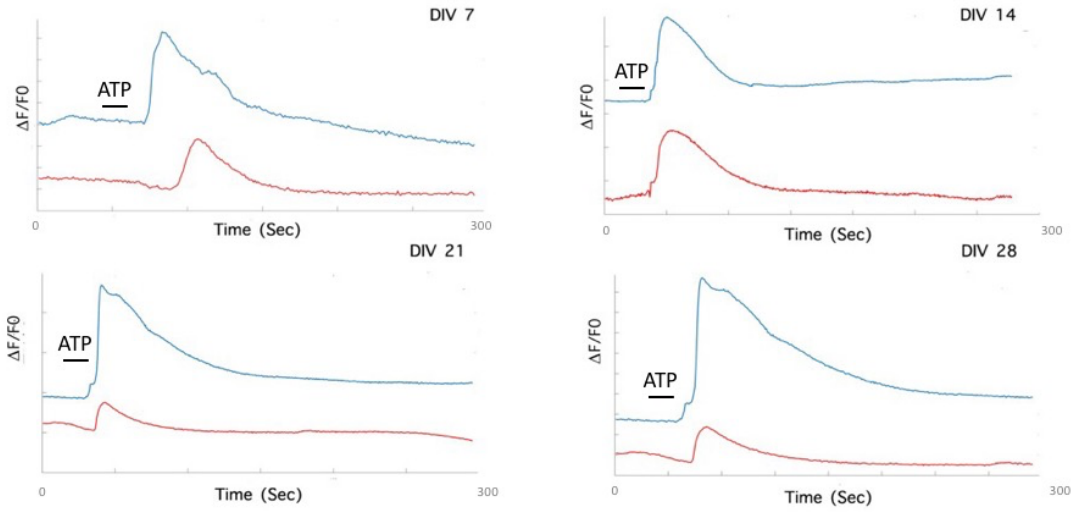

Figure 30: Suramin reveals involvement of purinergic receptors in mESCDA calcium dynamics. Bath incubation of mESCDA with suramin reveal stunted calcium dynamics across DIVs (DIV 7-28) confirming involvement of intracellular dynamics and purinergic receptors in mESCDA calcium dynamics. Red trace – suramin treated dynamics, blue trace – non suramin treated dynamics of representative traces.

Although the signal profile of the evoked calcium responses was similar (Fig. 30), the signal responses were stunted, at DIV 21 and DIV 28 (Fig. 30). This was further confirmed via peak difference analysis, where the peak of ATP was compared to the peak of suramin. The peak differences showed a stepwise reduction in peaks, with a significant reduction mainly at DIV 21 (Fig. 30: 50.02 ±2.71 n=4, $p<0.05$) and DIV 28 (Fig. 30: 58.8± 3.15 n=4, $p<0.05$). when compared to ATP. There was a 50% reduction in signal at DIV 21, with a slight return at DIV 28.

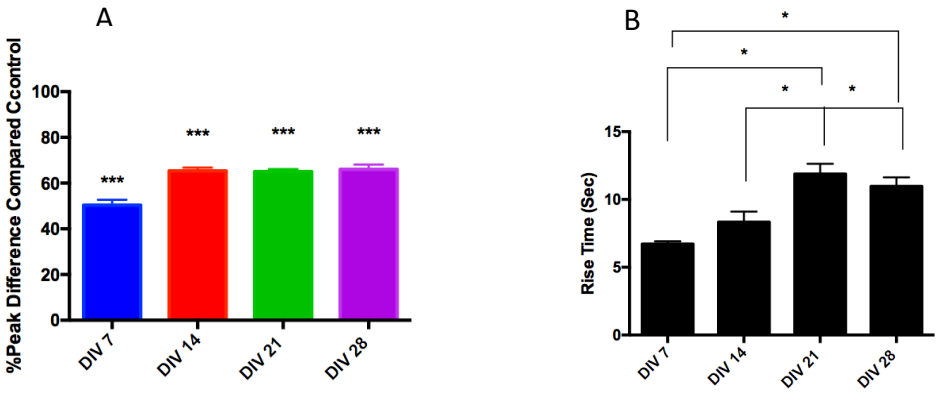

Figure 31: Suramin treated mESCDA. (A) Percentage peak differences was measured between suramin and non suramin treated mESCDA. Assessment show significant difference across DIVs (mainly later DIVs) when compared to control. (B) Rise time (RT) of n = 30 astrocytes from 3 separate experiments. All data are means ± SEM from three experiments. n.s., no significant difference ($P > 0.05$); *$P < 0.05$, **$P < 0.001$ ANOVA with Bonferroni's Multiple Comparison post-hoc tests.

There was a significant ($p<0.05$) increase in rise time of DIV 7 (Fig. 30B: 6.71s ± 0.192s, n=3) astrocytes when compared to DIV 21 (Fig. 30B: 1.43 ± 0.73s, n=3) and DIV28 (Fig. 30B: 11.88s ± 2.06s, n=3), alongside significant increase when comparing DIV 14 (Fig. 30B: 8.33 ± 2.11s, n=3) to DIV 28 (Fig. 30B: 11.88s ± 2.06s, n=3). Collectively, these results add support to the tenet that in mESCDA ATP induced transient calcium elevation and the calcium decay are dependent on the activation of different subtypes of P2 purinoceptors and suggest that the sustained calcium signalling is mediated by activation of calcium-permeable $P2X_7$-like receptors.

4.3.7. P2X7 provides minor contribution to purinergic calcium dynamics

Having established that purinergic receptor mechanisms in the generated mESCDA contribute to the calcium dynamics, receptor-specific antagonists to block the signalling pathways were used. Initially, contributions of the $P2X_7$ receptor were assessed. Bath incubation of mESCDA with the $P2X_7$ antagonist, BBG (50 µM), revealed no significant changes in evoked ATP calcium transients (Fig. 32).

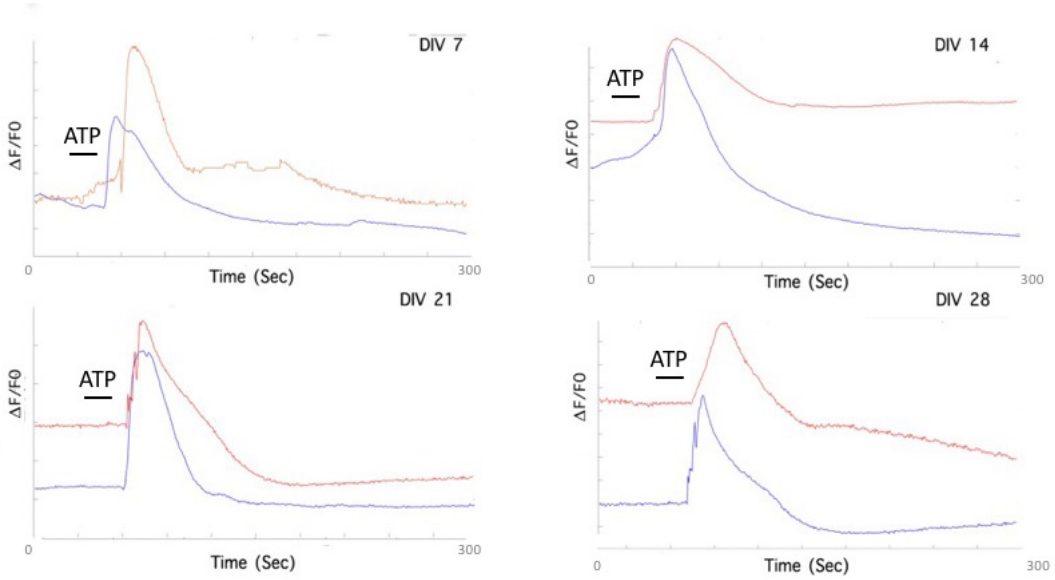

Figure 32: BBG reveals involvement of P2X7 receptors in calcium dynamics. Bath incubation of mESCDA with BBG reveals attenuated calcium dynamics across DIVs (DIV 7-28). Red trace – BBG treated dynamics, blue trace – non BBG treated dynamics of representative traces.

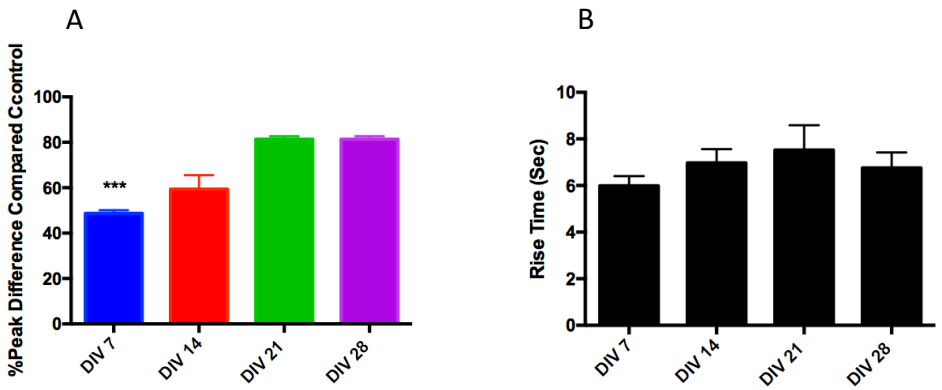

Figure 33: BBG treated mESCDA. (A) Percentage peak differences was measured between BBG and non BBG treated mESCDA. Assessment show significant difference at DIV 7 when compared to control. (B) Rise time (RT) of n = 30 astrocytes from 3 separate experiments. All data are means ± SEM from three experiments. n.s., no significant difference ($P > 0.05$); *$P < 0.05$, **$P < 0.001$ ANOVA with Bonferroni's Multiple Comparison post-hoc tests

A temporal inspection revealed a reduction in baseline and an attenuated response (Fig. 32), however, the reduction in signal was less pronounced when compared to suramin. There was no difference in rise time, where peak difference analysis of BBG treated cells revealed a significant reduction in the peak at DIV7 (Fig. 33: 53.11 ± 2.11 n=4), when compared to ATP, with an increase in peaks comparable to control at later DIVs (DIV 14-28). Further to this, a closer examination of the calcium kinetics revealed changes in decay tau when compared to ATP responses, but these could be due to noise or artificial signals due to summation of many signals in figure (Fig. 32). The results here show some involvement of the $P2X_7$ receptor in calcium dynamics and involvement of $P2X_7$ receptor involvement in calcium response of mECSDA.

4.3.8. P2YR1 contributes majorly towards mESCDA calcium transients

P2YR1 plays a prominent role in the rise time component in calcium kinetics (Zhu & Kimelberg[2] 2001; James & Butt 2001). Furthermore, metabotropic signalling and downstream pathways have been majorly linked with astrocyte calcium dynamics and further changes brought to the CNS via astrocyte calcium signalling (Martin et al. 2015). Therefore, it was essential to assess whether generated mESCDA responded to ATP via the activation of P2YR1 and the subsequent pathway. To test this, MRS2179: P2YR1 antagonist was used to selectively inhibit receptor specific response.

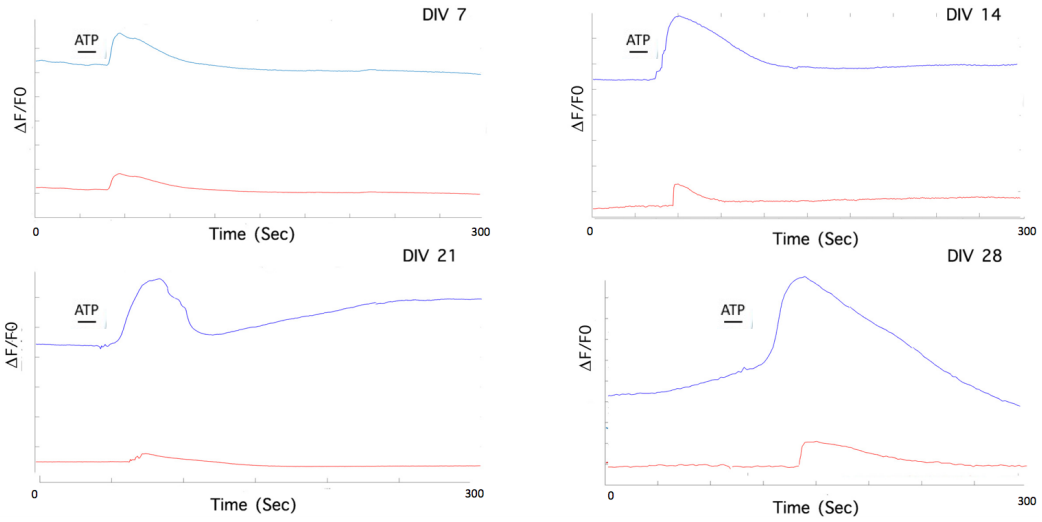

Figure 34: MRS2179 reveals involvement of purinergic receptors in mESCDA calcium dynamics. Bath incubation of mESCDA with MRS2179 reveals stunted calcium dynamics across DIVs (DIV 7-28). Red trace – MRS2179 treated dynamics, blue trace – non MRS2179 treated dynamics of representative traces.

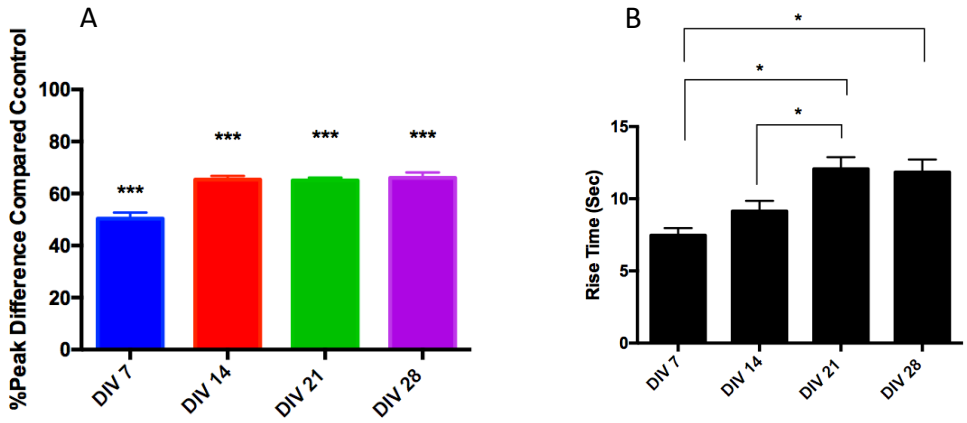

Figure 35: MRS2179 treated mESCDA. Percentage peak differences was measured between MRS2179 and non MRS2179 treated mESCDA. Assessment show significant difference at across DIVs (DIV 7-28) compared to control. All data are means ± SEM from three experiments. n.s., no significant difference ($P > 0.05$); *$P < 0.05$, **$P < 0.001$ ANOVA with Bonferroni's Multiple Comparison post-hoc tests

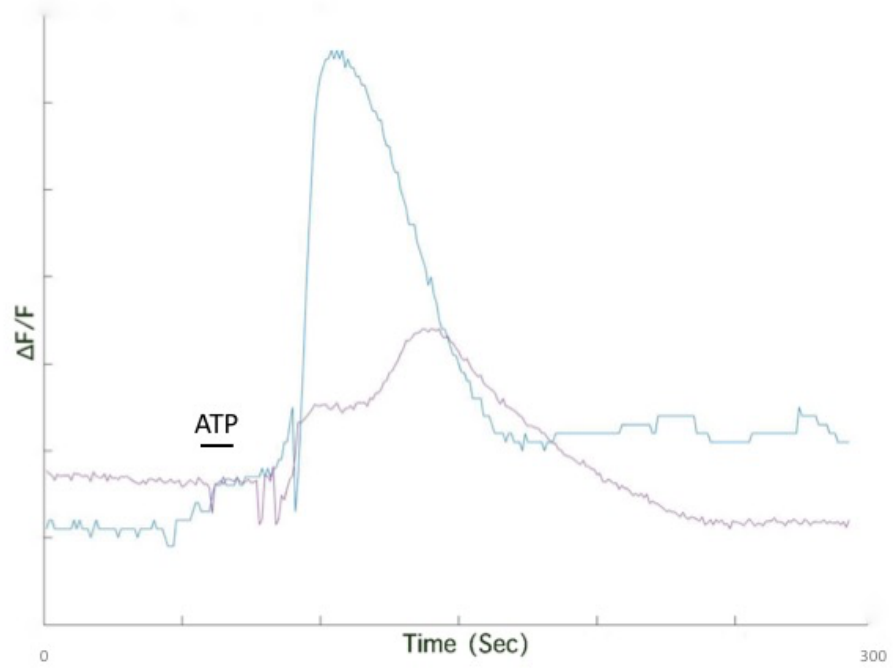

Figure 36: Inhibition of downstream PLC reveals involvement Gq-GPCR/PLC/IP_3 signalling in mESCDA calcium dynamics. Bath incubation of mESCDA with U73122 reveals stunted calcium dynamics at DIV 28. Purple trace – U73122 treated dynamics, blue trace – non U73122 treated dynamics.

The response to ATP was significantly and reversibly inhibited by the P2Y1 receptor antagonist MRS2179. Observing the calcium kinetics across the DIVs, there were a significant attenuation and dampening of the response – similar to the effect of suramin responses. There was a significant ($p<0.05$) increase in rise time of DIV 7 (Fig. 35B: 7.46s ± 1.10s, n=3) astrocytes when compared to DIV 21 (Fig. 35B: 12.06 ± 2.13s, n=3) and DIV28 (Fig. 35B: 11.84s ± 2.56s, n=3), alongside significant increase when comparing DIV 14 (Fig. 35B: 9.14 ± 1.92s, n=3) to DIV 21 (Fig. 35B: 11.84s ± 2.11s, n=3). Comparison of peak differences revealed a significant difference across the DIVs (Fig.33A). There was a significant decrease in peaks across all of the DIVs, DIV 7 (Fig. 35A: 53.02 ± 1.33 n=4, $p<0.05$), DIV 14 (Fig. 35A: 64.66 ± 2.01 n=4, $p<0.05$), DIV 21 (Fig. 35A: 63.66 ± 1.13 n=4, $p<0.05$) and DIV 28 (Fig35A. 33: 65.01 ± 3.15 n=4, $p<0.05$), with majority of the significant difference occurring at DIV 7 (Fig. 35: 53.02 ± 1.33 n=4, $p<0.05$). The results revealed P2YR1 as a major contributor towards evoked ATP signalling observed within mESCDA.

4.4. Discussion

In the brain, astrocytes are associated intimately with neurons and surround synapses. Due to their close proximity to synaptic clefts, astrocytes are in a prime location for receiving synaptic information from released neurotransmitters. Evidence *in vitro* and *in vivo* has shown that astrocytes express all of the neurotransmitter receptors and respond to neuronal transmitter release by further releasing their own transmitters – termed gliotransmitters (Michael M. Halassa et al. 2007; Volterra et al. 2015). As astrocytes are electrically passive cells, they mediate the changes and response via elevating their intracellular calcium levels (Khakh et al. 2015). Therefore, it was essential to test whether the generated mESCDA a) possessed the necessary receptors (mainly purinergic) b) possessed the ability to respond to the environmental niche via responding to exogenous transmitters c) possessed the ability to display calcium transients d) whether these transients were due to response to their environment.

The purinergic signalling system is, arguably, one of the main extracellular signalling system that integrates neuronal-glial and glial–glial circuits in the nervous system (Pascual et al. 2005). Adenosine 5'-triphosphate (ATP), which is the principal purinergic signaller, is released from cells by several mechanisms, such as exocytosis, diffusion through plasmalemmal channels and transporters mediated release. In addition, ATP is released also released from pathological astrocytes, as an immunocompromised signal response. Evidence has shown that purinergic signalling mediates reciprocative signalling between neurons and astrocytes (Fields & Stevens-Graham 2002). For example, Hassinger et al 1996 displayed extracellular ATP being involved in mediating calcium waves which propagate in situ, showing purines and pyrimidines provide for multiple signalling pathways within the astrocytic network, and are responsible for mediating calcium waves (Burnstock 1978; Hassinger et al. 1996; Hamilton et al. 2008). The family of purinoceptors is coupled with numerous dowsntream signalling cascades such as calcium or metabolites pathways which governing astrocytes physiological and pathological responses, therefore purinergic signalling was chosen to be scrutinised within the generated mESCDA.

The functional ATP responses that hinted at several receptor classes were recognized rather early. Burnstock & Kennedy (1978) proposed the first clear subdivision of P2 purinoceptors into P2X purinoceptors and P2Y purinoceptors (Burnstock 1978) Recent accumulation of evidence has indicated that ATP mediated calcium changes within astrocytes are brought about mainly via P2YR1 and $P2X_7$ receptors (Scemes & Giaume

2007; Suadicani et al. 2009). Furthermore, based on evidence from pioneering studies from Centimeri et al 1997, James and Butt 2001, and Sudacani et al 2009, these two main subtypes of purinoreceptors are responsible for the majority of purinergic signalling occurring within astrocytes (Centemeri et al. 1997; James & Butt 2001; Suadicani et al. 2009).

Genetic assessment on P2YR1 and $P2X_7$ revealed temporal changes in expression, where both P2YR1 and $P2X_7$ expression mainly increased across DIVs (Fig.18). This observed increase in receptor expression may be due to the result of increased proliferation and differentiation of astrocytes as observed within mESCDA (see chapter 2). Further to this, purinergic receptor expression is also visible in GFAP negative cells (Fig. 15-17). This further confirms ubiquitous expression of the receptors in generated mESCDA. Chick and murine assessments of purinergic receptors show expression of receptor $P2X_7$ at E18 and P2YR1 at E10 and this subsequently increases until adulthood where it reaches a plateau (Majumder et al. 2007; Burnstock et al. 2010). Furthermore, *in vitro* studies have shown increased expression of each receptor as the culture matures, as each receptor performs its functions such as proliferation, cell growth and mitogenic signalling leading to accelerated differentiation (Burnstock et al. 2010). For example, Tsao et al 2013 show upregulation of P2 receptors during development of mice, and their involvement in neurogenesis and gliogenesis via intracellular signalling cascades (Tsao et al. 2013). The results here agree with the literature and show purinergic receptor expression increases during development. However, on closer inspection, the P2YR1 receptor expression display a dip in expression at DIV 14. This may be due to culture conditions such as changes in developmental regulation, changes in glucose and energy metabolism, or changes in differentiation patterns to match the demands of the culture, as observed previously via S100B expression. However, this has not been reported elsewhere. Further to this, the P2YR1 expression comparatively was more that $P2X_7$ expression – comparatively across DIVs (Fig.21). The reduced in expression in $P2X_7$ shows that developed mESCDA are not reactive in nature. Evidence has shown that increased expression of $P2X_7$ has shown to occur mainly in pathological conditions and cause the release of proinflammatory cytokines and nitric oxide leading to diseases such as multiple sclerosis (Zou et al. 2011; Amadio et al. 2017). This genetic assessment was further confirmed via immunostaining, and these results here showed receptors are indeed expressed during development. Both P2YR1 and $P2X_7$ showed reliable staining and also showed co-localisation with astrocytes – shown via GFAP positive staining (Fig. 17). The results provided here display novelty in terms of receptor expression in stem cell derived astrocytes. The temporal assessment of these receptors within stem cell derived astrocytes

(mainly mouse) has not been performed. Although studies do provide a detailed genetic profile of stem cells derived astrocytes (Krenick et al. 2011; Zhang et al. 2016), they only utilise one time point and set this as a basis of future studies. Therefore, a detailed temporal analysis of receptors, is needed when trying to set out any future functional studies.

4.4.1. Purinergic assessment of mESCDA

Developed astrocytes were successfully loaded using Fluo-4 AM and agreement with the previous literature (Parri et al. 2001), the majority of the Fluo-4-loaded cells exhibited astrocytic morphology – extensive branching and elaborate morphology (Fig. 20). Astrocytes display both spontaneous and evoked intracellular calcium increases. Evoked calcium responses have been extensively studied using a variety of stimulation protocols such as mechanical and evoked (pharmacological) (Venance et al. 1997; Hamilton et al. 2008). Therefore, for comparative analysis here the developed mESCDA were tested for their ability to display evoked (pharmacological) calcium transient via ATP application.

Application of ATP displayed clear transients across the DIVs (Fig. 22). These transients had a rise phase, a peak response and a decay phase. These responses were analogous to primary (Fig. 48) (Nobile et al. 2003; Hamilton et al. 2008) and other stem derived astrocytes (Zhang et al. 2016; Lundin et al. 2018) in which they also showed a clear rise and decay phase, showing the mESCDA are functional and readily respond to their environment. The temporal assessment showed that the number of astrocytes which did not respond decreased significantly, indicating that temporal maturity in culture leads to increased functionality (Khakh et al. 2015). This increased in functionality could be due to developmental maturity of the cultures, as astrocytes begin to stably express the majority of the astrocyte specific genes (see chapter 2) which are involved in mediating astrocyte function (IP3R2, GJB6), or increased number of receptors subsequently increased binding sites for ATP (Fig. 21B). Additionally, the intracellular machinery of astrocytes, such as downstream pathways which lead to elevation of calcium from intracellular stores also gains complexity and intricacy, and these reasons could be related to increased responses in astrocytes across the DIVs.

Although no direct evidence exists which displays and compares temporal changes in the functional response of purified astrocyte cultures from stem cells, co-culture studies have shown that developmentally increased numbers of astrocytes have shown to respond as culture matures. For example, Shtrahman et al 2017 showed that astrocytes began to

show increased calcium activity when cultured with neurons and this activity increases as the cultured matured (Shtrahman et al. 2018). Furthermore, this increased in functionality across DIVs may be occurring due to stimulation mitogen-activated protein kinases which lead to increased 'readiness' in astrocytes to respond to external stimuli(Lundin et al. 2018) .

Closer inspection of the calcium transients reveal the ATP induced kinetics to be similar across the DIVs - therefore showing that mainly purinergic responses are involved in providing calcium dynamics due to ATP stimulation (Nobile et al. 2003). Each DIV provides a clear rise and decay phase, therefore analysis of modalities of calcium signalling mediated by purinoreceptor activation may offer insight in determining astrocyte intracellular machinery (Centemeri et al. 1997; Nobile et al. 2003). Recently, when developing astrocytes from stem cells, a number of studies have performed calcium imaging as a method of functional assessment (Santos et al. 2017; Lundin et al. 2018). However, none have shown the breakdown of calcium dynamics into individual components, and the present study is the first to do so, especially mESC derived astrocytes. Although it is not clear why the component breakdown of purinergic mediated activity in stem cell derived astrocytes have not previously been reported. It may be partly attributed towards a narrow focus adopted by studies, where quicker generation of cells is more important than providing a robust characterisation, hence overlooking the necessity of individual component assessment. Assessment of individual components in primary astrocytes is based on the universally observed characteristics that the astrocytic calcium changes exhibit slower kinetics and higher amplitude rises. Rise time is universally defined as the time required for the transient to increase from 10% to 90% of its maximal amplitude, and data here shows that there were statistically significant increases – almost double when comparing DIV 7 to DIV 28, in mESCDA.

For simplicity, the majority of researchers use the peak calcium response (Hamilton et al 2008, Bernardinelli et al 2011), but alongside rise time, the entire calcium transient can also be quantified using area under the curve (AUC) and rate of calcium exit from cell i.e. decay tau (DT) (James et al. 2011). Assessment of area under the curve (AUC) and decay tau (DT) displayed significant differences between earlier and later DIVs. Both parameters displayed a reduction in response where there was significance mainly occurring between DIV 7 and DIV21/28. This suggests that cellular ability to display calcium dynamics levels out as the culture matures, as there is increased capacity of the cell to hold and diffuse calcium through changes in its expression of receptors and complexity in pathways (Volterra et al 2014; Shigetomi et al 2016). Similar to rise time,

there is no data which measures changes AUC and DT in stem cell derived astrocytes, subsequently providing novelty in temporal parameter assessment of purinergic mediated calcium response. Although direct comparisons between DIVs and studies cannot be performed, observation and comparison of results with primary cell cultures reveal mESCDA display similar decay and AUC properties (Centimeri et al. 1997; James et al. 2011; Hashioka et a.l 2014). For example, rat primary cultures display decay tau kinetics similar to mESCDA – shown by Centimeri et al. 1997 and James et al. 2014. The decay phase of ATP stimulated rat cortical astrocytes lasted >60 seconds similar to mESCDA and showed a time dependent decline.

Isolation of another robust parameter(s) apart from peak calcium response would allow researchers to better isolate and understand calcium mechanics in a more robust manner (Charlton and Vaquelin 2010). Furthermore, as the datasets for calcium dynamics are quite large, individual cellular or temporal identity may be lost (Mukamel et al. 2009). Here Principle components analysis (PCA) at DIV 28 was performed to understand which parameter is best for isolating and characterising astrocyte response. The results indicated that RT alone is sufficient in isolating and measuring astrocytic response, as it was shown to be one of the main components. As RT and DT made up more than 40% of mESCDA picked up, more than 26% of mESCDA are able to be reliably be picked up by PCA. The results here show that alongside peak response, rise time should be used in characterising and identifying astrocytes functionally. At this point, this detailed breakdown of purinergic calcium dynamics shown here has not been performed.

Biological “noise” in expression levels of the calcium signalling apparatus overwhelms any difference observed when the individuals’ components are analysed. The hypothesis that calcium signal shape allows discrimination between stimuli is therefore almost certainly plausible, however assessing this hypothesis in a quantitative way has provided some issues. One of these challenges is the presence of noise and biphasic signals within the cultures. Although noise can be filtered out, biphasic calcium dynamics may require further analysis (Nobile et al 2001). Biphasic responses are characterised by calcium dynamics which contain a prolonged component during the decay phase, which is reported to be due to the influx of calcium from extracellular niche via store-operated channels (SOCE) or due to pore enlargement ionotropic receptors (e.g. P2XR7) (Hashioka et al. 2014). Within the culture, when biphasic responses were analysed across DIVs, there was an increase in average biphasic calcium dynamics - mainly in later DIVs (Fig. 28 and Fig. 29). Although the number of cells which had an increase in bipasic responses were negligible, this required further probing to fully elucidate the calcium

dynamics. Hence, receptor-specific assessments, such as pharmacological inhibition of receptors, to decouple metabotropic and ionotropic receptor contributions to the cellular calcium dynamics offer valuable insight into the differences in the responses seen of the generated mESCDA.

4.4.2. Intracellular dynamics are responsible for ATP mediated signalling

Analysis of receptor specific pathways was determined by using receptor specific antagonists. However, before receptor specific assessment, it was vital to understand whether ATP evoked calcium dynamics were a) not noise and b) were due to the rise of endogenous calcium and subsequent activation of further astrocytes. After having established that exogenous ATP application leads to calcium signalling in mESCDA via purinergic receptor stimulation, it was necessary to elucidate the significance of endogenous calcium in bringing about the characteristic calcium wave dynamics. Ionomycin– a calcium ionophore (Muller et al 2013) was used as a positive control. Application of 100 μM triggered a phasic increase in cytosolic calcium post ATP evoked calcium transient (Fig. 25). Post application there was a peak which was significantly different from ATP evoked calcium transients. This indicated an all or nothing response and this has occurred due to release of calcium within the intracellular (cytosolic) stores – via IP3 mediated release (Sherwood et al 2017). The results here confirmed intracellular machinery present in mediating and releasing intracellular calcium and disclosed the involvement of intracellular calcium in the observed ATP induced calcium dynamics (Fig 22).

4.4.3. Purinergic receptors mediate ATP evoked calcium response

Once it was established that the ATP evoked responses were indeed due intracellular calcium and signalling cascades, the non-selective purinergic antagonist was used to confirm purinergic involvement in mediating calcium transients. Initially, application of non-selective antagonist suramin was used. Bath application of suramin significantly downregulated calcium dynamics across DIVs (Fig. 30). Peak analysis of the signals revealed a significant difference in DIVs 21/DIV28, with non-significant but reduced peak differences at earlier DIVs – 7/14, when compared non-treated cells (Fig. 31). This indicates an involvement of P2 receptors in calcium dynamics evoked by ATP. Additionally, the increase in potency of suramin leading to a stunted response may also be correlated due to increase receptors that it can bind to - as shown by PCR and

immunocytochemistry, leading to an increased ability of the antagonist to prevent calcium dynamics (Ceruti & Abbracchio 2006). Similar to the component breakdown of ATP mediated responses, there is a lack of data on temporal dynamics of antagonist treated cells. Although, sufficient data lacks on stem cell derived astrocytes, recently Mizuno et al 2018 measured spontaneous calcium activity of human Down syndrome iPSC model of astrocytes. The study bath applied suramin after DIV 120 differentiation of astrocytes and measured spontaneous calcium dynamics, and saw a significant reduction in amplitude (around 2 fold). Similarly using P15 mice, analysis of white matter tract astrocytes Hamilton et al 2008 observed a similar reduction in ATP evoked suramin astrocytes. They observed 40% reductions in calcium response when compared to control ATP responses, comparable to what is observed at mESCDA at DIV 21. This subsequently confirmed and provided novelty in that the purinergic receptors were involved in mediating ATP evoked calcium dynamics in mESCDA, and these responses differed temporally. Furthermore, since PCA analysis displayed RT to be a significant parameter, subsequent analysis of RT dynamics displayed significant differences across DIVs. This novel analysis revealed inhibition of ATP receptors leads to longer time spent getting to peak maxima (Burnstock et al. 2014)

Suramin results indicate the involvement of P2YR1 receptors in calcium dynamics evoked by ATP, as the Gq-GPCR-PLC-IP_3 cascade is blocked, leading to reduced uncaging of calcium - showing intracellular cascade is necessary for calcium elevation observed. To further solidify P2YR1 involvement in mediating evoked calcium response, receptor specific antagonist MRS2719 was applied. The antagonist stunted the ATP evoked a response, and there was a significant decrease in activity in all of the DIVs when compared to ATP evoked transients (50% decrease when compared to ATP). This solidified the role of P2YR1 in mediating calcium dynamics that are visible with the mESCDA. These significant stunted responses have not been previously reported in stem cell derived astrocytes and were comparable to primary astrocytes. Studies conducted by Hamilton et al 2008, and Monar et al 2011 revealed similar truncation in responses . Hamilton et al 2008 saw a 50% reduction in responses, similar to what is observed in mESCDA at DIV 7. These stunted responses were similar to mESCDA observed at all the DIVs. This provided novel evidence of P2YR1 being involved in mediating calcium dynamics in stem cell derived astrocytes. Furthermore, these comparable observations were also observed *in vivo*, where Delekate et al 2014 report normalisation of astrocyte hyperactivity by blocking P2YR1 receptor on astrocytes (Delekate et al. 2014).

4.4.4. Ionotropic receptor contributes rather than dictates calcium dynamics

An alternative pathway involved in calcium transient is provided by activation of inotropic $P2X_7$ (Nobile et al. 2003; Bartlett et al. 2014). Astrocytes can express a range of ionotropic P2X receptor subtypes, principally $P2X_1$, $P2X_2$, $P2X_3$, $P2X_4$, $P2X_6$, and $P2X_7$ with the exception of $P2X_5$ (Kukley et al., 2001), however, $P2X_7$ has shown to be, to some extent, involved in calcium signalling (James and Butt 2002, Pascual et al. 2005). Immunostaining and genetic analysis revealed $P2X_7$ existence and variability across the DIVs (Fig…). $P2X_7$ displays a significant permeability to calcium in astrocytes (North 2002; Pascual et al. 2005). Therefore, to fully elucidate the role of $P2X_7$ in mESCDA, BBG was added and calcium transients observed. The addition of $P2X_7$ selective antagonist BBG revealed negligible involvement of the receptor in calcium transients. There were no significant changes observed in calcium dynamics at later DIVs, however at DIV7 there was a significantly weakened response. This was further confirmed during the qualitative assessment of the waves, where alongside reduction in peak differences and changes in resting calcium, there was no presence of bi-phasic transients (Hashioka et al. 2014). The abolishment of bi-phasic response may show involvement of $P2X_7$ in the decay phase, although this is yet to be fully shown by other studies. Nevertheless, due to no significant quantitative changes observed, it is essential to rule these changes out as an artefact or saturation in signal after ATP simulation. Furthermore, as there is no conclusive evidence of $P2X_7$ involvement in other components such as rise time, this shows $P2X_7$ as an auxiliary receptor, rather than dictating calcium responses within mESCDA (James and Butt 2002, Burnstock et al. 2010; Puchałowicz et al. 2015).

Thus, in mESCDA P2YR1 provide major and comparable components to calcium signalling at the application of agonist ATP. Activation of P2Y1 receptors results in a rapid but transient release of calcium from intracellular stores and, this is followed by a slower and prolonged influx of calcium through $P2X_7$ receptors and other store operated calcium entry (SOCE) machinery, which continues long after the application of the agonist. The results are consistent with the proposed principal role of P2YR1 receptors in physiological signalling and an accompanying supplementary role for $P2X_7$ (James and Butt 2002). The expression of multiple P2 receptors with different affinities for ATP, different sources of calcium, and different kinetics of the calcium signal provides a mechanism for a graded astrocyte response that depends on the extracellular level of ATP which further needs to be considered.

4.4.5. Study improvements and future directions

The evidence here shows ATP caused an increase in of calcium dynamics from generated mESCDA, and these changes are mediated by involvements of purinergic receptors. The concentration of ATP used was decided by extensive literature review, however the study here could benefit from a dose dependent assessment of the mESCDA. For example, Azzic & Nedeljkovic 2018 show there are changes in calcium dynamics in terms of peak differences when ATP at different concentration is applied onto astrocytes isolated from mice (Adzic & Nedeljkovic 2018). Nevertheless, regardless of the concentration, there is a clear rise and decay which is seen and therefore justifies the usage of one specific concentration of ATP to confirm the presence of calcium dynamics (Hamilton et al. 2008). Nevertheless, *in vivo*, the dynamic interplay between neurons and astrocytes would lead to different concentration of ATP (Adzic & Nedeljkovic 2018), and this would be essential to fully test the role of mESCDA within co-cultures. Additionally, alongside testing different concentrations of ATP, one could also test augmenting receptor specific responses. For example, (Zeng et al. 2008) selectively activated P2YR1 by applying ADPbetaS, and observed a significant increase in calcium dynamics. Therefore, alongside antagonist responses, mESCDA ability to attenuate a response should also be measured (Zeng et al 2008).

Astrocytic Gq-GPCR/PLC/IP_3 signalling pathway has been extensively studied *in vivo* and *in vitro* (Sherwood et al 2017). Available evidence indicates that astrocytes release gliotransmitters and mediate their calcium dynamics in a Gq G-protein-coupled receptor (GPCR)/IP_3R-mediated calcium dependent manner (Pasti et al. 1997; Jeremic et al. 2001; Tang et al. 2016). Three IP_3R subtypes have been identified, IPR1, 2, and 3, and majority of evidence pointed towards heavy IP_3R2 involvement in astrocyte calcium dynamics (Petravicz et al. 2008; Sherwood et al. 2017). Analysis of IP_3R2 in generated mESCDA revealed extensive expression of IP_3R2 across all DIVs in generated mESCDA (Fig. 6). Furthermore, as P2YR1 is a Gq-GPCR, the activation Gq-GPCR/PLC/IP_3 signalling mediated signalling should be assessed using receptor specific blockers for IP_3R2. However, during the assessment of calcium dynamics, study from Petravicz et al 2014 reported an unexpected finding that ablation of IP_3R2 in GFAP positive astrocytes leads to no detectable alteration behaviour and neuronal activity in mice (Petravicz et al 2014). Although evidence has now criticised, where Sherwood et al 2017 show involvement of astrocyte IP_3R2 in long term potentiation (LTP) in mouse hippocampus. More recently, evidence on the involvement of IP_3R3 has now also been brought forward (Sherwood et

al 2017), where it has been postulated that IP_3R2 and IP_3R3 work in tandem to mediate calcium response. Therefore, due to the scope of the study, and also due to reduce availability of highly selective IP_3 blockers (Saleem et al. 2014), IP_3 mediated receptor specific antagonism was not pursued. Therefore, in light of recent evidence and significant interest of the field, the generated mESCDA could benefit from performing this analysis. Nevertheless, as a proof of principle and to fully elucidate the involvement of P2YR1 receptor and the downstream pathways involved in rise in calcium dynamics, phosphate PLC was selectively blocked via application of U73122 (Fig.36). DIV 28 mESCDA revealed a significant reduction in calcium kinetics when compared to ATP mediated signals. However, the result is performed on n=1 and on DIV 28 mESCDA. Subsequent increase in n numbers and further analysis on the rest of the DIVs would beneficial.

Similarly, the role of $P2X_7$ could also be tested by applying an agonist such as Bz-ATP (Nobile et al 2003). The evidence of biphasic and monophonic responses that are mediated by $P2X_7$ receptors (Hashioka et al. 2014) could also be assessed by applying $P2X_7$ agonists. By application of Bz-ATP Nobile et al 2003 evoked a small peak post maximal peak at the plateau phase on rat cortical astrocytes, similar to what is observed here in some of the mESCDA across the DIVs.

5. Integration and isolation ability of mESCDA

5.1. Introduction

Cell culture (*in vitro*) models have an advantage of virtually unlimited availability and quick reproducible results which allow rapid screening for diseases and drug candidates (Hanna & Hubel 2009). *In vitro* models offer advantages over *in vivo* models in multiple aspects. For example, *in vitro* models have an advantage of providing unlimited availability of cell type of interest via creating a cell bank (Stacey 2012). Subsequently providing a model for quick and reproducible results which allow rapid screening for plethora of assays such as measurement of disease pathogenesis in neurodegenerative diseases or assessment of drug candidates for pharmacological assays (Stacey 2012). Furthermore, these *in vitro* models prevent the need of ubiquitous use of animals. Nevertheless, the majority of the *in vitro* models used do not represent the conditions seen *in vivo*. Most culture conditions have cellular homogeneity, where one cell type which of interest is grown (Altschuler & Wu 2010). For example, when unravelling the complexity of neurodegenerative and neurodevelopment disorders, experiments are mainly performed on neurons rich cultures. Despite the fact that neuronal monocultures are extensively used extensively to recapture CNS niche, these cultures represent unnatural environmental conditions, since *in vivo* neurons are heavily surrounded by glial cells such as astrocytes (Ullian et al. 2001; Boehler et al. 2008). In the past, astrocytes have traditionally been considered as passive elements, providing a metabolic support for neurons and regulating the extracellular homeostasis (MacVicar et al 2017). However, evidence in the last decade has revealed that astrocytes are also actively involved in the control of neuronal functions and neuronal survival (Fellin 2009; Covelo & Araque 2015). Therefore, to mimic *in vivo* environmental niche, and since neurons in the brain are embedded in a complex interaction network together with astrocytes, a co-culture model of both cell types are currently being adopted (Farhy-Tselnicker et al. 2018).

The most used method for obtaining astrocytes is isolation from murine resources (Schildge et al. 2013). These methods are hampered by inter-laboratory variability and contamination with a high amount of microglia, oligodendrocytes, neurons, and endothelial cells (Martin 1981; Schwartz & Wilson 1992; Schildge et al. 2013). Therefore, the newly generated pure astrocytes cell lines have received much attention. The mESCDA generated here (chapter 2) provide a suitable model to develop a co-culture system, as they are heterogeneous group of astrocytes which display characterises in form and function similar to the *in vivo* counterparts.

5.1.1. Isolation techniques

Efficient isolation protocols have been established and can be usually broken down into two main groups, mechanical and enzymatic (Jager et al. 2016). Mechanical dissociation methods may involve a combination of, cell scraping, usage of filters, use of devices such as homogenisers, and various other approaches. Enzymatic dissociation methods include the application of proteolytic enzymes such as Trypsin/EDTA, Accutase, alone or in combination. One of the most ubiquitous enzymes used is Trypsin/EDTA (Pan et al. 2014; Fong et al. 2017). Trypsin is a pancreatic serine protease which cleaves to peptide bonds involving the carboxyl group amino acids. Purified trypsin alone is usually ineffective for tissue dissociation since it shows little selectivity for extracellular proteins (Hui et al. 2015). Combinations of purified trypsin and other enzymes such as EDTA (disodium ethylenediaminetetraacetic acid) which chelates the divalent cations (Ca^{2+}, Mg^{2+}), allows trypsin to work effectively and efficient removal of cells (Beers et al. 2013). Evidence has shown that Trypsin/EDTA is a harsh enzyme which causes cell lysis and changes in cellular function, and reduces the ability to replace and reuse cells for future (Li et al. 2014). Additionally, when working with stem cells, trypsin doesn't effectively break up the large clusters and leads to increased cellular clumping (Cowan et al. 2004). Therefore, more recently less harmful enzymes such as accutase are used. Accutase does not contain EDTA and is a marine-origin enzyme with proteolytic and collagenolytic activity, leading to effective breaking down of cells (Bajpai et al. 2008). Accutase has mainly been used when cultivating cells such as stem cells, and has shown to be more effective leading to increased cell viability, and increased plating efficiency (TCW et al 2017).

However, aspects of enzymatic dissociation such as an understanding of the mechanisms regulating adhesion and incorporation into tissue, the time required for effective and increased cell removal and the right type of enzyme for the right type of cell are not well understood (Jager et al. 2016). There has been no comprehensive study of the impact of different methods of detachment of cells on the functionality, viability and structural ability of the cells. Moreover, there is also no comprehensive study on stem cell derived astrocytes, which shows effective removal of cells from a substrate, and which measures removed cells functional and structural ability. Therefore, the study here aims to assess first the efficient method of removal of generated mESCDA. Once an efficient method was chosen, the study aims to assess whether these isolated mESCDA are able to have similar functional and expression ability as the generated mESCDA and primary

astrocytes. Finally, the isolated mESCDA will be tested for their integration ability into a neuron rich culture and will be tested for their ability to rescue neurons, this will aim to contribute towards *in vitro* model which can be used for co-culture studies to test for neurodevelopment and neurodegenerative studies.

5.2. Materials and Method

5.2.1 Materials

Culture Materials	Catalog Number	Provider
Calcium Chloride (CaCl2)	12074	Sigma
HEPES	H3375	Thermo Fisher
HBSS, calcium, magnesium, no phenol red	14025092	Thermo Fisher
Bovine serum albumin (BSA)	A2058	Sigma
DPBS	A1285801	Thermo Fisher
ß-Mercaptoethanol	1350	Gibco
ADMEM/F-12	12634028	Thermo Fisher
B-27™ Supplement (50X), serum free	17504044	Thermo Fisher
Fetal Bovine Serum (FBS)	F2442	Gibco
Leukaemia Inhibitory Factor (LIF)	L5158	Thermo Fisher
N2 Supplement	17502048	Thermo Fisher
Pen/Strep	15140	Invitrogen
L-Glutamic Acid	G1624	Sigma
ß-Mercaptoethanol	1350	Gibco
Laminin	L2020	Sigma
Accutase	A1110501	Thermo Fisher
Triton-X100	9002931	Sigma
Formaldehyde (PFA)	130525894	Sigma
Hoechst 33342	H3570	Molecular Probes
Trypsin Solution	59427C	Thermo Fisher
Fluo 4	12312	Molecular Probes
ATP	2135791	Sigma
E18 mouse cortex	C57ECX	BrainBits
Papain	P4762	Sigma
Cell Scraper	734-2602	VWR

Table 7: Materials used for isolation and integration of mESCDA

5.2.2. Generation of mESCDA for mechanical assessment

The EB based isolation of mESCDA was for these experiments (see chapter 3). Briefuly, 20 intact EB's were seeded directly onto laminin-coated 13mm coverslips containing astrocyte differentiation media (ADMEM/F12, 2% FBS, N2, 1% L-glutamine, 1% Pen/Strep, 100uM β-mercaptoethanol and 50ug/mL heparin (Robertson and Goldstein 1988; Nagayasu et al. 2005) (Sigma Aldrich, Poole, UK), were grown for 28 DIVs.

5.2.3. Generation of neuron-rich culture for integration

Cultures of mESC were used when they reached 80% confluency, with a serum based media containing DMEM and FBS with 1uM of LIF to prevent spontaneous differentiation.

Media Recipe

Aggregation Medium (ADFNK)

- Advanced DMEM/F12 – Neurobasal (1:1)
- 10% Knockout Serum Replacement
- 1% Penicillin/Streptomycin
- 1% L-Glutamine
- 100uM 2-Mercaptoethanol

Neuronal Medium (ADFNB)

- Advanced DMEM/F-12 - Neurobasal medium (1:1)
- B-27 supplement
- 1% L- Glutamine
- 100uM β-mercaptoethanol
- 1% Pen/Strep

Step by step method

1. Confluent flask of mESC cells (around 80%) was taken and medium aspirated from the flask.

2. The flask was then washed in 5 ml PBS.
3. PBS was aspirated and cells in flask were exposed to 2 mL Trypsin/EDTA for 2 minutes
4. Flask was gently agitatated until top layer of mESC cells were detached
5. Trypsin/EDTA was inactivated with 3 mL mESC media (See above) and the lifted cells were transferred to a 20mL universal tube.
6. Cells were centrifuged for 5 minutes at 180g
7. Supernatant aspirated and cells were resuspend cells in 2mL ADFNK medium
8. Cells counted haemocytometer
9. Cells were seeded in mESC cells in ADFNK medium, at a density from 2 x 10^4 to 2.5 x 10^5, (recommended 50,000 cells/mL) in either non-tissue culture treated 6-well plates or petri dishes. For a petri dish, 500,000 cells per 10 mL is sufficient.
10. Cells were incubated at 37°C for 2 days, by which time aggregates were formed and found to be floating in the medium.
11. After 2 days EBs were exposed to fresh ADFNK media containing either containing retinoic acid (RA) at 1uM or no retinoic acid (depending on the methodology required and tested, see results). Media was also changed to remove non-EB formed cells and any debris
12. At day five, if RA was added it was removed and fresh ADFNK media was added by transferring medium containing EBs to a 15 mL centrifuge tube. The EBs were allowed settle under gravity.
13. The supernatatnt was aspirated and EBs were gently resuspend in fresh ADFNK media and transfered to petri dish for further incubation
14. At DIV 6 EBs were treated with 0.05% trypsin for 60 seconds, re- suspended in ADFNB medium
15. Cells were passed through 70 μm cell strainer and centrifuged at 500g for 5 min
16. Cells were resuspended in ADFNB medium
17. Cells were plated at a density of 50,000 cells/cm^2 in 12/24 plates coated with 2μg/cm^2 laminin
18. The cells were assessed via bright field microscopy every day and differentiated for up to 7 days with the media changed every other day and assessed via bright field microscopy every day and differentiated for up to 7 days.

5.2.4. Primary astrocyte rich cultures

E18 mouse cortex was obtained from BrainBits (BrainBits UK). Tissues were dissasociated in 2mg/ml papain containing Hibernate E and GlutaMax (Sigma Aldrich, Poole, UK) for 10 minutes at 37C. Tissue was triturated using silanised pasture pipette for 1 minute, at a gentle speed, to avoid air bubbles and the cell was left to settle for 60 seconds. The cells were then centrifuged at 1100 rpm for 60 seconds and the supernatant discarded. Cells were then resuspended in nbAstro medium (Neurobasal, 10% Fetal Bovine Serum (FBS) and Glutamax (Thermo Fisher). Suspended cells were counted, with the aid of Neubauer chamber (Sigma Aldrich, Poole, UK) and cells were plated at the density of 7,500 cells/cm2 in laminin-coated coverslips and grown for 6 DIVs and stained to assess the growth of astrocytes.

5.2.5. mESC derived astrocyte and neuronal co-cultures

Primary astrocyte rich cultures

E18 mouse cortex was obtained from BrainBits (BrainBits UK).

Media Recipe

Dissociating media

- Hibernate E
- 1% GlutaMax
- 2mg/ml papain

Primary astrocyte medium

- Neurobasal,
- 10% Fetal Bovine Serum (FBS)
- 1% Glutamax

1. Tissues were disassociated in dissociating media for 10 minutes at 37°C, 5% CO_2
2. Tissue was triturated using salinized pasture pipette for 1 minute, at a gentle speed, to avoid air bubbles and the cell was left to settle for 60 seconds
3. The cells were then centrifuged at 1100 rpm for 60 seconds and the supernatant discarded
4. Cells were then resuspended in Primary astrocyte medium
5. Suspended cells were counted, with the aid of Neubauer chamber and cells were plated at the density of 7,500 cells/cm^2 in laminin-coated coverslips and grown for 6 DIVs and stained to assess the growth of astrocytes

5.2.6. Enzymatic dissociation of mESCDA

For enzymatic disassociations, cells were centrifuged, re-suspended in 1 mL enzymes (Accutase or Trypsin/EDTA - ThermoFisher, UK), and incubated at 37C in the water bath for time-points 15, 30 or 60 minutes. Cells were then centrifuged and re-suspended in astrocyte media and incubated at 37C in the water bath for 10 min. Half-way through both incubation periods, tubes were shaken lightly to re-suspend cells. Cells were then centrifuged and resuspended in 1 mL of astrocyte media and plated onto laminin-coated coverslips, as above.

5.2.7. Mechanical dissociation

To test the efficacy of enzymatic dissociation, mechanical dissociation was also performed. At DIV 28, mESCDA grown on laminin-coated coverslips were scraped using corning cell scraper (Sigma Aldrich, Poole, UK). Post scraping, cells were passed through a 70 μm cell strainer to derive a suspension of single cells and prevent embryoid bodies (EBs) to occur in culture. Cells were then triturated 2 or 3 times at 200 mL astrocyte media maintaining a consistent speed of approximately 3 times per 2 seconds. Large clusters were allowed to settle before 180 mL was transferred to a new tube. Another 200 mL DMEM was added and cells were again triturated, settled, and transferred. The process was repeated for a total of 10 or 15 trituration and a final volume of 1 mL.

4.2.8. Immunocytochemistry

Antibody	Type	Concentration	Source
GFAP	Chicken Polyclonal	1:500	Aves
ALDH1L1	Rabbit Polyclonal	1:100	Abcam
BIII (TUJ1)	Rabbit Polyclonal	1:250	Abcam
Vinculin	Rabbit Polyclonal	1:500	Abcam
488	Anti-Rabbit	1:500	Alexa Fluor
594	Anti-Chicken	1:500	Alexa Fluor
594	Anti-Rabbit	1:250	Alexa Fluor

Table 8: Antibodies used for immunofluorescence

Immunocytochemistry was performed with same methodology as in previous chapters (see chapter 2) with antibodies that are detailed in Table 8. Isolated mESCDA were fixed at DIV 2 and washed three times with PBS at fixed with 3.7% formaldehyde in PBS for 30 minutes, and permeabilised with 0.02% Triton X-100 diluted in 10% goat serum for 10 minutes. Nuclei were counterstained with H-33342 (Hoechst dye). Images were taken using an Axio Imager microscope (Zeiss, Germany).

Separate digital images (red 568nm, green 468nm, blue 350nm - RGB) of astrocyte stains (green and red light) and DNA (Hoechst 33342) were captured with a ×20 objective (1040x1388 pixels). Focus was adjusted for each new field, but fluorescent illumination and exposure were kept constant to improve consistency during analysis. Scale bars were calibrated using AxioVision software (release 4.6.3; Carl Zeiss). Files were saved in tagged image file format (.tif) and JPEG (.jpeg).

5.2.9. Calcium Imaging of isolated mESCDA and primary astrocytes

Calcium imaging was performed as before (Chapter 3). Briefly, isolated, generated, and primary astrocytes were imaged using Fluo-4 acetoxymethyl ester dye at 2.5 μM in HEPES buffer same as above methods (see chapter 3). Post loading, cells were then moved to the recording chamber and all fluorescence measurements were made at 37C (Warner Instruments) with no CO2 control for 5 minutes – 300 Seconds. Excitation and

emission wavelengths were 494 nm and 516 nm respectively. Changes in calcium were detected with an inverted Nikon Eclipse TE2000-S microscope (Nikon) equipped with a xenon arc lamp (Sutter Instruments). Imaging Workbench 6.0 (INDEC Bio- Systems) was used to control a Lambda 10-2 shutter system (Sutter Instruments).

5.3. Results

Removal of EBs is essential to obtain a pure astrocyte rich culture for future studies. Additionally, creating a cell bank is also essential (Lange et al 2012, Waang et al 2012). This will allow a non-stop supply of cells, to allow future studies to be conducted and a cell line to be created (Altschuler et al 2010). Hence, removal of anchored cells to coverslips was examined via mechanical and enzymatic isolation techniques (Aronowitz et al 2015, Jager et al 2016). Generated DIV 28 mESCDA were incubated in enzymes Trypsin/EDTA and Accutase for 15, 30 and 60 minutes, and then re-plated onto laminin coated coverslips. Furthermore, to determine if enzymatic treatments is an ideal methodology for efficient cell removal, cells were also scraped using a cell scraper and re-plated laminin coated coverslips (Aronowitz & Hakakian 2015). Using immunocytochemistry, cells were assessed for astrocytic markers, ALDH1L1 and GFAP to determine the effectiveness of treatment.

5.3.1. Single cell dissociation with Trypsin/EDTA

Treatment and incubation of DIV 28 mESCDA with Trypsin/EDTA, led to effective dissociation of the majority of the cells at all the time points – observed via brightfield images (Fig. 37). From the 15 minute period, the monolayer of cells were seen to be detached from the laminin coated coverslips, suggesting Trypsin/EDTA effectively detached anchor proteins such as integrins, leading to effective cell removal (Pan et al 2014). Nevertheless, Trypsin/EDTA also compromised the EBs integrity and detached cells within the EBs, subsequently suggesting the accumulation of debris (Fig. 37B - arrow) (Huang et al 2010).

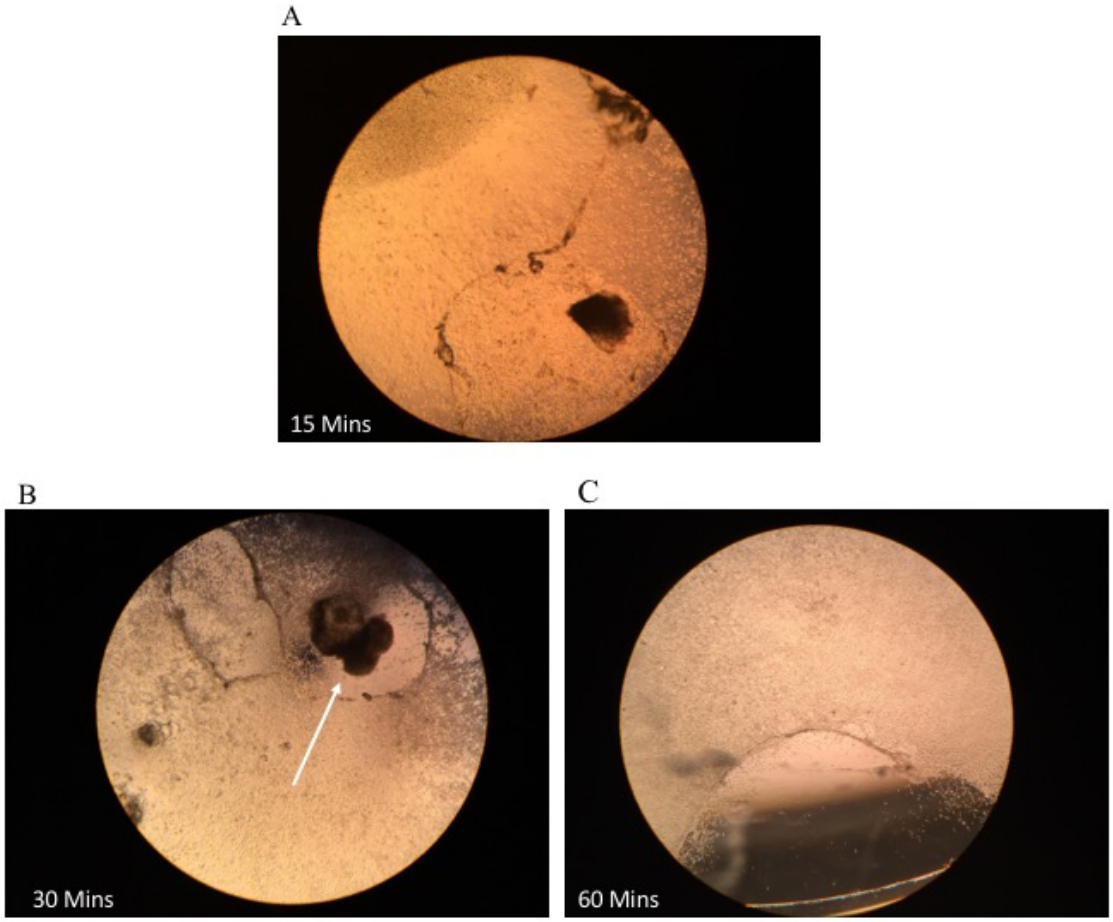

Figure 37: Brightfield micrographs of astrocytes incubated with (A) 15, (B) 30 and (C) 60 minutes with Tryspin/EDTA. Arrows point to disintegrated EB. Image acquired a x20 magnification.

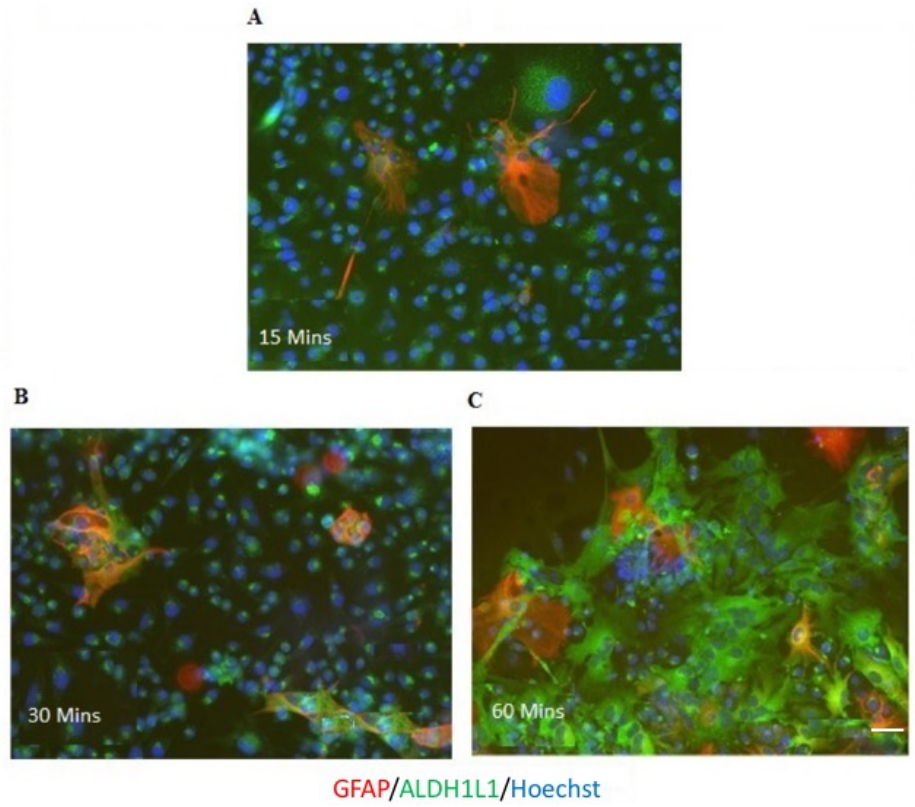

Figure 38: Immunocytochemistry images of astrocytes incubated with (A) 15, (B) 30 and (C) 60 minutes with Tryspin/EDTA. Isolated mESCDA reliably labelling for GFAP (Red), and ALDH1L1 (Green) at DIV2 post isolation from Trypsin/EDTA. Cultures have been counterstained for cell nuclei marker H- 33342 (blue stain). Scale bar = 20µm.

To effectively remove debris, cells were filtered through a 70um cell strainer and repeated onto laminin coated coverslips for 2 days. Assessment of re-plated cells onto laminin coated coverslips post incubation with Trypsin/EDTA was performed for astrocyte markers (Fig. 38). Assessment of GFAP positive cells revealed a stable expression of cells (>100 cells/mm2) at groups of cells obtained from 15 and 30 minutes (Fig. 38/Fig. 39). However, in comparison there was a significant increase at the group of cells plated from 60 minutes (273.3 cells/mm2 ± 40.24 n=3) when compared to both 15 (>125.5 cells/mm2, ± 21.25 n=3) and 30 (144.7 cells/mm2, ± 20.16 n=3) minutes groups (Fig. 39A). Inspection of ALDH1L1 cells revealed a stable expression across all time-points (Fig. 38B). There was a non-significant increase at 60 minutes group (955.80 cells/mm2 ± 90.04 n=3), when compared to both 15 minutes (818.0 cells/mm2 ± 110.19 n=3) and 30 minutes (655.80 cells/mm2 ± 310.24 n=3) respectively. Additionally, when

comparing the number of cells, there are significantly more ALDH1L1 positive cells (>900 cells/mm2) when compared to GFAP positive cells (>200 cells.mm2) (Fig. 39). The morphological assessment also revealed the GFAP positive cells displayed an enlarged cytoplasm, with protrusions extending from the cytoplasm (Fig. 36).

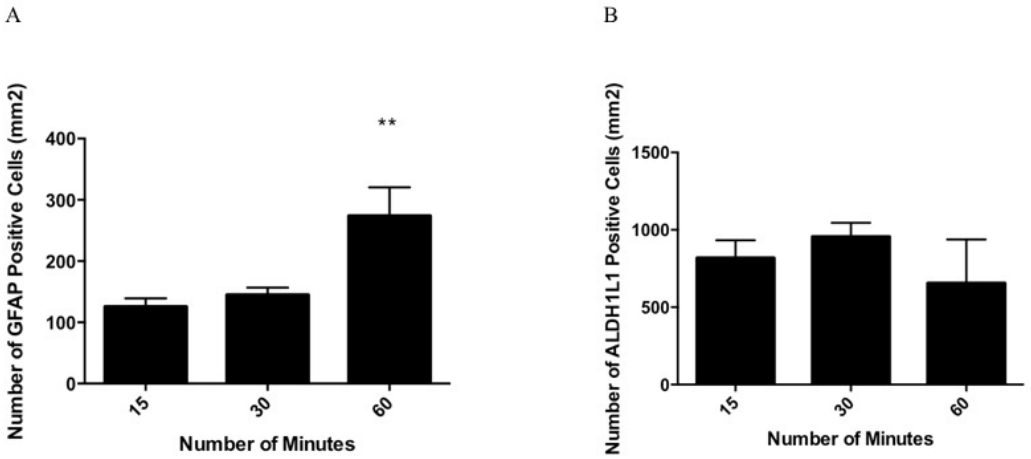

Figure 39: Quantification of marker expression. (A) Number of GFAP positive cells per mm2. (B) Number of ALDH1L1 positive cells per mm2. All data are expressed as mean ± SEM from three separate experiments, *P < 0.05, **P < 0.01, ***P < 0.001) Mann-Whitney statistical tests

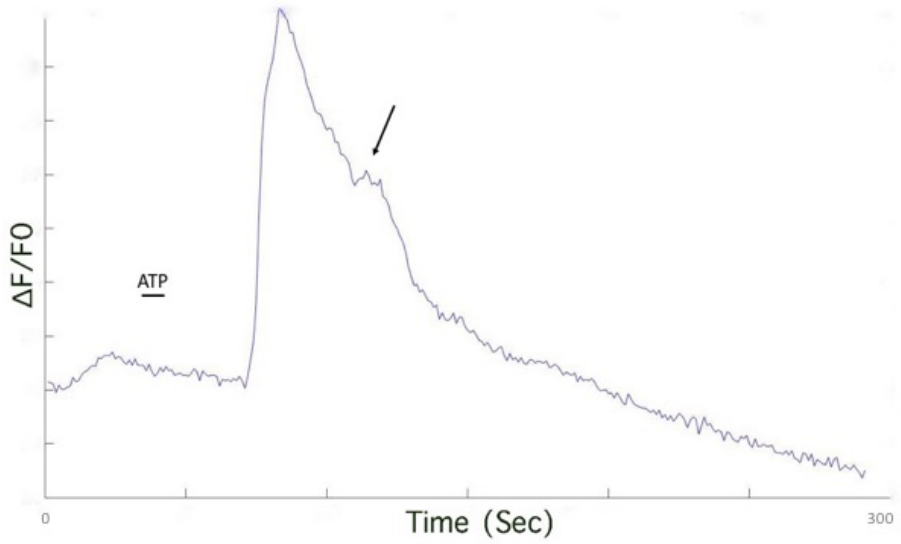

Figure 40: Representative ATP evoked responses of isolated mESCDA with Trypsin/EDTA. Isolated mESCDA reveals purinergic response similar to generated mESCDA and revealed transients which are bi-phasic in nature (black arrow at DIV 7 showing bi-phasic response).

Based on the immunocytochemical analysis, calcium assessment of 60 minute group was performed - as this group yielded the most number of astrocytes. Similar to previous experiments, Flou-4 loaded cells were stimulated with ATP, subsequently leading to intracellular calcium rise and a calcium response (Fig. 40). The 60 minute group provided a typical purinergic calcium response comparable to previous mESCDA calcium dynamics and displayed a clear rise and decay phase. Nevertheless, on closer inspection, there were clear dual peaks observed within the peak response of the curve (Fig. 40 - arrow). The second peak occurred at a significantly later time point. This suggests changes in mechanisms of actions brought about by Trypsin/EDTA.

5.3.2. Single cell dissociation with Accutase of mESCDA

Similar to Trypsin/EDTA, DIV 28 mESCDA were also treated with Accutase (Bajpai et al 2008). Assessment of accurate displayed effective dissociation of cells at all the time points, similar to Trypsin/EDTA – observed via brightfield images (Fig. 41).

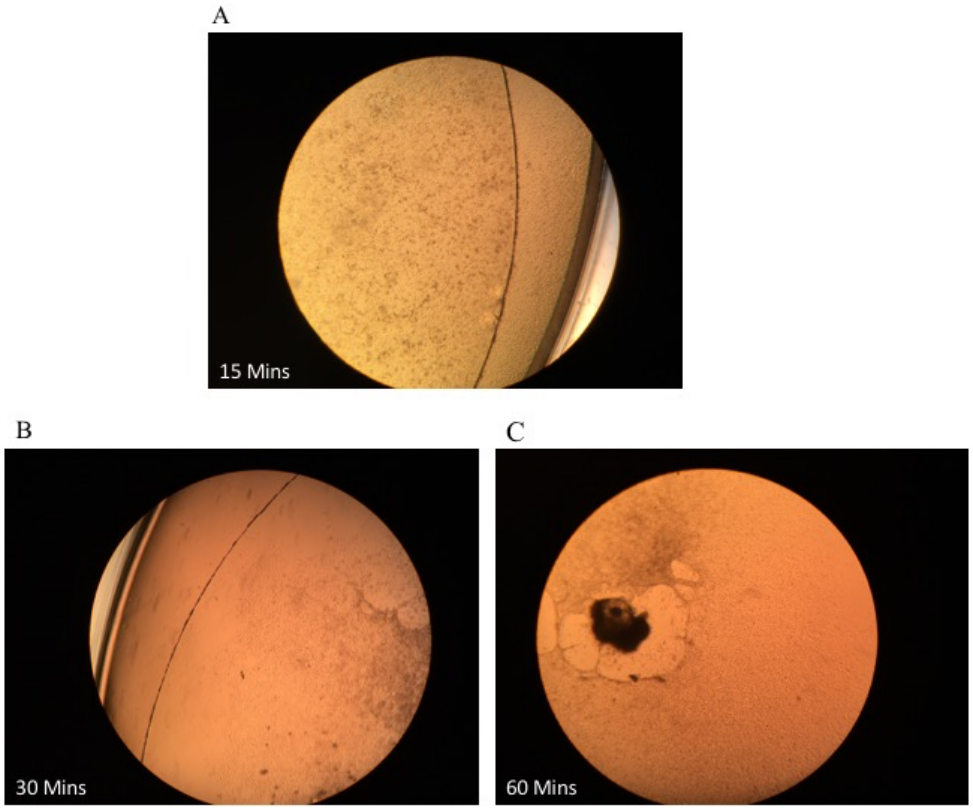

Figure 41: Brightfield micrographs of astrocytes incubated with (A) 15, (B) 30 and (C) 60 minutes with Accutase. Image acquired a x20 magnification.

Nevertheless, the EBs integrity was not compromised (Fig. 41). Inspection of all the groups (15-60 minutes) also displayed reduced removal of monolayer when compared to Trypsin/EDTA, suggesting Accutase does not effectively dissociate cells from laminin coated coverslips. Nevertheless, cells were still passed through a 70um cell strainer to remove debris. Similar to Trypsin/EDTA, assessment of re-plated cells onto laminin coated coverslips post incubation was performed for astrocyte markers (Fig. 42).

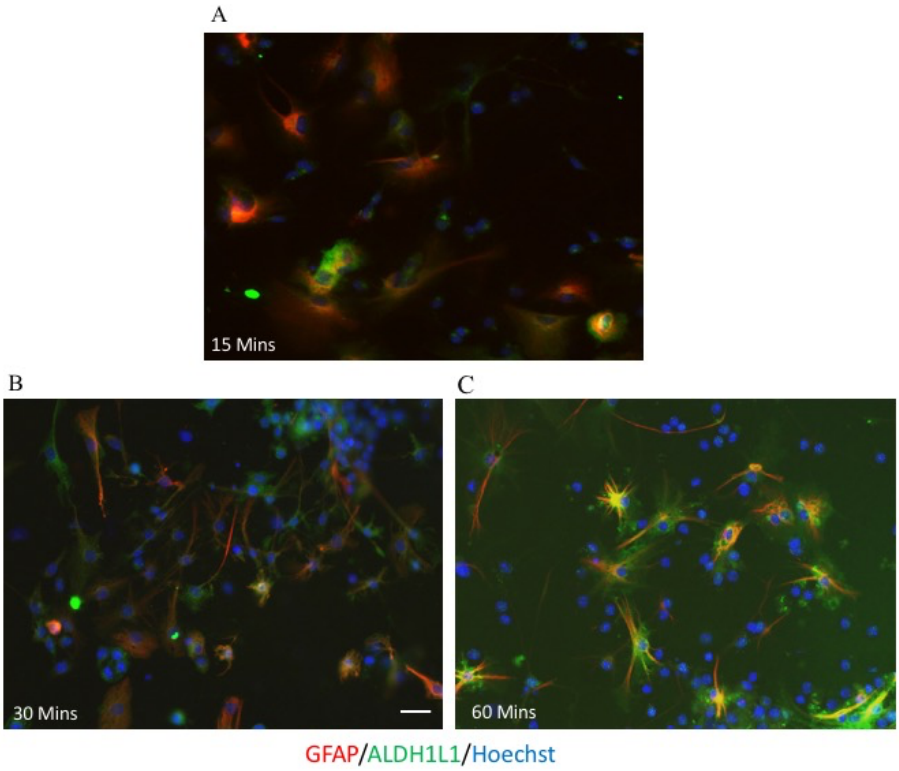

Figure 42: Immunocytochemistry images of astrocytes incubated with (A) 15, (B) 30 and (C) 60 minutes with Accutase. Isolated mESCDA reliably labelling for GFAP (Red), and ALDH1L1 (Green) at DIV2 post isolation from Accutase. Cultures have been counterstained for cell nuclei marker H- 33342 (blue stain). Scale bar = 20µm.

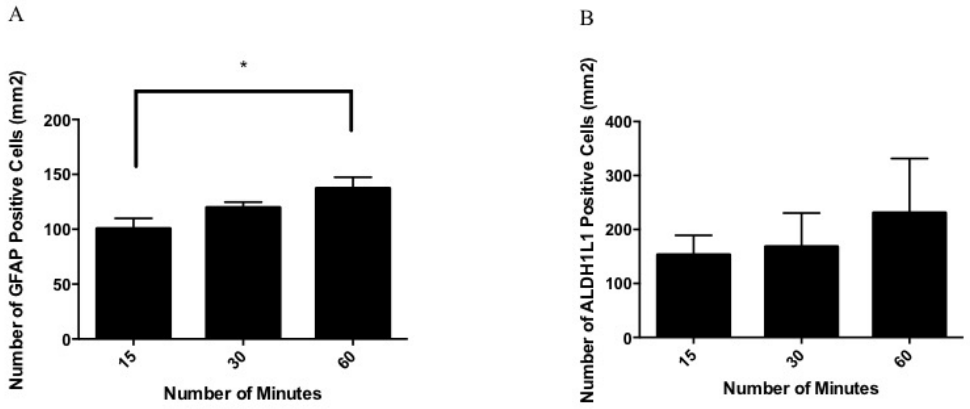

Figure 43: Quantification of marker expression. (A) Number of GFAP positive cells per mm2. (B) Number of ALDH1L1 positive cells per mm2. All data are expressed as mean ± SEM from three separate experiments, *P < 0.05, **P < 0.01, ***P < 0.001) from unpaired T-test.

Assessment of GFAP positive cells revealed a stepwise increase in cell numbers (>100 cells/mm2). Group comparison revealed a significant increase between 60 minutes (137.2 cells/mm2 ± 8.11 n=3) when compared with 15 minutes (>100.5 cells/mm2, ± 11.15 n=3) (Fig. 42/43A). Inspection of ALDH1L1 cells revealed a stepwise by non-significant expression across all time-points (Fig. 43B). There was a non-significant increase at 60 minutes group (230.8 cells/mm2 ± 121.04 n=3), when compared to both 15 minutes (153.0 cells/mm2 ± 66.91 n=3) and 30 minutes (168.80 cells/mm2 ± 84.24 n=3) respectively. Additionally, when comparing the number of cells, both markers display a similar number of cell expression with >100 cells/mm2. Similarly, in comparison to Trypsin/EDTA, morphological assessment of GFAP positive Accutase treated cells revealed morphology reduced cell size and less but elaborate protusions with high co-localisation with ALDH1L1 (Fig. 42C), comparable to mESCDA at DIV 28 - see previous chapter.

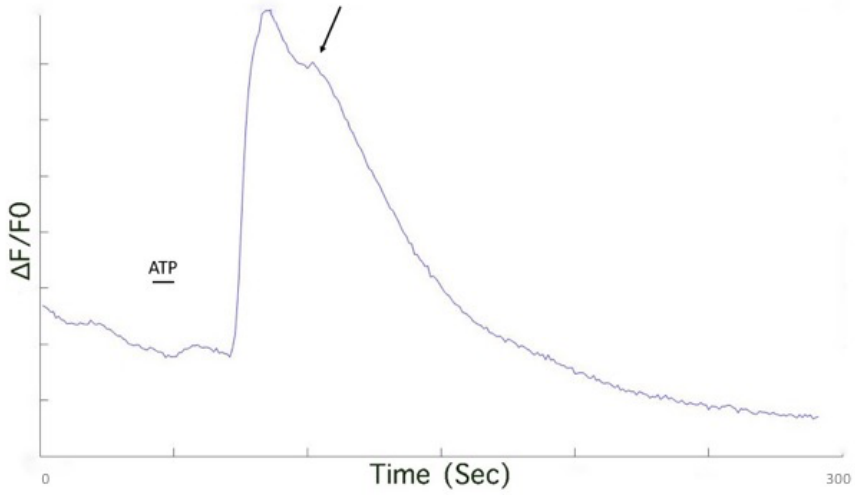

Figure 44: Representative ATP evoked responses of isolated mESCDA with Accutase. Isolated mESCDA reveals purinergic response similar to generated mESCDA and revealed transients which are bi-phasic in nature – similar to Trypsin/EDTA (black arrow at DIV 7 showing bi-phasic response).

Similar to Trypsin/EDTA, calcium assessment of 60 minutes group was performed. Cells were loaded with Flou-4 and stimulated with ATP. This led to an intracellular calcium rise and a calcium response (Fig. 44). The 60 minute group provided a typical purinergic calcium response comparable to previous mESCDA calcium dynamics (Fig. 24) and displayed a clear rise and decay phase. Nevertheless, on closer inspection, similar to Trypsin/EDTA, Accutase treated cells also displayed dual peaks (Fig. 42 - arrow).

5.3.3. Mechanical isolation of mESCDA

To solidify whether enzymatic treatments is truly necessary for effective removal and isolation of pure population of astrocytes, mechanical isolation was also performed (Beers et al 2012, Bellei et 2017) cells were scraped from the laminin coated coverslips using a cell scraper with 1.8cm blade, and cells were subsequently passed through a 70 um cell strainer - to remove debris and attached EBs. Similar to enzymatic treatments, re-plated cells were similarly assessed for astrocyte markers GFAP and ALDH1L1. There was a significant increase in ALDH1L1 (125.75 ± 25.24 n=3) positive cells when compared to GFAP positive cells (79.05 ± 45.15 n=3), with morphologies which resemble mESCDA - extensive cytoplasm with elaborate protrusions of GFAP positive cells (Fig. 45A/B).

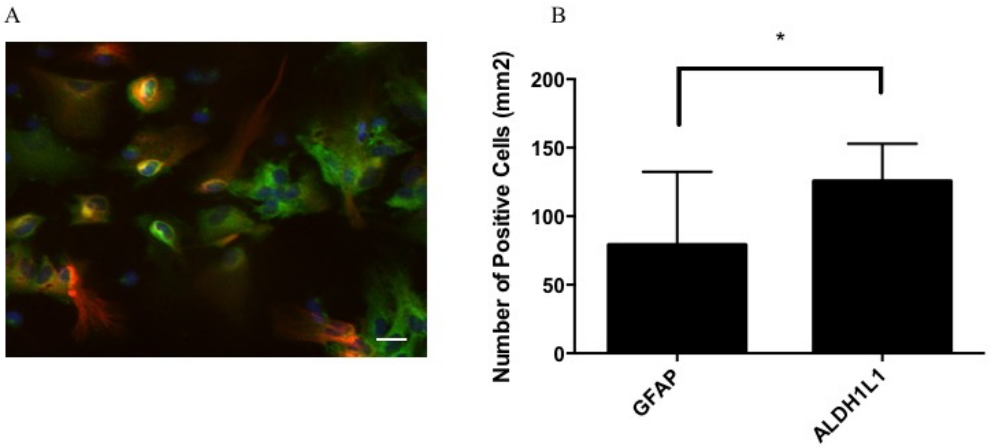

Figure 45: Immunocytochemistry images of mechanically isolated astrocytes. (A) Isolated mESCDA reliably labelling for GFAP (Red), and ALDH1L1 (Green) at DIV2 post isolation. (B) Quantification of marker expression. Number of GFAP and ALDH1L1 positive cells per mm2. All data are expressed as mean ± SEM from three separate experiments, *P < 0.05, **P < 0.01, ***P < 0.001) Cultures have been counterstained for cell nuclei marker H- 33342 (blue stain). Scale bar = 20µm.

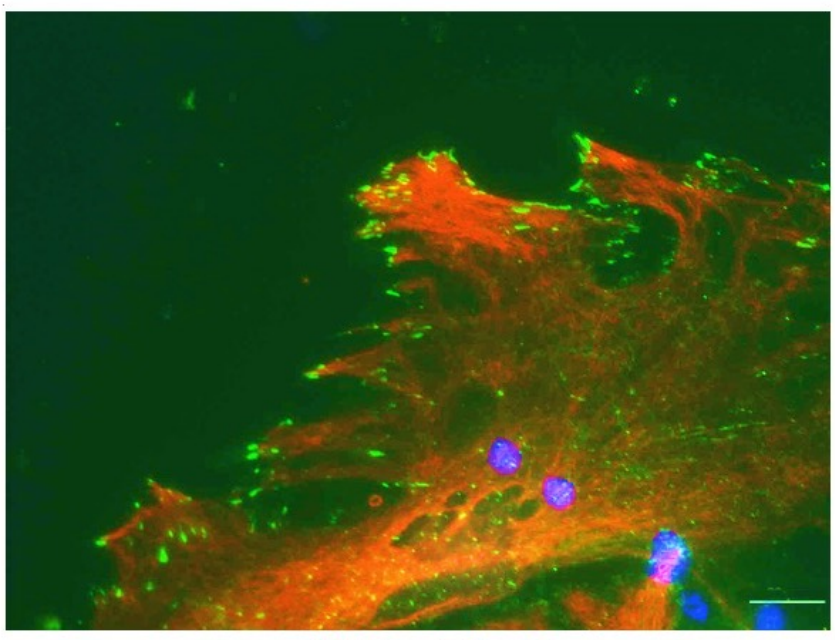

Figure 46: Immunocytochemistry images of mechanically isolated astrocytes. Isolated mESCDA reliably labelling for GFAP (Red), and Vinculin (Green) at DIV2 post isolation. Cultures have been counterstained for cell nuclei marker H- 33342 (blue stain). Scale bar = 50µm.

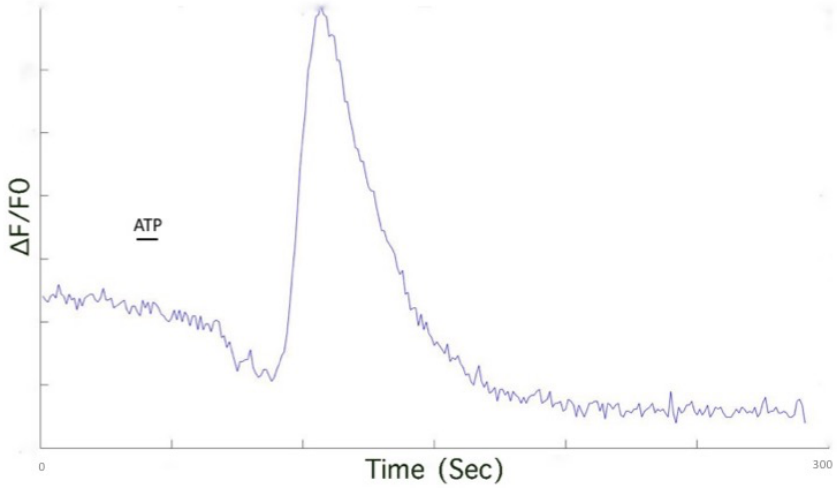

Figure 47: Representative ATP evoked responses of mechanically isolated mESCDA. Isolated mESCDA reveals purinergic response similar to generated mESCDA and revealed transients which are mono-phasic in nature.

Evidence dictates that significant force that is applied during mechanical isolation prevents focal adhesions, such as vinculin, to occur leading to significant cell loss (Grashoof et al 2010). To assess cellular ability to adhere to laminin coated coverslips, and to show mechanical isolation does not impair cell ability to anchor itself, vinculin staining was performed (Fig. 46). The staining revealed vinculin surrounding the cytoskeleton of re-plated astrocytes, further confirming the viability of isolated cells (Fig. 47). Similar to enzymatic isolation, when observing the calcium dynamics of scraped cells, there was a clear rise and decay transient with no presence of dual peaks (Fig. 47).

5.3.4. Comparison of primary astrocytes with isolated mESCDA

To confirm whether the isolated mESCDA cells are a viable tool for further research use, functional and morphological assessment of mESCDA and isolated mESCDA with primary cortical astrocytes was performed.

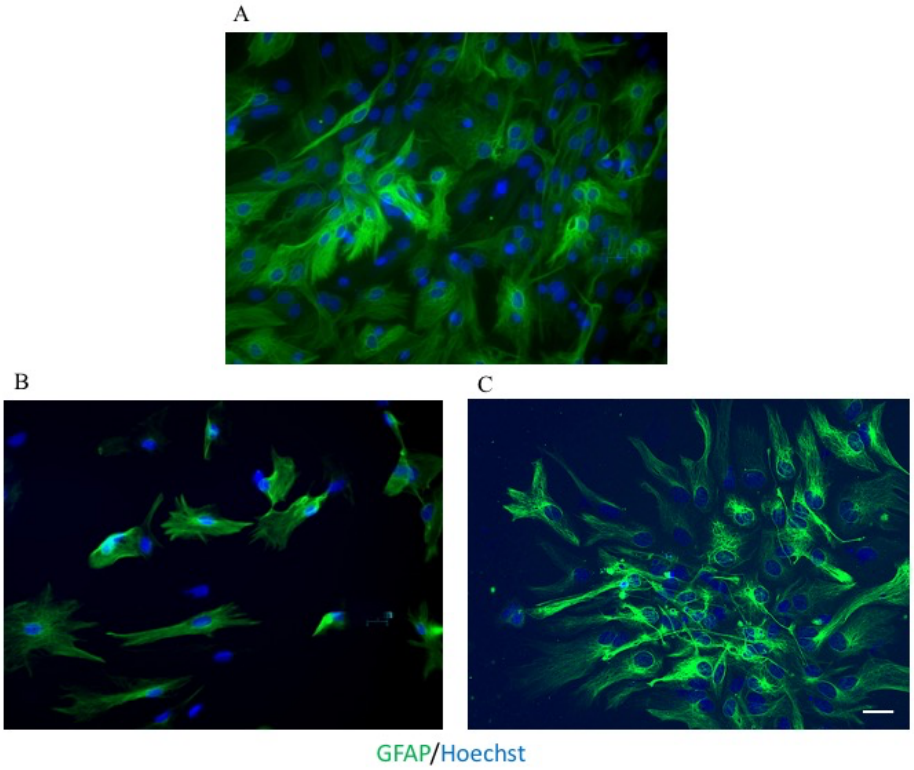

Figure 48: Immunocytochemistry images of astrocytes. (A) DIV 28 generated mESCDA (B) Mechanically isolated mESCDA (C) Primary cortical astrocytes reliably labelling for GFAP (Green) and showing similar morphology. Cultures have been counterstained for cell nuclei marker H- 33342 (blue stain). Scale bar = 20µm.

As cells with mechanical isolation provided comparable immunocytochemistry and calcium dynamics with generated mESCDA, these isolated cells were compared with primary cortical astrocytes (Fig. 48). Immunocytochemistry analysis for astrocyte marker GFAP of DIV 28 mESCDA, isolated astrocytes, and primary astrocytes revealed comparable staining (Fig. 48). All of the groups (DIV 28 mESCDA, Isolated mESCDA, and primary astrocytes) morphologies were comparable to each other - where there were extensive protrusions.

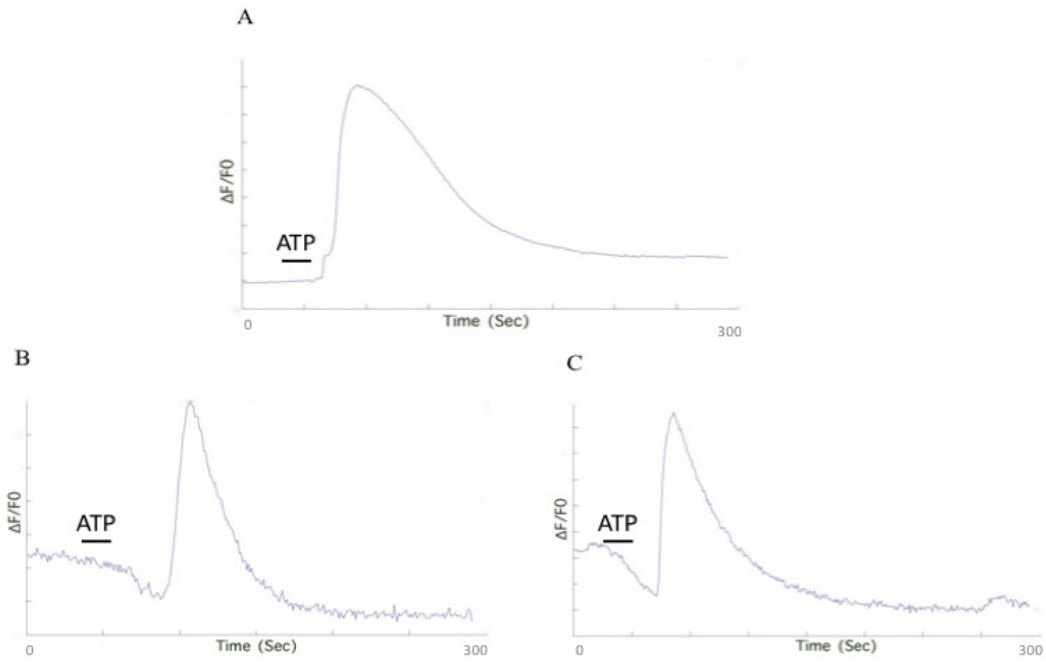

Figure 49: Comparative representative ATP evoked responses of astrocytes. (A) Biphasic responses of DIV 28 generated mESCDA (B) Mechanically isolated mESCDA (C) Primary cortical astrocytes reliably labelling showing similar calcium dynamics which are mono-phasic in nature.

Similarly, ATP evoked calcium dynamics of all these groups were compared and showed similar calcium transients (Fig. 49). There were a clear rise and decay phases, and when comparing the rise time were similar of DIV 28 mESCDA (6.50 seconds, n=1), isolated mESCDA (6.86 seconds, n=1) with a reduction in primary astrocytes (5.68 seconds, n=1). Similarly, decay tau also revealed no difference between the groups, DIV 28 mESCDA (78.68 seconds, n=1), isolated mESCDA (68.51 seconds, n=1) primary astrocytes (74.20 seconds, n=1), revealing the isolated and majority of generated mESCDA are comparable to their primary counterparts.

5.3.5. Neuron rich and isolated mESCDA ability to integrate

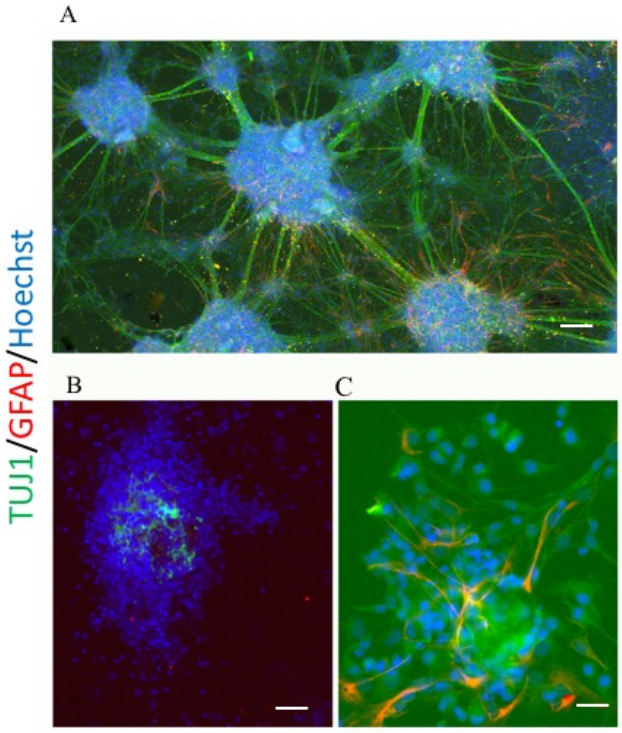

Figure 50: Integration ability of mESCDA. (A) Example of neuron rich culture (B) Treatment of neuron rich cultures with Ara-C results in extensive neuronal and astrocytic loss. (C) Direct seeding of mechanically isolated mESCDA show integration and survival ability of mESCDA and growth of neuronal cultures. Cells staining for b-Tubulin III (TUJ1) (Green) and GFAP (Red) counterstained for cell nuclei marker H- 33342 (blue stain). (A) Scale bar = 200µm, (B) Scale bar = 100µm, (C) Scale bar = 50µm

Cytosine arabinoside (AraC) treatment and integration ability of isolated mESCDA Neuron rich cultures were developed by following Pjelto et al 2012 protocol (Fig. 49A) to test isolated mESCDA ability to integrate and enhance network growth (Pjelto et al 2010). The neuron rich cultures were shown to contain astrocytes - observed by GFAP positive cells (Fig 50A). To selectively limit the number of natively produced astrocytes and limit further astrocyte division, anti-mitotic cytosine arabinoside (AraC) was used (Delivopoulos & Murray 2011). AraC was able to remove the majority of astrocytes (Fig. 50B), with few neuronal clusters remaining alongside it. These few neural clusters are not able to form elaborate networks seen from non-treated group (Fig. 50B). Mechanically isolated mESCDA at a density of 100 cells/mm2 were seeded onto Ara-C treated cultures. Immunostaining revealed that isolated mESCDA were able to integrate into the network of surviving neurons and promoted axonal and dendritic growth (Fig. 50C).

5.4. Discussion

Cell isolation and harvesting are principal techniques which are ubiquitously used in tissue culture research and cell biology studies to isolate populations of cells for future studies. In *in vitro* systems, trying to recapture what occurs in the brain is vital, therefore, isolation of one cell type and assessing their role is necessary to fully elucidate the function of that specific subtype of cell within the network (Altschuler & Wu 2010). A widespread of methodologies are employed for cell isolation, however, they can be usually broken down into two main groups, mechanical and enzymatic (Jager et al. 2016). Mechanical isolation has shown to be a harsh process which leads to accumulation of debris and has shown to have high contamination rates (Aronowitz & Hakakian 2015) therefore the widespread use of enzymes recently has been for isolating of cells over the years. Enzymatic methods have the advantages: they have been shown to be easy to use, provide reduced contamination with debris, and require no additional equipment (Beers et al. 2012). However, their mechanisms of action in dissociation and harvesting are not fully well understood. Moreover, there is the presence of a plethora of enzymes for enzymatic treatment, testing and identifying the optimal enzyme lead to increase time spent solidifying a protocol (Jager et a.l 2016). As a result, the choice of one technique over another is often subjective and it is based on past experiences and successes rather than on an understanding the method and what modifications could lead to even better results.

While this study is not the first study to approach the subject of how to best isolate cells from cultures, it provides novelty in its comparison of time points and its comparison with mechanical isolation.

5.4.1. Enzymatic treatment of mESCDA reveals presence of reactive astrocytes

The process of enzymatic treatment with enzymes such as, accurate and Trypsin/EDTA, cleaves proteins (such as cadherins, integrins, and dystroglycan) which enable the cells to adhere to the surface (Pan et al. 2014; Fong et al. 2017). Cleavage of these proteins allows detachment of the adhered cells (Pan et al. 2014). Nevertheless, it is necessary to not allow cells to be exposed to enzymes for too long, as they may permeabilise the membrane and essentially lyse the cells (Huang et al. 2010). Therefore, within the cultures, it was essential to discover the optimal time to get the maximal amount of astrocytes from enzymatic treatment. There is sparse evidence of long term incubation of stem derived cells in Trypsin/EDTA or accutase and what their effects are on structural

and functional ability (Cowan et al 2004; Hui et al. 2015), especially stem cell derived astrocytes, therefore it was essential to test long term incubation of these cells and what it yields.

Increased incubation led to increased removal and breakdown of cells (Fig. 37 - bright field). Immunocytochemical analysis of cells incubated with Trypsin/EDTA revealed the existence of astrocytes after trypsinisation - termed re-plated mESCDA. At different time points, there was reliable staining for ALDH1L1 and GFAP (Fig. 38). Analysis of GFAP positive cells revealed a significant increase in GFAP positive cells at the 60 minute group when compared to 15/30 minutes (Fig. 38). This was similarly observed by Hui et al 2015, they observed significantly more GFAP positive astrocytes derived from Sprague Dawley rats when cells were incubated for 40 minutes when compared to 20 minutes. The significant increase in GFAP positive cells could provide evidence of inflammatory reactive astrocytes, as trypsinisation is a harsh process in itself and GFAP is the most frequently used marker for inflammatory activation of astrocytes in the brain (Walz & Lang 1998; Fereidoni et al. 2013). Additionally, observing the morphology of GFAP positive cells revealed evidence towards reactivity, as the sating revealed enlarged protrusions and aberrant enlarged cytoplasm, similar to observed in APPPS1 Alzheimer mice model (Delekate et al. 2014). Further evidence towards reactivity induced by Trypsin/EDTA is shown by Fereidoni et al 2013. They revealed a dose dependent manner increase in Trypsin/EDTA concentration led to increased production of nitric oxide in cultured rat astrocytes (Fereidoni et al. 2013). Post 24 hours treatment of astrocytes with Trypsin/EDTA led to increased NF-κB activation and nitric oxide gene activity causing the development of reactive astrocytes. This may be what is occurring here, although this is to be further tested, the presence of ALDH1L1 astrocytes alongside GFAP positive astrocytes rules out the significant presence of reactive astrocytes (Boisvert et al. 2018), however this remains to be further tested. Further analysis showed that there were significantly more ALDH1L1 positive astrocytes when compared to GFAP positive astrocytes (Fig. 38), with no significant differences across the treated groups (although 60 minute group had a large variance). This suggests the presence of ALDH1L1 positive cells provides Trypsin/EDTA ability to filter out subtype of astrocytes - as there is heterogeneous population of astrocytes even at DIV 28 (see chapter 2). Furthermore, evidence dictates increased presence of anchor proteins in mature astrocytes (Hui et al 2015), therefore increased presence of GFAP positive cells in 60 minute group could be due to an increased ability of Trypsin/EDTA to cleave more anchor proteins yielding more mature astrocyte subtype (Peng et al. 2008). However, as previously discussed 60 minutes incubation is a long time for the cells to be exposed to trypsin, and the presence

of GFAP could be due to presence of reactive astrocytes (Boisvert et al. 2018). This could be further tested by performing genetic assessment to see which genes are up and downregulated to show the presence and absence of each subtype of astrocytes.

The removed and re-plated Trypsin/EDTA isolated mESCDA were analysed for they functionality at the 60 minute marks as it yielded an increased number of astrocytes across all time-points. As with previous analysis on generated mESCDA (chapter 3), isolated mESCDA were loaded with Fluo-4-AM dye and tested for purinergic mediated calcium dynamics. Cells loaded with Fluo-4 cells exhibited astrocytic morphology seen in generated mESCDA (Fig - chapter 3). Application of ATP displayed clear transient from isolated mESCDA (Fig. 40). The transients had a rise phase, a peak response, and a decay phase. The responses were analogous to generated mESCDA and other stem cell derived astrocytes (Zhang et al. 2016) showing isolated mESCDA are functional and readily respond to their environment, with no compromise in their ability to be functional. Nevertheless, closer observation of calcium dynamics revealed the presence of dual peaks, where there was a clear second rise which was smaller than the first rise (Fig. 27). These dual peaks observed have shown to be related to astrocyte reactivity (Morita et al 2003). For example, Morital et al 2003, using Wistar rats showed the presence of evoked dual peaks in the presence of pro-inflammatory cytokines TNF-a and IL-1a. This is further confirmed by Delekate et al 2014, as they observe increase hyperactivity and the presence of increased dual peaks when measuring calcium activity in APPPS1 (Alzheimer's) mice astrocyte mice. Additionally, uncharacteristic expression of purinoreceptors may also cause changes in calcium dynamics (Franke et al. 2012). During severe neurodegeneration, reactive astrocytes display hyperactivity altered calcium dynamics which are mediated by purinergic receptors. For example, Reichenbach et al 2018 in mice which have a human KM67/671NL mutation for Alzheimer's there are severe cases of increased dual peaks and frequency of spontaneous calcium events from astrocytes, similar to what is observed here. And blocking the P2YR1 normalised network dysfunction by normalising calcium dynamics (Reichenbach et al. 2018). This is what is observed here and shows that long incubation with Trypsin/EDTA leads to changes in receptor dynamics causing changes in calcium dynamics seen here. These changes in receptor dynamic can also be attributed to increase in GFAP positive staining, pointing towards the argument of presence of reactive astrocytes at 60 minutes. Nevertheless, this needs to be further tested, for example by performing genetic expression at all-time points or performing calcium analysis at earlier time-point to see at which time points the changes start to occur.

The evidence here shows, that the presence of Trypsin/EDTA for a prolonged period of time leads to changes in astrocyte behaviour causing them to become more reactive. Therefore, a gentler approach or removal of cells at an earlier time point is needed to procure cells which are functionally and genetically similar to their primary and stem cell derived counterparts. Accutase is an enzyme which contains a mixture of proteolytic, collagenolytic, and DNAse activities (Bajpai et al. 2008). Evidence dictates accutase leads to better cell viability and cell yield compared to Trypsin/EDTA (Li et al 2015), and more recently stem cells are being treated with accutase rather than trypsin for passaging and efficient cell generation (TCW et al 2017). Therefore, to prevent the presence of reactive astrocytes caused by Trypsin/EDTA, accutase was used on DIV 28 mESCDA. Accutase displayed reduced compromising the EBs and prevented the accumulation of debris (Fig. 40). Therefore, confirming straightaway the gentler approach of accutase when compared to trypsin. Similarly, with accutase, there was reliable staining with GFAP and ALDH1L1, showing accutase reliably being able to interact with anchor proteins on the laminin coated coverslips to remove astrocytes (Fig. 42). There is a significant increase in GFAP positive cells in 60 minutes when compared to 15 minutes – similar to Trypsin/EDTA treatment, pointing towards the presence of reactive astrocytes (Fig. 43). Additionally, analysis of ALDH1L1 staining revealed no differences in the number of astrocytes, again similar to Trypsin/EDTA. However, here accutase removed less number of ALDH1L1 positive cells when comparing the number/mm2 (Fig. 43). These similarities in long term incubation reveal long term incubation with enzymes produces reactive astrocytes. Therefore, focus of towards isolating astrocytes should be short term incubation, where there were a reduced number of astrocytes. Morphologically, isolated mESCDA seem to be comparable to generated mESCDA – across all time points, where there were extended protrusions from the cytoplasm and similar cell size from all of the time points. The result here shows that accutase seems to be gentler to the cells and less destructive to the cell surface and membrane proteins, yet long term incubation is as harmful as Trypsin/EDTA. These effects of accutase in long term incubation on stem cell derived astrocyte have not been reported, thus providing novelty. Comparative analysis with Mesenchymal Stromal Cells from Salzig et al 2016 shows 45 minute incubation leads to more viable cells when compared to other enzymatic treatment including Trypsin/EDTA, and this is represented by morphological differences observed – observed via GFAP positive staining (Salzig et al. 2016). Nonetheless, the number of cells from each treatment is the same, which what is observed here. Additionally, Bajpai et al 2008, report accutase prevents the ‘cellular crisis’ in human embryonic stem cells (hESC) and lead to high efficiency and cell numbers. Although there is reduced number of cells reported here when compared to trypsin/EDTA, the

maintenance of cellular integrity and similarity in numbers across the DIVs dictates usage of accutase compared to Trypsin/EDTA may be a better alternative.

Similar to Trypsin/EDTA, the removed and re-plated accutase treated mESCDA were analysed for their functionality at the 60-minute mark to allow direct comparison with Trypsin/EDTA treatment. As with previous analysis isolated mESCDA were loaded with Fluo-4-AM dye and tested for purinergic mediated calcium dynamics. Loaded cells exhibited astrocytic morphology and application of ATP displayed clear transient from isolated mESCDA (Fig. 44). The transients had a rise phase, a peak response, and a decay phase. The responses were analogous to generated mESCDA and Trypsin/EDTA mESCDA. Calcium dynamics revealed a rise and decay phase, with the peak rise showing the presence of dual peaks, where there was a clear second rise which was smaller than the first rise, and occurred in a similar manner to Trypsin/EDTA. Nevertheless, the peak rise was noticeably smaller. This smaller rise could be due to reduced reactivity in astrocyte with accutase treatment, however this further needs to be tested. The novel evidence here displays long term incubation with enzymes should be avoided. However, the study could benefit from analysis of calcium dynamics from previous timepoints. However as there were not any significant changes in morphology and marker expression, analysis of earlier incubation period may not provide any beneficial outcomes. Hence, enzymatic treatment, therefore, may not be a suitable option when isolating mESCDA.

5.4.2. Mechanical isolation yields healthier isolated mESCDA

As an alternative to enzymatic treatment, mechanical isolation of cells was also performed (Aronowitz et al. 2015). There is also various method for mechanical isolation for cell harvestings such as prolonged incubation on a rotator – the McCarthy and deVellis method for isolating astrocytes from a substrate from primary tissue (McCarthy 1980), isolation via cell scrapers (Beers et al. 2012), or heavy pipetting. Prior to enzymatic treatments, mechanical isolation was the standard technique utilised when isolating cells from a substrate (Jager et al. 2016). Additionally, assessment and comparison of mechanical and enzymatic treatments have been previously performed (Jager et al. 2016), however assessment on stem cell derived astrocytes and measurement of functionality via calcium dynamics is where the study provides novelty.

Here, mechanical isolation of DIV 28 mESCDA led successful removal from the substrate and cells reliably labelled for astrocyte markers. Analysis showed significant

more ALDH1L1 positive cells compared to GFAP and closer inspection to the numbers revealed isolation resembling accutase treatment (~100 cells/mm2 for each staining). This result displayed accutase treatment to be as good as mechanical treatment when comparing the number of astrocyte positive staining. Additionally, the morphology of mechanically isolated astrocytes (observed via GFAP positive staining), was similar to accutase treated cells (extended protrusions from the cytoplasm and similar cell size from all of the timepoints and comparable cell size to generated mESCDA from DIV 28). Nevertheless, when observing calcium dynamics, the responses here differed (Fig. 47). Mechanically isolated mESCDA were subjected to similar ATP stimulation and provided a clear and robust calcium transient, confirming the presence of purinergic receptors (Fig. 47). However, when comparing the calcium transient with mechanically isolated cells, there was a notable absence of dual peaks, which was similarly observed in generated mESCDA (Fig. 28). The lack of dual peaks observed shows mechanical isolation is better in maintaining cellular structural and functional integrity. Mechanical isolation of stem cell astrocytes has been performed previously by Santos et al 2017, where they use human iPSCs to derive astrocytes (See Table 1). However, the study does not measure the calcium dynamics of astrocytes. Therefore, the results obtained here are novel in terms of assessment of functional calcium aspects of enzymatic and mechanical disassociations.

5.3.3. Isolated and generated mESCDA are similar to the primary astrocytes and can be used as a tool for co-culture studies

Once the isolation methodology was established, the isolated cells were compared with their generated and primary cortical counterparts, to assess and confirm their ability to be utilised for future studies and create cell banks (Stacey 2012). The similar pattern of immunocytochemistry and functional analysis was used to provide comparative analysis (Fig. 48/49).

Immunocytochemistry revealed a similar pattern of expression of GFAP when isolated, and generated mESCDA were compared to primary cortical astrocytes. GFAP was shown to label astrocytes which displayed similar morphologies across the groups (Fig. 48). This showed that generated and mechanically isolated mESCDA are similar in expression to primary astrocytes. This similarity in expression is observed by other stem cell derived astrocyte studies. For example, Kleiderman et al 2016 observed similar expression in mouse neural stem cell derived astrocytes when compared to primary astrocytes derived from P1 pups (Kleiderman 2016). However, this isolated expression has not been

observed previously. These multiple comparisons with three different groups is novel and provide mESCDA to be used as a tool for future studies in determining the roles of astrocytes.

One of the fundamental roles of astrocytes is providing support and network integrity (Ullian et al. 2001; Perez-alvarez et al. 2010). Isolated mESCDA were assessed in their ability to support and rescue and improve altered neural network (Boehler et al. 2008). Neuron rich culture was grown by following Peljto et al protocol (Fig. 50) and the number of endogenous astrocytes was limited with anti-mitotic agent cytosine arabinoside (AraC) (Delivopoulos & Murray. 2011). The addition of AraC caused significant loss of neurons and endogenous astrocytes led to altered neural networks - observed via loss of neuronal clusters, reduction of TUJ1 and GFAP positive cells. This has been observed before, as Ahlemeyer et al 2003 have shown that AraC causes astrocytes to become reactive resulting in damage to neurons and astrocytes (Ahlemeyer et al. 2003; Delivopoulos & Murray 2011). Further evidence is shown by Geller et al 2001, and show AraC kills postmitotic neurons by a mechanism similar to neurotrophic factor deprivation and TUJ positive images demonstrate that neurons in AraC treated cultures appear unhealthy when compared to untreated cultures, similar to what is observed here.

Since the endogenous astrocytes were successfully removed (Fig. 49A), mechanically isolated mESCDA were directly plated onto the damaged neutron rich network (Fig. 50B). The introduced mESCDA were able to show integration into cells that were left post AraC treatment, and showed to promote neural survival, shown by TUJ1 positive staining (Fig. 50C), similar to what is observed *in vivo* (Farhy-Tselnicker et al. 2018), and displayed by their primary counterparts (Boehler et al. 2007). Although rudimentary, this observation provided evidence of mESCDA possessing ability to integrate into the neuronal network, confirming the future potential usage of mESCDA as a tool to study neurodegenerative diseases. This observation is in close agreement with multiple stem cell derived astrocytes studies (See Table 1). For example, Keugler et al 2012, Shaltouki et al 2013, Santos et al 2017 were able to show that derived astrocytes were able to rescue damaged neurons - shown via increased TUJ1 string, and were able to promote new synapses and dendrites by inducing release of trophic factors and promote synaptogenesis (Shaltouki et al. 2013, TCW et al 2017).

5.3.4. Study improvements and future directions

Although the study provides efficient method for isolation of mESCDA and their ability to integrate, improvements which time could not permit to perform, would enhance the results explained. For example, further improvements could be performed on isolated astrocytes. They could be tested for their expression for all of the relevant astrocyte markers that were used for generated mESCDA (see chapter 2 and 3). The expression of purinergic and some relevant astrocyte markers are present because isolated cells respond to ATP and exhibit expression of ALDH1L1, and GFAP, however a full characterisation would further solidify the results obtained. The study could benefit by initially providing calcium dynamics analysis from all of the time points for each enzymatic treatment. Although here providing calcium dynamics from Tryspin/EDTA would be not fully necessary, as immunocytochemistry has provided sufficient results that regardless of timepoint, the isolated cells have shown to be reactive - seen via morphology and expression via GFAP staining. Results for accutase could make accutase treatment the better candidate for isolating astrocytes, as earlier timepoints have shown to have reduced GFAP positive staining (Fig. 40). Furthermore, the dual peaks observed at 60 minutes mark are significantly attenuated when compared to Trypsin/EDTA (Fig. 42), thus do the dual peaks arise at earlier timepoints. Further to this, even though trypan blue analysis was performed before cell plating, cellular viability assays such as BrdU, MTT, and Live/Dead assays would further provide evidence on the effect of the enzyme on mESCDA.

The integration ability of isolated mESCDA could also be tested even further. It is established that these mESCDA are able to integrate and rescue a neuron rich culture. Further studies could assess how mESCDA rescue a disrupted network. For example Farhy-Tselnicker et al. 2018 recently displayed stabilisation of pre and post synapses occurs due to expression of glypican (heparan sulfate proteoglycans) by astrocytes. Removal of astrocytes leads to disruption in synapse stabilisation and neuronal signalling (Ullian et al 2001). The study here could test the expression of glypican pre and post introduction of mESCDA, and could also test for synaptic integrity and synapse formation by staining for pre and post synapses (Ullian et al. 2001). Additionally, the disruption of network via electrophysiological studies could also be performed. Evidence has shown that a single astrocyte can come into contact with many synapses – subsequently forming a tripartite synapse (Araque et al. 1999), hence astrocytes can communicate between them and simultaneously effect neurons. This effect has been demonstrated in the hippocampus, where astrocyte calcium elevations release

gliotransmitters causing synchronous excitation of clusters of pyramidal neurons, indicating that astrocyte activity contributing towards neuronal synchronisation (Fellin 2009). Neuronal network and mESCDA role in network activity could also be studied via tools such as multi electrode arrays (MEAs), and network level activity can be monitored. Furthermore, better analysis of the integration ability could be tested via performing co-localisation analysis of staining. Additionally, increasing n numbers, or conditioned media and astrocyte suspension study could be tested on neuronal population could provide better insight onto mESCA ability to integrate and rescue the neuronal population. For example, Boehler et al 2008 were able to show that conditioned media from astrocytes was sufficient enough to rescue damaged neural activity shown via electrophysiological recordings (Boehler et al 2008), and similar analysis could be performed here where before direct seeding, conditioned media or physical barrier studies could be performed to better understand integration ability of astrocytes.

Nevertheless, the isolated and generated mESCDA showed they contain the ability to form a co-cultures of neurons. This opens up new possibilities of studying the interplay of neurons and astrocytes during development, the influence of astrocyte during neurodegenerative diseases and inflammation.

6. Conclusion

A major breakthrough in the study of astrocytes was the description of a procedure to purify and culture astrocytes from neonatal rodent brains using serum-containing media (McCarthy and de Vellis, 1980). This protocol was used and modified for decades to culture not only rodent cells but also human astrocytes from foetal post-mortem tissue (Ennas et al., 1992; Lee et al., 1993). Recently, new methods of astrocyte purification using immunopanning combined with serum-free culture have been described for adult rodent and human brains (Zhang et al. 2016). However, these are invasive techniques. Thus, cellular models that rely on the differentiation of astrocytes from stem cells are the most accessible methods for *in vitro* disease modelling and can potentially allow for new discoveries and allow us to probe intricate function of astrocyte in different conditions.

In this study, significant effort has been made to contribute towards a standardisation of protocols for *in vitro* astrocytogenesis and generate astrocytes from stem cells. Similar to in vivo astrocytogenesis, majority of *in vitro* protocol require a prolonged time-course to generate functional and morphologically relevant cells, which can be used to probe further questions. Here, the protocol was able to generate different subpopulations of astrocytes, which are heterogeneous in form and function, in a quick and efficient manner. To our knowledge, our method is distinct from others recently reported (see Table 4). Its major advantages are the ease by which mESCDA can be differentiated – via semi directed approach and with reduced use of morphogens, and how they follow the *in vivo* astrocytegenesis signature – seen via genetic and staining analysis. This allows future studies to be conducted at different timelines to further to assess the developmental role of astrocytes, and contribute towards studies examining the factors controlling astrocyte differentiation. Furthermore, the mESCDA can be expanded and cryopreserved, serving as a source of cells to support an array of experiments, such as performing co-culture studies with neurons and other cell types.

In summary, reduction of the timeframe, together with data on the phenotype and function of the resultant cells, suggests that generation of astrocytes from mouse embryonic stem cells (mESCDA) is a viable alternative to the preparation of primary astrocytes for biological, pharmacological and toxicological studies. The comparison of mESCDA and primary astrocytes performed here provided new insights into stem cell derived functionality. In the future, the generation of mESCDA with different genetic back grounds opens up new possibilities in patient-specific research.

7. Appendix

A

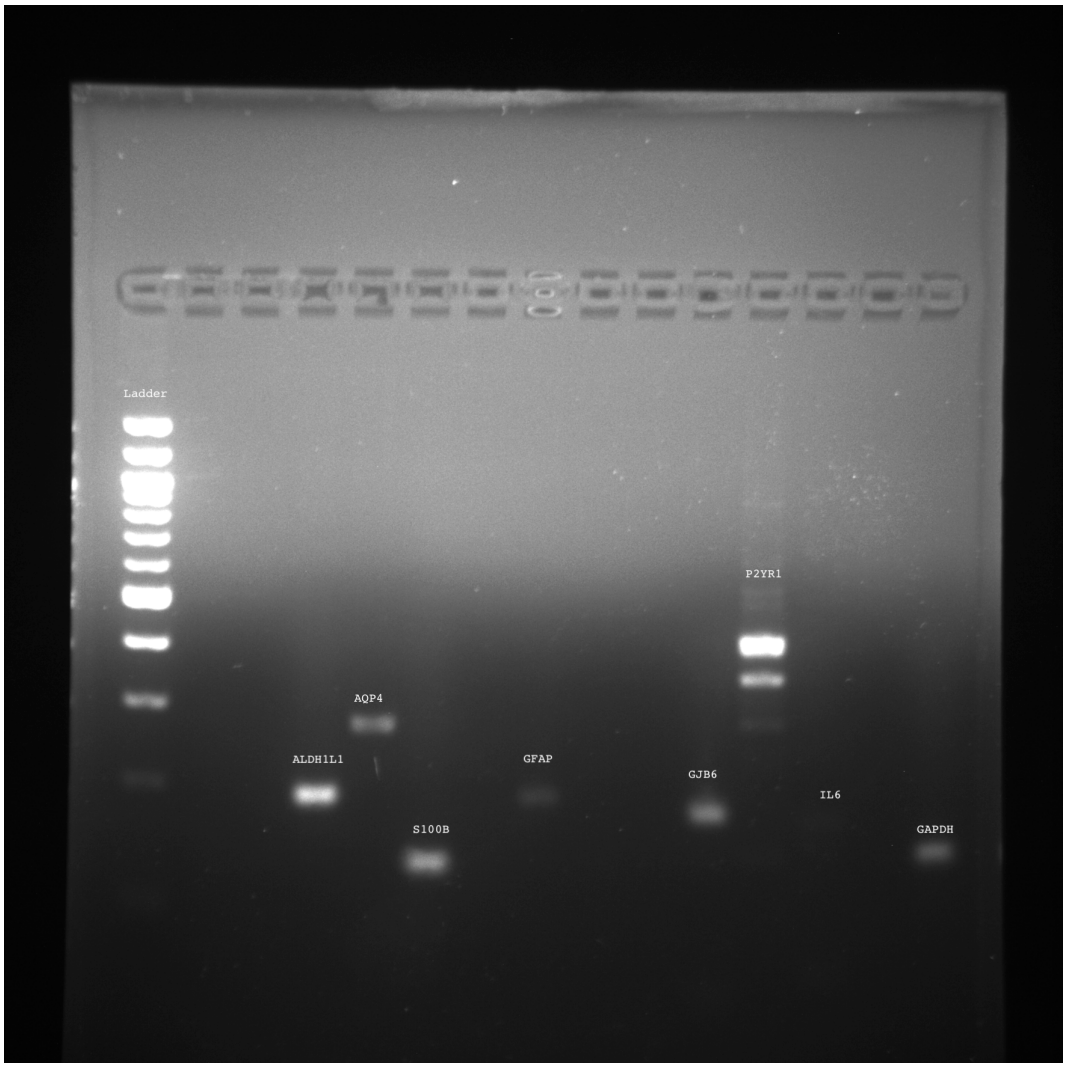

Figure 51A: Representative reverse transcriptase PCR image. (B) Expression of tested genes (Table 3). Each gene expression was compared against GAPDH to obtain absolute value via gel densitometry and ImageJ.

B

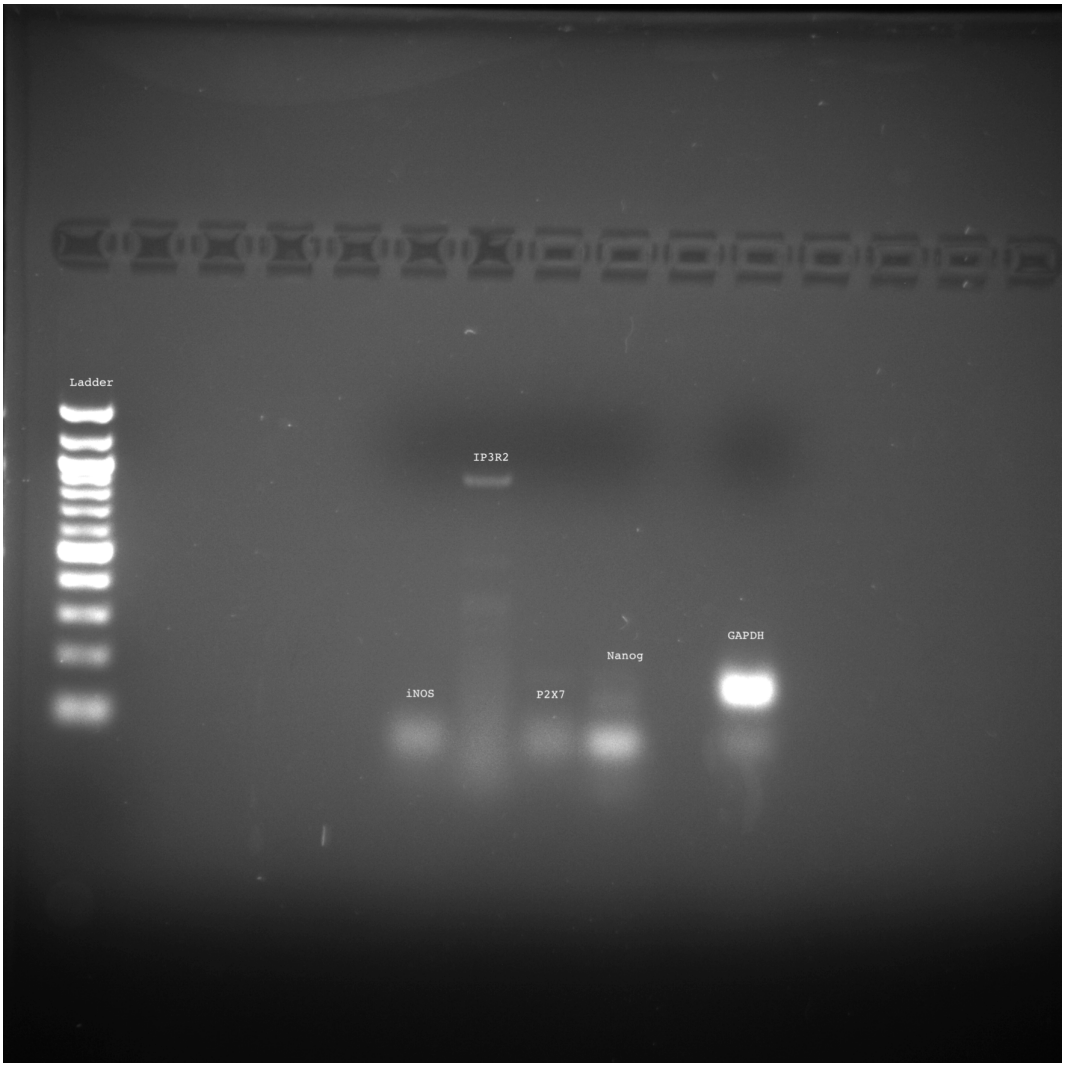

Figure 51B: Representative reverse transcriptase PCR image. Expression of tested genes (Table 3). Each gene expression was compared against GAPDH to obtain absolute value via gel densitometry and ImageJ.

A

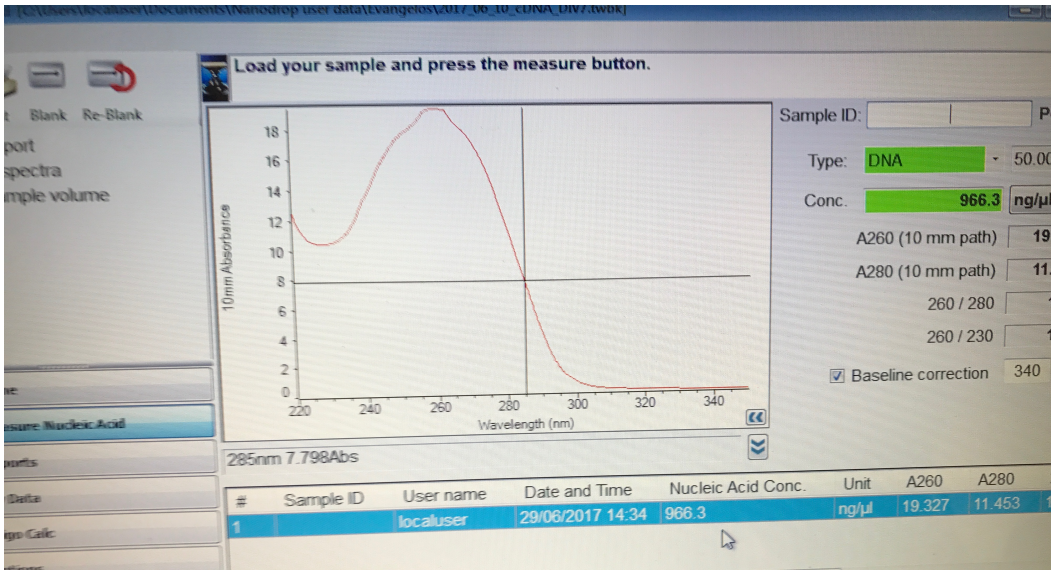

B

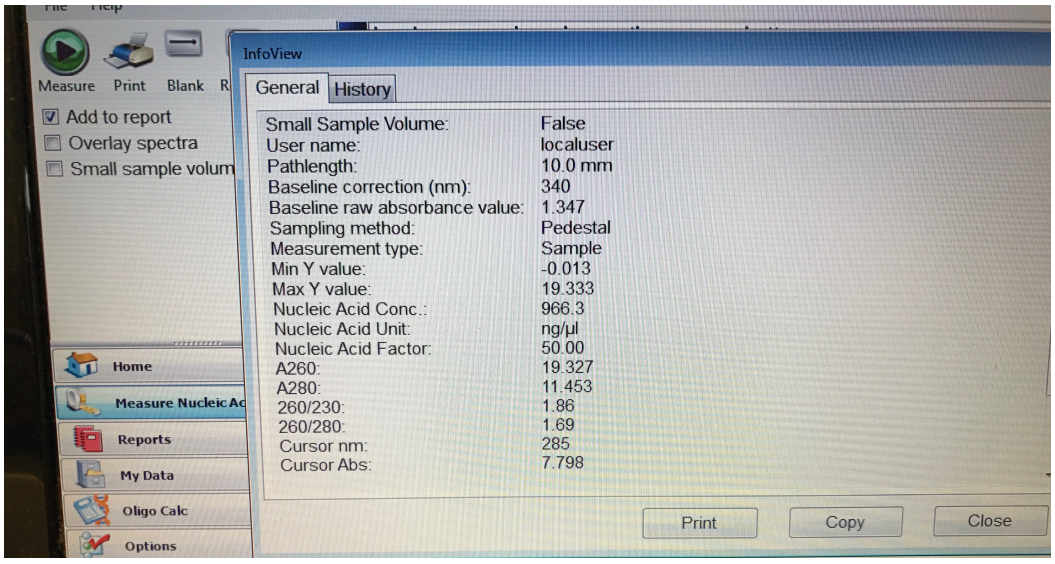

Figure 52: (A) Representative image of a graph of absorbance from the spectrophotometer (Nanodrop). (B) The values obtained from the spectrophotometer to be used to determine the yield of mRNA and cDNA.

A

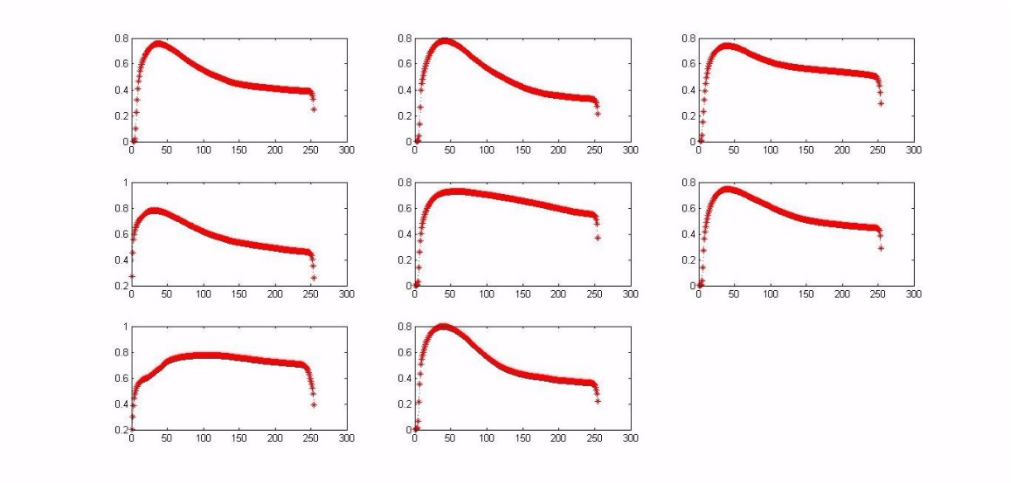

B

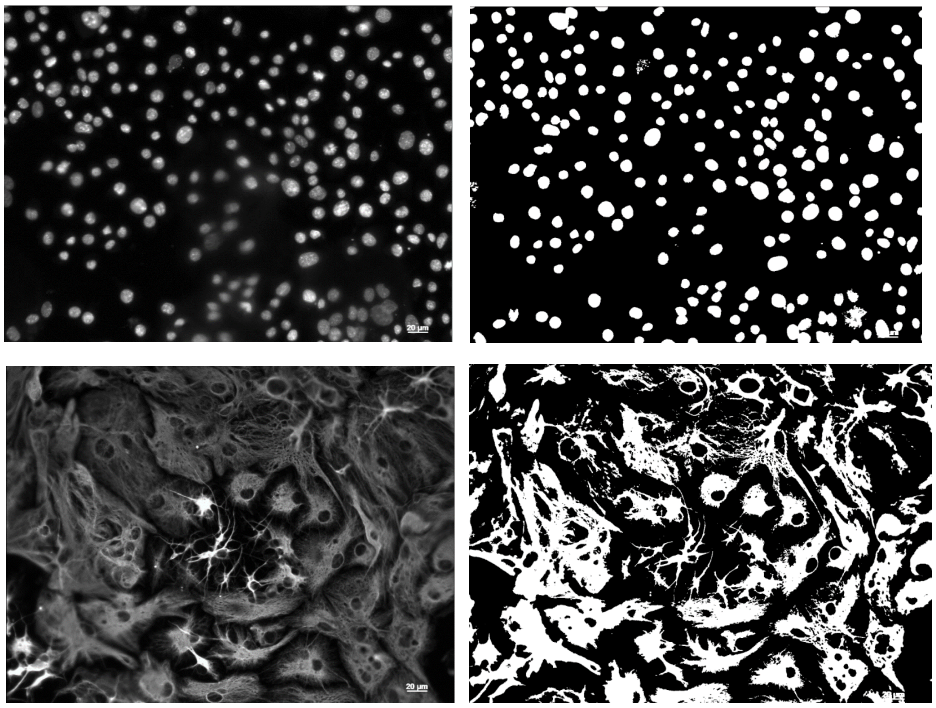

Figure 53: Image analysis. Each image was split into relevant channel and was analysed for its components. (A) Each image had a peak or optimal thresholding value seen. (B) Image was split into relevant channel, Green, Red, and Blue and was analysed for its components from the optimal value, further analysis was performed.

8. References

Adzic, M. & Nedeljkovic, N., 2018. Unveiling the role of Ecto-5'-nucleotidase/CD73 in astrocyte migration by using pharmacological tools. *Frontiers in Pharmacology*, 9(MAR), pp.1–19.

Agulhon, C. et al., 2008. What Is the Role of Astrocyte Calcium in Neurophysiology? *Neuron*, 59(6), pp.932–946.

Ahlemeyer, B. et al., 2003. Cytosine arabinofuranoside-induced activation of astrocytes increases the susceptibility of neurons to glutamate due to the release of soluble factors. *Neurochemistry International*, 42(7), pp.567–581.

Alliot, F. et al., 1999. Brain parenchyma vessels and the angiotensin system. *Brain Research*, pp.101–112.

Altschuler, S.J. & Wu, L.F., 2010. Cellular heterogeneity: when do differences make a difference? *Cell*, 141(4), pp.559–563.

Amadio, S. et al., 2017. Modulation of P2X7 receptor during inflammation in multiple sclerosis. *Frontiers in Immunology*, 8(NOV), pp.1–17.

Anderson, C.M., Bergher, J.P. & Swanson, R. a, 2004. ATP-induced ATP release from astrocytes. *Journal of neurochemistry*, 88(1), pp.246–256.

Anthony, T.E. & Heintz, N., 2007. The Folate Metabolic Enzyme ALDH1L1 Is Restricted to the Midline of the Early CNS , Suggesting a Role in Human Neural Tube Defects. *Journal of comparative neurobiology*, 383(March 2006), pp.368–383.

Araque, A. et al., 1999. Tripartite synapses: glia, the unacknowledged partner. *TINS*, 22(5), pp.207–208.

Araque, A. & Navarrete, M., 2010. Glial cells in neuronal network function. *Philosophical transactions of the Royal Society of London. Series B, Biological sciences*, 365(1551), pp.2375–81. Available at: http://www.pubmedcentral.nih.gov/articlerender.fcgi?artid=2894949&tool=pmcentrez&rendertype=abstract [Accessed November 5, 2014].

Aronowitz, J. & Hakakian, B., 2015. A novel and effective strategy for the isolation of adipose-derived stem cells: Minimally manipulated adipose-derived stem cells for more rapid and safe stem cell therapy. *Plastic and Reconstructive Surgery*, 133(6), pp.1406–1409. Available at: http://www.nejm.org/doi/abs/10.1056/NEJMsr040330.

Asano, H. et al., 2009. Astrocyte differentiation of neural precursor cells is enhanced by retinoic acid through a change in epigenetic modification. *Stem cells (Dayton, Ohio)*, 27(11), pp.2744–52. Available at: http://www.ncbi.nlm.nih.gov/pubmed/19609931 [Accessed October 24, 2014].

Bajpai, R. et al., 2008. Efficient propagation of single cells accutase-dissociated human

embryonic stem cells. *Molecular Reproduction and Development*, 75(5), pp.818–827.

Ban, J. et al., 2007. Embryonic stem cell-derived neurons form functional networks in vitro. *Stem cells (Dayton, Ohio)*, 25(3), pp.738–49. Available at: http://www.ncbi.nlm.nih.gov/pubmed/17110621 [Accessed December 4, 2014].

Barberi, T. et al., 2003. Neural subtype specification of fertilization and nuclear transfer embryonic stem cells and application in parkinsonian mice. *Nature biotechnology*, 21(10), pp.1200–7. Available at: http://www.ncbi.nlm.nih.gov/pubmed/14502203 [Accessed December 2, 2014].

Bayraktar, O.A. et al., 2015. Astrocyte Development and Heterogeneity.

Bazargani, N. & Attwell, D., 2016. Astrocyte calcium signaling: the third wave. *Nature Neuroscience*, 19(2), pp.182–189. Available at: http://www.nature.com/doifinder/10.1038/nn.4201.

Becker, A.J. McCulloch, E.A. Till, J.., 1963. Cytological Demonstration of the Clonal Nature of Spleen Colonies Derived from Transplanted Mouse Marrow Cells. *Nature*, 197, pp.452–454.

Beers, J. et al., 2013. Passaging and colony expansion of human pluripotent stem cells by enzyme-free dissociation in chemically defined culture conditions. *Nature Protocols*, 7(11), pp.2029–2040.

Bellot-Saez, A. et al., 2017. Astrocytic modulation of neuronal excitability through K+spatial buffering. *Neuroscience and Biobehavioral Reviews*, 77, pp.87–97. Available at: http://dx.doi.org/10.1016/j.neubiorev.2017.03.002.

Bernstein, M. et al., 1998. Pharmacological characterisation of metabotropic glutamatergic and purinergic receptors linked to Ca 2 + signalling in hippocampal astrocytes. , 37, pp.169–178.

Biehl, J.K. & Russell, B., 2009. Introduction to Stem Cell Therapy. *Journal of Cardiovascular Nursing*, 24(2), pp.98–103.

Boehler, M.D., Wheeler, B.C. & Brewer, G.J., 2008. Added astroglia promote greater synapse density and higher activity in neuronal networks. , 5, pp.127–140.

Boisvert, M. et al., 2018. The Aging Astrocyte Transcriptome from Multiple Regions of the Mouse Brain. *Cell Reports*, 15(1), pp.34–48.

Bouzier-Sore, A.-K. & Pellerin, L., 2013. Unraveling the complex metabolic nature of astrocytes. *Frontiers in Cellular Neuroscience*, 7(October), pp.1–13. Available at: http://journal.frontiersin.org/article/10.3389/fncel.2013.00179/abstract.

Bradley, R.A. & A, 2018. Heterogeneity and Function of Human Astrocytes By.

Brown, J. a et al., 2014. Metabolic consequences of interleukin-6 challenge in developing neurons and astroglia. *Journal of neuroinflammation*, 11(1), p.183. Available at:

http://www.ncbi.nlm.nih.gov/pubmed/25374324 [Accessed November 10, 2014].

Brozzi, F. et al., 2009. S100B Protein Regulates Astrocyte Shape and Migration via Interaction with Src Kinase: IMPLICATIONS FOR ASTROCYTE DEVELOPMENT, ACTIVATION, AND TUMOR GROWTH. *Journal of Biological Chemistry*, 284(13), pp.8797–8811. Available at: http://www.jbc.org/cgi/doi/10.1074/jbc.M805897200.

Burnstock, G., 1978. A basis for distinguishing two types of purinergic receptor. *Cell membrane receptors for drugs and hormones: a multidisciplinary approach*, pp.107–118.

Burnstock, G. et al., 2010. The birth and postnatal development of purinergic signalling. , (1929), pp.93–147.

Cahoy, J.D. et al., 2008. A transcriptome database for astrocytes, neurons, and oligodendrocytes: a new resource for understanding brain development and function. *The Journal of neuroscience : the official journal of the Society for Neuroscience*, 28(1), pp.264–78. Available at: http://www.ncbi.nlm.nih.gov/pubmed/18171944 [Accessed July 10, 2014].

Carpenter, M.K. et al., 2001. Enrichment of neurons and neural precursors from human embryonic stem cells. *Experimental Neurology*, 172(2), pp.383–397.

Centemeri, C. et al., 1997. Characterization of the Ca 2 + responses evoked by ATP and other nucleotides in mammalian brain astrocytes. *British Journal of Pharmacology*, pp.1700–1706.

Ceruti, S. & Abbracchio, M.P., 2006. Roles of P2 receptors in glial cells: focus on astrocytes. *Purinergic Signalling*, 2(4), pp.595–604. Available at: http://www.ncbi.nlm.nih.gov/pubmed/18404462%5Cnhttp://www.ncbi.nlm.nih.gov/pubmed/18404462?ordinalpos=4&itool=EntrezSystem2.PEntrez.Pubmed.Pubmed_ResultsPanel.Pubmed_DefaultReportPanel.Pubmed_RVDocSum.

Chagastelles, P.C. & Nardi, N.B., 2011. Biology of stem cells: An overview. *Kidney International Supplements*, 1(3), pp.63–67. Available at: http://dx.doi.org/10.1038/kisup.2011.15.

Chandrasekaran, A. et al., 2016. Astrocyte Differentiation of Human Pluripotent Stem Cells: New Tools for Neurological Disorder Research. *Frontiers in Cellular Neuroscience*, 10(September), p.215. Available at: http://journal.frontiersin.org/article/10.3389/fncel.2016.00215.

Cho, J.M. et al., 2013. Characterization of nestin expression in astrocytes in the rat hippocampal CA1 region following transient forebrain ischemia. *Anatomy & cell biology*, 46(2), pp.131–40. Available at: http://www.pubmedcentral.nih.gov/articlerender.fcgi?artid=3713277&tool=pmcentr

ez&rendertype=abstract.

Chung, W., Allen, N.J. & Eroglu, C., 2015. Astrocytes Control Synapse Formation, Function, and Elimination.

Clarke, L.E. & Barres, B. a, 2013. Emerging roles of astrocytes in neural circuit development. *Nature reviews. Neuroscience*, 14(5), pp.311–21. Available at: http://www.ncbi.nlm.nih.gov/pubmed/23595014 [Accessed July 11, 2014].

Conley, B.J. et al., 2004. Derivation, propagation and differentiation of human embryonic stem cells. *The international journal of biochemistry & cell biology*, 36(4), pp.555–67. Available at: http://www.ncbi.nlm.nih.gov/pubmed/15010323 [Accessed November 5, 2014].

Conti, L. et al., 2005. Niche-independent symmetrical self-renewal of a mammalian tissue stem cell. *PLoS biology*, 3(9), p.e283. Available at: http://www.pubmedcentral.nih.gov/articlerender.fcgi?artid=1184591&tool=pmcentrez&rendertype=abstract [Accessed July 10, 2014].

Covelo, a. & Araque, a., 2015. Lateral regulation of synaptic transmission by astrocytes. *Neuroscience*, (March). Available at: http://linkinghub.elsevier.com/retrieve/pii/S0306452215001888.

Cowan, C.A. et al., 2004. Derivation of Embryonic Stem-Cell Lines from Human Blastocysts. *New England Journal of Medicine*, 350(13), pp.1353–1356. Available at: http://www.nejm.org/doi/abs/10.1056/NEJMsr040330.

Crocker, S.J. et al., 2008. A novel method to establish microglia-free astrocyte cultures: comparison of matrix metalloproteinase expression profiles in pure cultures of astrocytes and microglia. *Glia*, 56(11), pp.1187–98. Available at: http://www.pubmedcentral.nih.gov/articlerender.fcgi?artid=2776034&tool=pmcentrez&rendertype=abstract [Accessed November 5, 2014].

Dallérac, G., Chever, O. & Rouach, N., 2013. How do astrocytes shape synaptic transmission? Insights from electrophysiology. *Frontiers in Cellular Neuroscience*, 7(October), pp.1–19. Available at: http://journal.frontiersin.org/article/10.3389/fncel.2013.00159/abstract.

Delekate, A. et al., 2014. Metabotropic P2Y1 receptor signalling mediates astrocytic hyperactivity in vivo in an Alzheimer's disease mouse model. *Nature communications*, 5, p.5422. Available at: http://www.ncbi.nlm.nih.gov/pubmed/25406732 [Accessed November 21, 2014].

Delivopoulos, E. & Murray, A.F., 2011. Controlled adhesion and growth of long term glial and neuronal cultures on Parylene-c. *PLoS ONE*, 6(9).

Desilva, T.M. et al., 2012. Expression of EAAT2 in neurons and protoplasmic astrocytes during human cortical development. *Journal of Comparative Neurology*, 520(17),

pp.3912–3932.

Dienel, G. a., 2015. The metabolic trinity, glucose–glycogen–lactate, links astrocytes and neurons in brain energetics, signaling, memory, and gene expression. *Neuroscience Letters*. Available at: http://linkinghub.elsevier.com/retrieve/pii/S0304394015001676.

Ding, S., 2014. Glutamate and ATP at the Interface of Metabolism and Signaling in the Brain. *Advances in Neurobiology*, 11, pp.189–211. Available at: http://link.springer.com/10.1007/978-3-319-08894-5.

Donato, R. et al., 2008. S100B's double life: Intracellular regulator and extracellular signal. *BBA - Molecular Cell Research*, 1793(6), pp.1008–1022. Available at: http://dx.doi.org/10.1016/j.bbamcr.2008.11.009.

Le Dréau, G. & Martí, E., 2012. Dorsal-ventral patterning of the neural tube: A tale of three signals. *Developmental Neurobiology*, 72(12), pp.1471–1481.

Emdad, L. et al., 2012. Efficient Differentiation of Human Embryonic and Induced Pluripotent Stem Cells into Functional Astrocytes. *Stem Cells and Development*, 21(3), pp.404–410.

Emsley, J.G. & Macklis, J.D., 2006. Astroglial heterogeneity closely reflects the neuronal-defined anatomy of the adult murine CNS. *Neuron Glia Biology*, 2(3), pp.175–186.

Eng, L.F. et al., 1971. An acidic protein isolated from fibrous astrocytes. *Brain Research*, 28(2), pp.351–354.

Eng, L.F., Ghirnikar, R.S. & Lee, Y.L., 2000. Glial fibrillary acidic protein: GFAP-thirty-one years (1969-2000). *Neurochemical research*, 25(9–10), pp.1439–1451.

Ennas, M.G. et al., 1992. Immunocompetent cell markers in human fetal astrocytes and neurons in culture. *Journal of Neuroscience Research*, 32(3), pp.424–436.

Espuny-Camacho, I. et al., 2013. Pyramidal Neurons Derived from Human Pluripotent Stem Cells Integrate Efficiently into Mouse Brain Circuits In Vivo. *Neuron*, 77(3), pp.440–456.

Falsig, J., Latta, M. & Leist, M., 2004. Defined inflammatory states in astrocyte cultures: correlation with susceptibility towards CD95-driven apoptosis. *Journal of neurochemistry*, 88(1), pp.181–193.

Fam, S.R. et al., 2003. Differential Frequency Dependence of P2Y 1 - and P2Y 2 - Mediated Ca 2 ∂ Signaling in Astrocytes. , 23(11), pp.4437–4444.

Farhy-Tselnicker, I. & Allen, N.J., 2018. Astrocytes, neurons, synapses: A tripartite view on cortical circuit development. *Neural Development*, 13(1), pp.1–12.

Farmer, W.T. & Murai, K., 2017. Resolving Astrocyte Heterogeneity in the CNS. *Frontiers in Cellular Neuroscience*, 11(September), pp.1–7. Available at:

http://journal.frontiersin.org/article/10.3389/fncel.2017.00300/full.

Fellin, T., 2009. Communication between neurons and astrocytes: Relevance to the modulation of synaptic and network activity. *Journal of Neurochemistry*, 108, pp.533–544.

Fereidoni, M. et al., 2013. The effects of trypsin on rat brain astrocyte activation. *Iranian journal of neurology*, 12(4), pp.129–35. Available at: http://www.pubmedcentral.nih.gov/articlerender.fcgi?artid=3829307&tool=pmcentrez&rendertype=abstract.

Fiacco, T.A. & Mccarthy, K.D., 2004. Intracellular Astrocyte Calcium Waves In Situ Increase the Frequency of Spontaneous AMPA Receptor Currents in CA1 Pyramidal Neurons. *Journal of Neuroscience*, 24(3), pp.722–732.

Fields, R.D. & Stevens-Graham, B., 2002. Neuroscience: New insights into neuron-glia communication. *Science*, 298(5593), pp.556–562.

Fields, R.D., Woo, D.H. & Basser, P.J., 2015. Perspective Glial Regulation of the Neuronal Connectome through Local and Long-Distant Communication. *Neuron*, 86, pp.374–386. Available at: http://dx.doi.org/10.1016/j.neuron.2015.01.014.

Fong, D., Duceppe, N. & Hoemann, C.D., 2017. Mesenchymal stem cell detachment with trace trypsin is superior to EDTA for in vitro chemotaxis and adhesion assays. *Biochemical and Biophysical Research Communications*, 484(3), pp.656–661. Available at: http://dx.doi.org/10.1016/j.bbrc.2017.01.171.

Foo, L.C. & Dougherty, J.D., 2013. Aldh1L1 is Expressed by Postnatal Neural Stem Cells In Vivo. *Glia*, 61(9), pp.1533–1541.

Franke, H. et al., 2012. Pathophysiology of astroglial purinergic signalling. *Purinergic Signalling*, 8(3), pp.629–657.

Freeman, M., 2010. Specification and Morphogenesis of Astrocytes. *Science*, 165(2), pp.255–269.

Furue, M.K. et al., 2008. Heparin promotes the growth of human embryonic stem cells..pdf. , 105(36), pp.13409–13414.

Gallagher, C.J. & Salter, M.W., 2003. Differential properties of astrocyte calcium waves mediated by P2Y1 and P2Y2 receptors. *The Journal of neuroscience : the official journal of the Society for Neuroscience*, 23(17), pp.6728–39. Available at: http://www.ncbi.nlm.nih.gov/pubmed/12890765.

Gao, L. et al., 2017. Direct Generation of Human Neuronal Cells from Adult Astrocytes by Small Molecules. *Stem Cell Reports*, 8(3), pp.538–547. Available at: http://dx.doi.org/10.1016/j.stemcr.2017.01.014.

Gardner, R.L., 2007. Stem cells and regenerative medicine: principles, prospects and problems. *Comptes Rendus - Biologies*, 330(6–7), pp.465–473.

Ginhoux, F. et al., 2013. Fate Mapping Analysis Reveals That Adult Microglia Derive from Primitive Macrophages. *Science*, 330(6005), pp.841–845.

Gleichman, A.J. & Carmichael, S.T., 2014. Astrocytic therapies for neuronal repair in stroke. *Neuroscience letters*, 565, pp.47–52. Available at: http://www.ncbi.nlm.nih.gov/pubmed/24184876 [Accessed November 7, 2014].

Gupta, K. et al., 2012. Human embryonic stem cell derived astrocytes mediate non-cell-autonomous neuroprotection through endogenous and drug-induced mechanisms. *Cell death and differentiation*, 19(5), pp.779–87. Available at: http://www.pubmedcentral.nih.gov/articlerender.fcgi?artid=3321621&tool=pmcentrez&rendertype=abstract [Accessed November 5, 2014].

Guthrie, P.B. et al., 1999. ATP released from astrocytes mediates glial calcium waves. *The Journal of neuroscience : the official journal of the Society for Neuroscience*, 19(2), pp.520–528.

Hachem, S. et al., 2007. Expression of S100B during embryonic development of the mouse cerebellum. *BMC developmental biology*, 7, p.17.

Halassa, M.M. et al., 2007. Synaptic Islands Defined by the Territory of a Single Astrocyte. *The Journal of neuroscience : the official journal of the Society for Neuroscience*, 27(24), pp.6473–6477.

Halassa, M.M., Fellin, T. & Haydon, P.G., 2007. The tripartite synapse: roles for gliotransmission in health and disease. *Trends in Molecular Medicine*, 13(2), pp.54–63.

Hamilton, N. et al., 2008. Mechanisms of ATP- and glutamate-mediated calcium signaling in white matter astrocytes. *Glia*, 56(7), pp.734–749.

Hamilton, N.B. & Attwell, D., 2010. Do astrocytes really exocytose neurotransmitters? *Nature reviews. Neuroscience*, 11(4), pp.227–38. Available at: http://www.ncbi.nlm.nih.gov/pubmed/20300101 [Accessed July 11, 2014].

Hanna, J. & Hubel, A., 2009. Preservation of stem cells. *Organogenesis*, 5(3), pp.134–137.

Hashioka, S. et al., 2014. Purinergic responses of calcium-dependent signaling pathways in cultured adult human astrocytes. *BMC neuroscience*, 15, p.18. Available at: http://www.pubmedcentral.nih.gov/articlerender.fcgi?artid=3903030&tool=pmcentrez&rendertype=abstract.

Hassinger, T.D. et al., 1996. An extracellular signaling component in propagation of astrocytic calcium waves. *Neurobiology*, 93(November), pp.13268–13273.

Haydon, P.G., 2001. GLIA: listening and talking to the synapse. *Nature reviews. Neuroscience*, 2(3), pp.185–193.

He, F. et al., 2005. A positive autoregulatory loop of Jak-STAT signaling controls the

onset of astrogliogenesis. *Nature Neuroscience*, 8(5), pp.616–625.

Henneberger, C. et al., 2010. Long-term potentiation depends on release of D-serine from astrocytes. *Nature*, 463(7278), pp.232–6. Available at: http://www.pubmedcentral.nih.gov/articlerender.fcgi?artid=2807667&tool=pmcentrez&rendertype=abstract [Accessed September 24, 2014].

Herculano-Houzel, S., 2014. The glia/neuron ratio: How it varies uniformly across brain structures and species and what that means for brain physiology and evolution. *Glia*, 62(9), pp.1377–1391.

Hewett, J.A. & Hewett, S.J., 2012. Induction of Nitric Oxide Synthase-2 Expression and Measurement of Nitric Oxide Production in Enriched Primary Cortical Astrocyte Cultures. , 814, pp.251–263. Available at: http://link.springer.com/10.1007/978-1-61779-452-0.

Hol, E.M. & Pekny, M., 2015. Glial fibrillary acidic protein (GFAP) and the astrocyte intermediate filament system in diseases of the central nervous system. *Current Opinion in Cell Biology*, 32, pp.121–130. Available at: http://linkinghub.elsevier.com/retrieve/pii/S0955067415000137.

Hong, S. & Song, M.-R., 2014. STAT3 but not STAT1 is required for astrocyte differentiation. *PloS one*, 9(1), p.e86851. Available at: http://www.pubmedcentral.nih.gov/articlerender.fcgi?artid=3900679&tool=pmcentrez&rendertype=abstract [Accessed November 2, 2014].

Hopperton, K.E. et al., 2018. Markers of microglia in post-mortem brain samples from patients with Alzheimer's disease: A systematic review. *Molecular Psychiatry*, 23(2), pp.177–198. Available at: http://dx.doi.org/10.1038/mp.2017.246.

Hu, X. et al., 2016. Heterogeneous astrocytes: Active players in CNS. *Brain Research Bulletin*, 125, pp.1–18. Available at: http://linkinghub.elsevier.com/retrieve/pii/S0361923016300600.

Huang, H.-L. et al., 2010. Trypsin-induced proteome alteration during cell subculture in mammalian cells. *Journal of Biomedical Science*, 17(1), pp.10–36. Available at: http://www.jbiomedsci.com/content/17/1/36%5Cnpapers3://publication/doi/10.1186/1423-0127-17-36.

Hughes, E.G., Elmariah, S.B. & Balice-Gordon, R.J., 2010. Astrocyte secreted proteins selectively increase hippocampal GABAergic axon length, branching, and synaptogenesis. *Molecular and Cellular Neuroscience*, 43(1), pp.136–145. Available at: http://dx.doi.org/10.1016/j.mcn.2009.10.004.

Hui, J.I.N. et al., 2015. Optimization of trypsin digestion intensity to obtain high-purity in vitro cultured astrocytes. *Acta Physiologica Sinica*, 67(2012), pp.103–109.

Imura, T. et al., 2006. Phenotypic and functional heterogeneity of GFAP-expressing cells

in vitro: Differential expression of LeX/CD15 by GFAP-expressing multipotent neural stem cells and non-neurogenic astrocytes. *Glia*, 53(3), pp.277–293.

Innocenti, B., Parpura, V. & Haydon, P.G., 2000. Imaging extracellular waves of glutamate during calcium signaling in cultured astrocytes. *The Journal of neuroscience : the official journal of the Society for Neuroscience*, 20(5), pp.1800–1808.

Jager, L.D. et al., 2016. Advances in Medical Sciences Effect of enzymatic and mechanical methods of dissociation on neural progenitor cells derived from induced pluripotent stem cells. *Advances in Medical Science*, 61, pp.78–84.

Jakoby, P. et al., 2014. Higher transport and metabolism of glucose in astrocytes compared with neurons: A multiphoton study of hippocampal and cerebellar tissue slices. *Cerebral Cortex*, 24(1), pp.222–231.

James, G. & Butt, A.M., 2001. P2X and P2Y purinoreceptors mediate ATP-evoked calcium signalling in optic nerve glia in situ. *Cell calcium*, 30(4), pp.251–259.

James, L.R. et al., 2011. High-throughput analysis of calcium signalling kinetics in astrocytes stimulated with different neurotransmitters. *PloS one*, 6(10), p.e26889. Available at: http://www.pubmedcentral.nih.gov/articlerender.fcgi?artid=3201978&tool=pmcentrez&rendertype=abstract.

Jeremic, A. et al., 2001. ATP stimulates calcium-dependent glutamate release from cultured astrocytes. *Journal of Neurochemistry*, 77(2), pp.664–675.

Johnson, M.A. et al., 2007. Functional neural development from human embryonic stem cells: accelerated synaptic activity via astrocyte coculture. *The Journal of neuroscience : the official journal of the Society for Neuroscience*, 27(12), pp.3069–3077.

Juopperi, T.A. et al., 2012. Astrocytes generated from patient induced pluripotent stem cells recapitulate features of Huntington's disease patient cells. *Molecular Brain*, 5(1), p.17. Available at: http://www.molecularbrain.com/content/5/1/17.

Kaja, S. et al., 2014. Differential subcellular Ca(2+) signaling in a highly specialized subpopulation of astrocytes. *Experimental neurology*. Available at: http://www.ncbi.nlm.nih.gov/pubmed/25542978 [Accessed January 6, 2015].

Kamnasaran, D., Hawkins, C. & Guha, A., 2008. Characterization and Transformation Potential of Synthetic Astrocytes Differentiated from Murine Embryonic Stem Cells. , 470(December 2007), pp.457–470.

Kamphuis, W. et al., 2012. GFAP isoforms in adult mouse brain with a focus on neurogenic astrocytes and reactive astrogliosis in mouse models of Alzheimer disease. *PLoS ONE*, 7(8).

Kang, M. & Othmer, H.G., 2009. Spatiotemporal characteristics of calcium dynamics in astrocytes. *Chaos*, 19(3), pp.1–21.

Kang, P. et al., 2012. Sox9 and NFIA Coordinate a Transcriptional Regulatory Cascade during the Initiation of Gliogenesis. *Neuron*, 74(1), pp.79–94. Available at: http://dx.doi.org/10.1016/j.neuron.2012.01.024.

Kaufman, M.H. et al., 1983. Establishment of pluripotential cell lines from haploid mouse embryos. *Journal of Embryology and Experimental Morphology*, 73(1), pp.249–261. Available at: http://dev.biologists.org/content/73/1/249.abstract.

Kempermann, G., Song, H. & Gage, F.H., 2015. Neurogenesis in the Adult Hippocampus. *Cold Spring Harbor Perspectives in Biology*, 7(9), p.a018812. Available at: http://www.ncbi.nlm.nih.gov/pubmed/26330519%0Ahttp://www.pubmedcentral.nih.gov/articlerender.fcgi?artid=PMC4563705%0Ahttp://cshperspectives.cshlp.org/lookup/doi/10.1101/cshperspect.a018812.

Kessaris, N., Pringle, N. & Richardson, W.D., 2008. Specification of CNS glia from neural stem cells in the embryonic neuroepithelium. *Philosophical Transactions of the Royal Society B: Biological Sciences*, 363(1489), pp.71–85.

Kettenmann, H. & Verkhratsky, A., 2008. Neuroglia: the 150 years after. *Trends in Neurosciences*, 31(12), pp.653–659.

Khakh, B.S. et al., 2015. Diversity of astrocyte functions and phenotypes in neural circuits. *Nature Neuroscience*, 18(7), pp.942–952.

Khakh, B.S. & McCarthy, K.D., 2015. Astrocyte calcium signaling: From observations to functions and the challenges therein. *Cold Spring Harbor Perspectives in Biology*, 7(4), pp.1–17.

Kimelberg, H.K., 2010. Functions of mature mammalian astrocytes: a current view. *The Neuroscientist : a review journal bringing neurobiology, neurology and psychiatry*, 16(1), pp.79–106.

Kleiderman, S. et al., 2016. Functional and phenotypic differences of pure populations of stem cell-derived astrocytes and neuronal precursor cells. *GLIA*.

Kleiderman, S.M., 2016. The Generation of Astrocytes from Stem Cells and their Potency to Regain Stem Cell Potential.

Kleiderman, S.M. & Kirner, N., 2017. The Generation of Astrocytes from Stem Cells and their Potency to Regain Stem Cell Potential. Available at: http://nbn-resolving.de/urn:nbn:de:bsz:352-0-363060.

Kohyama, J. et al., 2010. BMP-induced REST regulates the establishment and maintenance of astrocytic identity. *Journal of Cell Biology*, 189(1), pp.159–170.

Krencik, R. & Zhang, S.-C., 2011. Directed Differentiation of Functional Astroglial

Subtypes from Human Pluripotent Stem Cells. *Nat Biotechnology*, 6(11), pp.1710–1717.

Kuegler, P.B. et al., 2012. GFAP-independent inflammatory competence and trophic functions of astrocytes generated from murine embryonic stem cells. *Glia*, 60(2), pp.218–228. Available at: http://www.ncbi.nlm.nih.gov/pubmed/22072312 [Accessed November 5, 2014].

Kuga, N. et al., 2011. Large-scale calcium waves traveling through astrocytic networks in vivo. *The Journal of neuroscience : the official journal of the Society for Neuroscience*, 31(7), pp.2607–2614.

Lalo, U. et al., 2011. Ionotropic receptors in neuronal-astroglial signalling: What is the role of "excitable" molecules in non-excitable cells. *Biochimica et Biophysica Acta - Molecular Cell Research*, 1813(5), pp.992–1002. Available at: http://dx.doi.org/10.1016/j.bbamcr.2010.09.007.

Lange, S.C. et al., 2012. Primary cultures of astrocytes: their value in understanding astrocytes in health and disease. *Neurochemical research*, 37(11), pp.2569–88. Available at: http://www.ncbi.nlm.nih.gov/pubmed/22926576 [Accessed November 3, 2014].

Lee, H.S. et al., 2014. Astrocytes contribute to gamma oscillations and recognition memory. *Proceedings of the National Academy of Sciences*. Available at: http://www.pnas.org/cgi/doi/10.1073/pnas.1410893111 [Accessed July 29, 2014].

Lee, J. et al., 2015. Ca 2 + Entry is Required for Mechanical Stimulation-induced ATP Release from Astrocyte. *Experimental Neurobiology*, 24(1), pp.17–23.

Li, D. et al., 2013. New tools for investigating astrocyte-to-neuron communication. *Frontiers in Cellular Neuroscience*.

Li, Q. et al., 2014. Interaction between four flavonoids and trypsin: Effect on the characteristics of trypsin and antioxidant activity of flavonoids. *International Journal of Food Science and Technology*, 49(4), pp.1063–1069.

Li, X. et al., 2018. Fast Generation of Functional Astrocytes from Human Pluripotent Stem Cells. *Stem Cell Reports*, 11(4), pp.998–1008. Available at: http://dx.doi.org/10.1016/j.stemcr.2018.08.019.

Liu, X. et al., 2008. Yamanaka factors critically regulate the developmental signaling network in mouse embryonic stem cells. *Cell Research*, 18(12), pp.1177–1189.

Lock, J.T., Parker, I. & Smith, I.F., 2015. A comparison of fluorescent Ca2+ indicators for imaging local Ca2+ signals in cultured cells. *Cell Calcium*, 58(6), pp.638–648. Available at: http://linkinghub.elsevier.com/retrieve/pii/S0143416015001633.

López-Hidalgo, M. & Schummers, J., 2014. Cortical maps: a role for astrocytes? *Current opinion in neurobiology*, 24(1), pp.176–89. Available at:

http://www.ncbi.nlm.nih.gov/pubmed/24419141 [Accessed November 7, 2014].

Lundin, A. et al., 2018. Human iPS-Derived Astroglia from a Stable Neural Precursor State Show Improved Functionality Compared with Conventional Astrocytic Models. *Stem Cell Reports*, 10(3), pp.1030–1045.

Macleod, G.T., 2012. Calcium imaging at the Drosophila larval neuromuscular junction. *Cold Spring Harbor Protocols*, 7(7), pp.758–766.

Majumder, P. et al., 2007. New insights into purinergic receptor signaling in neuronal differentiation, neuroprotection, and brain disorders. *Purinergic Signalling*, 3(4), pp.317–331.

Mamber, C. et al., 2012. GFAPδ Expression in Glia of the Developmental and Adolescent Mouse Brain. *PLoS ONE*, 7(12), pp.1–15.

Martin, G.R., 1981. Isolation of a pluripotent cell line from early mouse embryos cultured in medium conditioned by teratocarcinoma stem cells. *Proceedings of the National Academy of Sciences of the United States of America*, 78(12), pp.7634–7638.

Martin, R. et al., 2015. Circuit-specific signaling in astrocyte-neuron networks in basal ganglia pathways. *Science*, 349(6249), pp.730–734. Available at: http://www.sciencemag.org/cgi/doi/10.1126/science.aaa7945.

Matyash, V. & Kettenmann, H., 2010. Heterogeneity in astrocyte morphology and physiology. *Brain research reviews*, 63(1–2), pp.2–10. Available at: http://www.ncbi.nlm.nih.gov/pubmed/20005253 [Accessed September 16, 2014].

Mccarthy, K. & Vellis, J. De, 1980. Preparation of Separate Astroglial and Oligodroglial Cell Cultures from Rat Cerebral Tissue. *The Journal of Cell Biology*, 85(June).

Miller, F.D. & Gauthier, A.S., 2007. Timing Is Everything: Making Neurons versus Glia in the Developing Cortex. *Neuron*, 54(3), pp.357–369.

Miller, R.H. & Raff, M.C., 1984. Fibrous and protoplasmic astrocytes are biochemically and developmentally distinct. *The Journal of neuroscience : the official journal of the Society for Neuroscience*, 4(2), pp.585–592.

Miller, W., 2010. *Mechanisms of Astrocytic Calcium Wave Propagation and In Vitro Hippocampal Cell Death Are Determined By The Magnitude Of Mechanical Injury*, Available at: http://repository.upenn.edu/edissertationshttp://repository.upenn.edu/edissertations/172.

Molofsky, A. V. et al., 2013. Expression profiling of Aldh1l1-precursors in the developing spinal cord reveals glial lineage-specific genes and direct Sox9-Nfe2l1 interactions. *Glia*, 61(9), pp.1518–1532.

Molofsky, A. V et al., 2014. Astrocyte-encoded positional cues maintain sensorimotor circuit integrity. *Nature*, 509(7499), pp.189–94. Available at:

http://www.ncbi.nlm.nih.gov/pubmed/24776795 [Accessed October 7, 2014].

Molofsky, A.V. & Deneen, B., 2015. Astrocyte development: A Guide for the Perplexed. *Glia*, pp.1–10. Available at: http://doi.wiley.com/10.1002/glia.22836.

Morrow, T., Song, M.R. & Ghosh, a, 2001. Sequential specification of neurons and glia by developmentally regulated extracellular factors. *Development (Cambridge, England)*, 128(18), pp.3585–3594.

Mukamel, E.A., Nimmerjahn, Axel & Schnitzer, M.J., 2009. Automated analysis of cellular signals from large-scale calcium imaging data. *Neuron*, 1(2), pp.65–69. Available at: http://augean.ua.oz.au/personal/dabbott/publications/FNL_ferguson2001.pdf.

Muratore, C.R. et al., 2014. Comparison and optimization of hiPSC forebrain cortical differentiation protocols. *PLoS ONE*, 9(8).

Muroyama, Y. et al., 2005. Specification of astrocytes by bHLH protein SCL in a restricted region of the neural tube. *Nature*, 438(November), pp.360–363.

Nagao, M. et al., 2016. Zbtb20 promotes astrocytogenesis during neocortical development. *Nature Communications*, 7, p.11102. Available at: http://www.nature.com/doifinder/10.1038/ncomms11102.

Nagayasu, T. et al., 2005. Heparin structures in FGF-2-dependent morphological transformation of astrocytes. *Journal of Biomedical Materials Research - Part A*.

Nakashima, K. et al., 1999. Astrocyte differentiation mediated by LIF in cooperation with BMP2. *FEBS Letters*, 457(1), pp.43–46.

Namihira, M. et al., 2009. Committed Neuronal Precursors Confer Astrocytic Potential on Residual Neural Precursor Cells. *Developmental Cell*, 16(2), pp.245–255. Available at: http://dx.doi.org/10.1016/j.devcel.2008.12.014.

Navarrete, M. et al., 2013. Astrocyte calcium signal and gliotransmission in human brain tissue. *Cerebral Cortex*, 23(5), pp.1240–1246.

Neary, J.T. et al., 1999. Mitogenic signaling by ATP/P2Y purinergic receptors in astrocytes: involvement of a calcium-independent protein kinase C, extracellular signal-regulated protein kinase pathway distinct from the phosphatidylinositol-specific phospholipase C/calcium pathway. *The Journal of neuroscience : the official journal of the Society for Neuroscience*, 19(11), pp.4211–4220.

Nedergaard, M., Ransom, B. & Goldman, S. a, 2003. New roles for astrocytes: redefining the functional architecture of the brain. *Trends in neurosciences*, 26(10), pp.523–30. Available at: http://www.ncbi.nlm.nih.gov/pubmed/14522144 [Accessed October 3, 2014].

Nobile, M. et al., 2003. ATP-induced, sustained calcium signalling in cultured rat cortical astrocytes: evidence for a non-capacitative, P2X7-like-mediated calcium entry.

FEBS Letters, 538(1–3), pp.71–76. Available at: http://linkinghub.elsevier.com/retrieve/pii/S0014579303001297.

Oberheim, N.A., Goldman, S.A. & Nedergaard, M., 2012. Heterogeneity of Astrocytic Form and Function. *Methods*, 814, pp.23–45. Available at: http://link.springer.com/10.1007/978-1-61779-452-0.

Okada, Y. et al., 2012. Preinspiratory calcium rise in putative pre-Botzinger complex astrocytes. *The Journal of physiology*, 590(Pt 19), pp.4933–44. Available at: http://www.ncbi.nlm.nih.gov/pubmed/22777672.

Okada, Y. et al., 2004. Retinoic-acid-concentration-dependent acquisition of neural cell identity during in vitro differentiation of mouse embryonic stem cells. *Developmental biology*, 275(1), pp.124–42. Available at: http://www.ncbi.nlm.nih.gov/pubmed/15464577 [Accessed November 5, 2014].

Okuda, H., 2018. A review of functional heterogeneity among astrocytes and the CS56-specific antibody-mediated detection of a subpopulation of astrocytes in adult brains. *Anatomical Science International*, 93(2), pp.161–168.

Olude, M. a. et al., 2015. Astrocyte morphology, heterogeneity, and density in the developing African giant rat (Cricetomys gambianus). *Frontiers in Neuroanatomy*, 9(May), pp.1–10. Available at: http://www.frontiersin.org/Neuroanatomy/10.3389/fnana.2015.00067/abstract.

Otsu, Y. et al., 2014. Calcium dynamics in astrocyte processes during neurovascular coupling. *Nature Neuroscience*, (December), pp.1–11. Available at: http://www.nature.com/doifinder/10.1038/nn.3906 [Accessed December 23, 2014].

Palm, T. et al., 2015. Rapid and robust generation of long-term self-renewing human neural stem cells with the ability to generate mature astroglia. *Scientific Reports*, 5(October), p.16321. Available at: http://www.nature.com/articles/srep16321.

Pan, L. et al., 2014. ??1-Integrin and Integrin Linked Kinase Regulate Astrocytic Differentiation of Neural Stem Cells. *PLoS ONE*, 9(8).

Panatier, a. & Robitaille, R., 2015. Astrocytic mGluR5s and the tripartite synapse. *Neuroscience*, (April), pp.6–11. Available at: http://linkinghub.elsevier.com/retrieve/pii/S0306452215003127.

Pannasch, U. & Rouach, N., 2013. Emerging role for astroglial networks in information processing: from synapse to behavior. *Trends in neurosciences*, 36(7), pp.405–17. Available at: http://www.ncbi.nlm.nih.gov/pubmed/23659852 [Accessed August 19, 2014].

Parri, H., Gould, T. & Crunelli, V., 2001. Spontaneous astrocytic Ca2+ oscillations in situ drive NMDAR- mediated neuronal excitation H. *Nature*, pp.369–456.

Pascual, O. et al., 2005. Astrocytic Purinergic Signaling Coordinates Synaptic Networks.

Science, 310(5745), pp.113–116.

Pascual, O. et al., 2016. Astrocytic Purinergic Signaling Coordinates Synaptic Networks. *Science*, 310(5745), pp.113–116.

Pasti, L. et al., 1997. Intracellular calcium oscillations in astrocytes: a highly plastic, bidirectional form of communication between neurons and astrocytes in situ. *The Journal of neuroscience : the official journal of the Society for Neuroscience*, 17(20), pp.7817–7830.

Patro, N., Naik, A. & Patro, I.K., 2015. Differential temporal expression of S100β in developing rat brain. *Frontiers in cellular neuroscience*, 9(March), p.87. Available at: http://journal.frontiersin.org/article/10.3389/fncel.2015.00087/abstract.

Peljto, M. et al., 2010. Functional diversity of ESC-derived motor neuron subtypes revealed through intraspinal transplantation. *Cell stem cell*, 7(3), pp.355–66. Available at: http://www.pubmedcentral.nih.gov/articlerender.fcgi?artid=2933095&tool=pmcentrez&rendertype=abstract [Accessed November 5, 2014].

Peng, H. et al., 2008. Integrins and dystroglycan regulate astrocyte wound healing: The integrin B1 subunit is necessary for process extension and orienting the microtubular network. *Developmental Neurobiology*, 68(5), pp.559–574.

Perea, G. & Araque, A., 2010. GLIA modulates synaptic transmission. *Brain Research Reviews*, 63(1–2), pp.93–102. Available at: http://dx.doi.org/10.1016/j.brainresrev.2009.10.005.

Perea, G., Sur, M. & Araque, A., 2014. Neuron-glia networks: integral gear of brain function. *Frontiers in Cellular Neuroscience*, 8(November), pp.1–8. Available at: http://www.frontiersin.org/Cellular_Neuroscience/10.3389/fncel.2014.00378/abstract [Accessed November 13, 2014].

Perez-alvarez, A. et al., 2010. LTP-Inducing Stimuli Increase Astrocytic Motility. *The New England journal of medicine*, 363(38), p.2090.

Petravicz, J.C. et al., 2010. Challenging the Dogma : Reevaluating the Role of Astrocyte Calcium Signaling in Physiology .

Petrelli, F. & Bezzi, P., 2016. Novel insights into gliotransmitters. *Current Opinion in Pharmacology*, 26(Table 1), pp.138–145. Available at: http://linkinghub.elsevier.com/retrieve/pii/S1471489215001484.

Phatnani, H. & Maniatis, T., 2015. Astrocytes in Neurodegenerative Disease. , pp.1–18.

Pickford, C.E. et al., 2011. Specific glycosaminoglycans modulate neural specification of mouse embryonic stem cells. *Stem Cells*, 29(4), pp.629–640.

Puchałowicz, K. et al., 2015. Purinergic Signaling and the Functioning of the Nervous System Cells. *Cellular and Molecular Biology Letters*, 0(0). Available at:

http://www.degruyter.com/view/j/cmble.ahead-of-print/cmble-2015-0050/cmble-2015-0050.xml.

Raichle, M.E. & Gusnard, D.A., 2002. Appraising the brain's energy budget. *Proceedings of the National Academy of Sciences*, 99(16), pp.10237–10239. Available at: http://www.pnas.org/cgi/doi/10.1073/pnas.172399499.

Rajan, P. & McKay, R.D., 1998. Multiple routes to astrocytic differentiation in the CNS. *The Journal of neuroscience : the official journal of the Society for Neuroscience*, 18(10), pp.3620–3629.

Raponi, E. et al., 2007. S100B Expression Defines a State in Which GFAP- Expressing Cells Lose Their Neural Stem Cell Potential and Acquire a More Mature Developmental Stage. *Glia*.

Reichenbach, N. et al., 2018. P2Y1 receptor blockade normalizes network dysfunction and cognition in an Alzheimer ' s disease model. *The Journal of experimental medicine*, pp.1–15. Available at: https://doi.org/10.1084/jem.20171487.

Reubinoff, B.E. et al., 2000. Embryonic stem cell lines from human blastocysts: somatic differentiation in vitro. *Nature biotechnology*, 18(4), pp.399–404.

Rezaie, Ulfig & Male, 2003. Distribution and Morphology of GFAP-Positive Astrocytes in the Human Fetal Brain at Second Trimester.

Riol, H., Fages, C. & Tardy, M., 1992. Transcriptional regulation of glial fibrillary acidic protein (GFAP)-mRNA expression during postnatal development of mouse brain. *Journal of Neuroscience Research*, 32(1), pp.79–85.

Risher, W.C. et al., 2014. Astrocytes refine cortical connectivity at dendritic spines. *eLife*, 3, pp.1–24. Available at: http://elifesciences.org/lookup/doi/10.7554/eLife.04047.

Rose, C.R. & Chatton, J.-Y., 2015. Astrocyte sodium signaling and neuro-metabolic coupling in the brain. *Neuroscience*. Available at: http://linkinghub.elsevier.com/retrieve/pii/S0306452215002134.

Rowitch, D.H. & Kriegstein, A.R., 2010. Developmental genetics of vertebrate glial-cell specification. *Nature*, 468(7321), pp.214–22. Available at: http://www.ncbi.nlm.nih.gov/pubmed/21068830 [Accessed July 9, 2014].

Roybon, L. et al., 2013. Human stem cell-derived spinal cord astrocytes with defined mature or reactive phenotypes. *Cell Reports*, 4(2011), pp.1035–1048.

Rujano, M.A. et al., 2004. Retinoic acid-induced differentiation into astrocytes and glutamatergic neurons is associated with expression of functional and activable phospholipase D. *Biochemical and Biophysical Research Communications*, 316(2), pp.387–392.

Rusakov, D.A. et al., 2014. Diversity of astroglial functions alludes to subcellular specialisation. *Trends in Neurosciences*, 37(4), pp.228–242. Available at:

http://dx.doi.org/10.1016/j.tins.2014.02.008.

Sadler, T.W., 2005. Embryology of neural tube development. *American Journal of Medical Genetics - Seminars in Medical Genetics*, 135 C(1), pp.2–8.

Saleem, H. et al., 2014. Interactions of antagonists with subtypes of inositol 1,4,5-trisphosphate (IP3) receptor. *British Journal of Pharmacology*, 171(13), pp.3298–3312.

Salter, M.W. & Hicks, J.L., 1995. ATP causes release of intracellular Ca2+ via the phospholipase C beta/IP3 pathway in astrocytes from the dorsal spinal cord. *The Journal of neuroscience : the official journal of the Society for Neuroscience*, 15(4), pp.2961–2971.

Salzig, D. et al., 2016. Attachment, Growth, and Detachment of Human Mesenchymal Stem Cells in a Chemically Defined Medium. *Stem Cells International*, 2016.

Santos, R. et al., 2017. Differentiation of Inflammation-Responsive Astrocytes from Glial Progenitors Generated from Human Induced Pluripotent Stem Cells. *Stem Cell Reports*.

Savtchouk, I. & Volterra, A., 2018. Gliotransmission: Beyond Black-and-White. *The Journal of Neuroscience*, 38(1), pp.14–25. Available at: http://www.jneurosci.org/lookup/doi/10.1523/JNEUROSCI.0017-17.2017.

Scemes, E. & Giaume, C., 2007. Astrocyte Calcium Waves: What They Are and What They Do. *Glia*, 55(May), pp.1416–1425.

Schildge, S. et al., 2013. Isolation and Culture of Mouse Cortical Astrocytes. *Journal of Visualized Experiments*, (71), pp.1–7. Available at: http://www.jove.com/video/50079/isolation-and-culture-of-mouse-cortical-astrocytes.

Schousboe, A. & Waagepetersen, H.S., 2005. Role of astrocytes in glutamate homeostasis: Implications for excitotoxicity. *Neurotoxicity Research*, 8(3–4), pp.221–225.

Schwartz, J.P. & Wilson, D.J., 1992. Preparation and characterization of type 1 astrocytes cultured from adult rat cortex, cerebellum, and striatum. *Glia*, 5(1), pp.75–80.

Selinfreund, R.H. et al., 1991. Neurotrophic protein S100 beta stimulates glial cell proliferation. *Proceedings of the National Academy of Sciences of the United States of America*, 88(9), pp.3554–3558.

Shaltouki, A. et al., 2013. Efficient generation of astrocytes from human pluripotent stem cells in defined conditions. *Stem Cells*, 31(5), pp.941–952. Available at: http://www.ncbi.nlm.nih.gov/pubmed/23341249 [Accessed November 5, 2014].

Sherwood, M.W. et al., 2017. Astrocytic IP3Rs: Contribution to Ca2+signalling and hippocampal LTP. *Glia*, 65(3), pp.502–513.

Shi, Y., Kirwan, P. & Livesey, F.J., 2012. Directed differentiation of human pluripotent stem cells to cerebral cortex neurons and neural networks. *Nature Protocols*, 7(10), pp.1836–1846.

Shigetomi, E., Patel, S. & Khakh, B.S., 2016. Probing the Complexities of Astrocyte Calcium Signaling. *Trends in Cell Biology*, xx, pp.1–13. Available at: http://dx.doi.org/10.1016/j.tcb.2016.01.003.

Shtrahman, E. et al., 2018. Understanding Spatial and Temporal Patterning of Astrocyte Calcium Transients via Interactions Between Network Transport and Extracellular Diffusion. *Physical Biology*, 165(2), pp.255–269.

Sloan, S. a. & Barres, B. a., 2014. Mechanisms of astrocyte development and their contributions to neurodevelopmental disorders. *Current Opinion in Neurobiology*, 27, pp.75–81. Available at: http://dx.doi.org/10.1016/j.conb.2014.03.005.

Sloan, S.A. et al., 2017. Human Astrocyte Maturation Captured in 3D Cerebral Cortical Spheroids Derived from Pluripotent Stem Cells. *Neuron*, 95(4), p.779–790.e6.

Sofroniew, M. V. & Vinters, H. V., 2010. Astrocytes: Biology and pathology. *Acta Neuropathologica*, 119(1), pp.7–35.

Stacey, G., 2012. *Banking stem cells for research and clinical applications* 1st ed., Elsevier B.V. Available at: http://dx.doi.org/10.1016/B978-0-444-59575-1.00003-X.

Stadtfeld, M. et al., 2010. Induced pluripotency : history , mechanisms , and applications. , 5, pp.582–596.

Suadicani, S.O. et al., 2009. Point mutation in the mouse P2X 7 receptor affects intercellular calcium waves in astrocytes. , 1(1), pp.55–63.

Suda, Y. et al., 1987. Mouse embryonic stem cells exhibit indefinite proliferative potential. *Journal of cellular physiology*, 133(1), pp.197–201. Available at: http://www.ncbi.nlm.nih.gov/pubmed/3667706.

Sun, W. et al., 2017. SOX9 Is an Astrocyte-Specific Nuclear Marker in the Adult Brain Outside the Neurogenic Regions. *The Journal of Neuroscience*, 37(17), pp.4493–4507. Available at: http://www.jneurosci.org/lookup/doi/10.1523/JNEUROSCI.3199-16.2017.

Sun, Y. et al., 2001. Neurogenin promotes neurogenesis and inhibits glial differentiation by independent mechanisms. *Cell*, 104(3), pp.365–376.

Suzuki, A. et al., 2011. Astrocyte-neuron lactate transport is required for long-term memory formation. *Cell*, 144(5), pp.810–823. Available at: http://dx.doi.org/10.1016/j.cell.2011.02.018.

Szu, J.I. & Binder, D.K., 2016. The Role of Astrocytic Aquaporin-4 in Synaptic Plasticity and Learning and Memory. *Frontiers in Integrative Neuroscience*, 10(February),

pp.1–16. Available at: http://journal.frontiersin.org/Article/10.3389/fnint.2016.00008/abstract.

Tabar, V. et al., 2005. Migration and differentiation of neural precursors derived from human embryonic stem cells in the rat brain. *Nature Biotechnology*, 23(5), pp.601–606.

Tabata, H., 2015. Diverse subtypes of astrocytes and their development during corticogenesis. *Frontiers in Neuroscience*, 9(April), pp.1–7. Available at: http://journal.frontiersin.org/article/10.3389/fnins.2015.00114.

Takahashi, K. et al., 2006. Induction of Pluripotent Stem Cells from Mouse Embryonic and Adult Fibroblast Cultures by Defined Factors. *Cell*, 126(4), pp.663–676. Available at: http://linkinghub.elsevier.com/retrieve/pii/S0092867406009767.

Takouda, J., Katada, S. & Nakashima, K., 2017. Emerging mechanisms underlying astrogenesis in the developing mammalian brain. *Proceedings of the Japan Academy, Series B*, 93(6), pp.386–398. Available at: https://www.jstage.jst.go.jp/article/pjab/93/6/93_PJA9306B-03/_article.

Tang, J. et al., 2016. Effect of calcium channel noise in astrocytes on neuronal transmission. *Communications in Nonlinear Science and Numerical Simulation*, 32, pp.262–272. Available at: http://linkinghub.elsevier.com/retrieve/pii/S1007570415002968.

Tang, W. et al., 2015. Stimulation-Evoked Ca2+ Signals in Astrocytic Processes at Hippocampal CA3-CA1 Synapses of Adult Mice Are Modulated by Glutamate and ATP. *Journal of Neuroscience*, 35(7), pp.3016–3021. Available at: http://www.jneurosci.org/cgi/doi/10.1523/JNEUROSCI.3319-14.2015.

TCW, J. et al., 2017. An Efficient Platform for Astrocyte Differentiation from Human Induced Pluripotent Stem Cells. *Stem Cell Reports*.

Tordjmann, T. et al., 1997. Coordinated intercellular calcium waves induced by noradrenaline in rat hepatocytes: Dual control by gap junction permeability and agonist. *EMBO Journal*, 16(17), pp.5398–5407.

Tsai, H. et al., 2012. Regional astrocyte allocation regulates CNS synaptogenesis and repair. *Science*, 337(6092), pp.358–362.

Tsao, H.K., Chiu, P.H. & Sun, S.H., 2013. PKC-dependent ERK phosphorylation is essential for P2X7 receptor-mediated neuronal differentiation of neural progenitor cells. *Cell Death and Disease*, 4(8), pp.e751-11. Available at: http://dx.doi.org/10.1038/cddis.2013.274.

Tyzack, G., Lakatos, A. & Patani, R., 2016. Human Stem Cell-Derived Astrocytes: Specification and Relevance for Neurological Disorders. *Current Stem Cell Reports*. Available at: http://link.springer.com/10.1007/s40778-016-0049-1.

Ullensvang, K. et al., 1997. Differential developmental expression of the two rat brain glutamate transporter proteins GLAST and GLT. *European Journal of Neuroscience*, 9(8), pp.1646–1655.

Ullian, E.M. et al., 2001. Control of synapse number by glia. *Science (New York, N.Y.)*, 291(2001), pp.657–661.

Uzzaman, M. et al., 2005. Embryonic stem cell-derived astrocytes: a novel gene therapy vector for brain tumors. *Neurosurgical focus*, 19(3), p.E6.

Vala, M.H.J. & Baxi, A., 2013. A review on Otsu image segmentation algorithm. *International Journal of Advanced Research in Computer Engineering and Technology*, 2(2), pp.387–389.

Vasiliou, V. & Nebert, D.W., 2005. Analysis and update of the human aldehyde dehydrogenase (ALDH) gene family. *Human Genomics*, 2(2), p.138. Available at: http://www.humgenomics.com/content/2/2/138.

Velkey, J. & O'Shea, K., 2015. Expression of Neurogenin 1 in mouse embryonic stem cells directs the differentiation of neuronal precursors and identifies unique patterns of down-stream gene expression. *Development*, 143(5), pp.951–959.

Venance, L. et al., 1997. Mechanism Involved in Initiation and Propagation of Receptor-Induced Intercellular Calcium Signaling in Cultured Rat Astrocytes. *The Journal of Neuroscience*, 17(6), pp.1981–1992. Available at: http://www.jneurosci.org/content/17/6/1981.abstract%5Cnhttp://www.jneurosci.org/content/17/6/1981.full.pdf.

Verkhratsky, A. & Butt, A., 2018. The History of the Decline and Fall of the Glial Numbers Legend. *Neuroglia*, 1(1), pp.188–192. Available at: http://www.mdpi.com/2571-6980/1/1/13.

Verkhratsky, A., Nedergaard, M. & Hertz, L., 2014. Why are Astrocytes Important? *Neurochemical Research*.

Verkhratsky, A. & Parpura, V., 2014. Store-operated calcium entry in neuroglia. *Neuroscience Bulletin*, 30(1), pp.125–133.

Virchow, R., 1858. Die Cellularpathologie in ihrer Begrundung auf physiologische and pathologische Gewebelehre. Zwanzig Vorlesungen gehalten wahrend der Monate Februar, Marz und April 1858 im pathologischen Institut zu Berlin: August Hirschwald.

Vizi, E.S., Wirkner, K. & Illes, P., 2006. P2X 7 receptors in the nervous system. , 78, pp.327–346.

Volterra, A. & Meldolesi, J., 2005. Astrocytes, from brain glue to communication elements: the revolution continues. *Nature reviews. Neuroscience*, 6(8), pp.626–40. Available at: http://www.ncbi.nlm.nih.gov/pubmed/16025096 [Accessed July 11,

2014].

Volterra, A., Sahlender, D.A. & Savtchouk, I., 2015. What do we know about gliotransmitter release from astrocytes? *Philosophical transactions of the Royal Society of London. Series B, Biological sciences*. Available at: http://dx.doi.org/10.1098/rstb.2013.0592.

Walz, W. & Lang, M.K., 1998. Immunocytochemical evidence for a distinct GFAP-negative subpopulation of astrocytes in the adult rat hippocampus. *Neuroscience Letters*, 257(3), pp.127–130.

Wang, D.D. & Bordey, A., 2008. The astrocyte odyssey. *Progress in Neurobiology*, 86, pp.342–367.

Wang, F. et al., 2012. Astrocytes Modulate Neural Network Activity by Ca2+ -Dependent Uptake of Extracellular K+. , 5(218).

Wang, T. et al., 2014. The role of the JAK-STAT pathway in neural stem cells, neural progenitor cells and reactive astrocytes after spinal cord injury (Review). *Biomedical Reports*, pp.1–6. Available at: http://www.spandidos-publications.com/10.3892/br.2014.401 [Accessed December 30, 2014].

Wilczynska, K.M. et al., 2009. Nuclear factor i isoforms regulate gene expression during the differentiation of human neural progenitors to astrocytes. *Stem Cells*, 27, pp.1173–1181.

Xin, W. & Bonci, A., 2018. Functional Astrocyte Heterogeneity and Implications for Their Role in Shaping Neurotransmission. *Frontiers in Cellular Neuroscience*, 12(May), pp.1–7. Available at: https://www.frontiersin.org/article/10.3389/fncel.2018.00141/full.

Yanagisawa, M. et al., 2001. Signaling crosstalk underlying synergistic induction of astrocyte differentiation by BMPs and IL-6 family of cytokines. *FEBS Letters*, 489(2–3), pp.139–143.

Yang, Y. et al., 2011. Molecular comparison of GLT1+ and ALDH1L1+ astrocytes in vivo in astroglial reporter mice. *Glia*, 59(2), pp.200–207.

Yang, Y., Higashimori, H. & Morel, L., 2013. Developmental maturation of astrocytes and pathogenesis of neurodevelopmental disorders. *Journal of Neurodevelopmental Disorders*, 5(1), p.22. Available at: http://jneurodevdisorders.biomedcentral.com/articles/10.1186/1866-1955-5-22.

Ying, Q.-L. et al., 2003. Conversion of embryonic stem cells into neuroectodermal precursors in adherent monoculture. *Nature biotechnology*, 21(2), pp.183–186. Available at: http://www.ncbi.nlm.nih.gov/pubmed/12524553 [Accessed July 9, 2014].

Yong, V.W. et al., 1990. Morphologic heterogeneity of human adult astrocytes in culture:

Correlation with HLA-DR expression. *Journal of Neuroscience Research*, 27(4), pp.678–688.

Zeng, J.W. et al., 2008. P2Y1 receptor-mediated glutamate release from cultured dorsal spinal cord astrocytes. *Journal of Neurochemistry*, 106(5), pp.2106–2118.

Zhang, S.C. et al., 2001. In vitro differentiation of transplantable neural precursors from human embryonic stem cells. *Nature Biotechnology*, 19(12), pp.1129–1133.

Zhang, Y. et al., 2016. Purification and Characterization of Progenitor and Mature Human Astrocytes Reveals Transcriptional and Functional Differences with Mouse. *Neuron*, 89(1), pp.37–53. Available at: http://www.cell.com/article/S0896627315010193/fulltext.

Zhang, Y. & Barres, B. a., 2010. Astrocyte heterogeneity: An underappreciated topic in neurobiology. *Current Opinion in Neurobiology*, 20(5), pp.588–594. Available at: http://dx.doi.org/10.1016/j.conb.2010.06.005.

Zhou, Q. & Anderson, D.J., 2002. The bHLH transcription factors OLIG2 and OLIG1 couple neuronal and glial subtype specification. *Cell*, 109(1), pp.61–73.

Zhu, Y. & Kimelberg[2], H.K., 2001. Developmental expression of metabotropic P2Y 1 and P2Y 2 receptors in freshly isolated astrocytes from rat hippocampus. *Journal of Neurochemistry*, 77, pp.530–541.

Zorec, R. et al., 2015. Astrocytic vesicles and gliotransmitters: Slowness of vesicular release and synaptobrevin2-laden vesicle nanoarchitecture. *Neuroscience*, (March). Available at: http://linkinghub.elsevier.com/retrieve/pii/S0306452215001852.

Zorec, R. et al., 2012. Astroglial excitability and gliotransmission: an appraisal of Ca2+ as a Signalling Route. *Asn Neuro*, 4(2), pp.103–119.

Zou, J. et al., 2011. Down-regulation of glutamine synthetase enhances migration of rat astrocytes after in vitro injury. *Neurochemistry International*, 58(3), pp.404–413. Available at: http://dx.doi.org/10.1016/j.neuint.2010.12.018.